Quantitative cue-signal-response analysis of EGF-induced cell migration

by

Brian David Harms

B.A. Chemistry
Rice University, 1998

Submitted to the Department of Chemical Engineering
in partial fulfillment of the requirements for the degree of

Doctor of Philosophy

at the

Massachusetts Institute of Technology

September 2004

Signature of Author:.....
Department of Chemical Engineering
July 12, 2004

Certified by:.....
Douglas A. Lauffenburger
Professor of Chemical Engineering
Thesis Supervisor

Accepted by:.....
Daniel Blankschtein
Professor of Chemical Engineering
Chairman, Committee for Graduate Students

Quantitative cue-signal-response analysis of EGF-induced cell migration

by

Brian David Harms

Submitted to the Department of Chemical Engineering on July 12, 2004
in partial fulfillment of the requirements for the degree of
Doctor of Philosophy in Chemical Engineering

Abstract

The physiological importance of cell motility has resulted in intense efforts dedicated towards deconstructing its molecular control mechanisms. Most research employs qualitative approaches, yet quantitative understanding of how altering the function of genes or proteins changes migration responses is critical for engineering therapies targeting pathological cell motility. In this work, we deconstruct hierarchical quantitative relationships between biochemical, biophysical, and phenomenological descriptions of cell motility. Specifically, this thesis establishes quantitative correlations between the activation of key intracellular signaling proteins by extracellular motility cues and the effects of these signals on both the biophysical processes comprising motility and parameters describing the overall paths of translocating cells.

Our model system consisted of Chinese Hamster Ovary (CHO) cells transfected with the epidermal growth factor (EGF) receptor. In initial experiments employing EGF and fibronectin (Fn) as extracellular cues, we found that adhesion-mediated stabilization of lamellipodial protrusions governed the magnitude of directional persistence in cell paths. To connect this biophysical control of persistence to intracellular signaling, a second study examined the role of extracellular signal-related kinase (ERK) and phosphatidylinositol 3-kinase (PI3K) signaling in EGF-induced migration. Both molecules controlled directional persistence biphasically, with maximal persistence at intermediate signal strength. Studies of lamellipodial protrusion, in concert with experiments using soluble anti-adhesion peptides to modulate persistence, indicated that the ERK, but not the PI3K, biphasic curve is explained mechanistically by the results of the first study. In a final study, we investigated the phenomenological structure of CHO-EGFR cell paths using turn angle distribution and time series analyses. Increased local cell speed correlated with increased likelihood of local directional persistence, a result independent of biochemical modulation of overall cell motility. Time-based directional autocorrelations were observed that indicate an unusual non-Markov behavior in CHO migration. Overall, these studies demonstrate how biophysical analysis is an effective tool for gaining insight into the quantitative regulation of motility by intracellular signaling.

Thesis Supervisor: Douglas A. Lauffenburger
Professor of Chemical Engineering

Acknowledgements

My six years of doctoral training have been a period of incredible intellectual and personal growth in my life. I am indebted to all those who have been a part of my experiences in Boston and MIT.

I am greatly appreciative of my thesis advisor, Doug Lauffenburger, for his guidance and support during my thesis. Doug was the primary force behind my intellectual maturation as a scientist, giving me the freedom to fail while challenging me to succeed. The other members of my thesis committee, Rick Horwitz (University of Virginia), Linda Griffith (MIT), and Frank Gertler (MIT), deserve thanks for their valuable intellectual feedback regarding my research. Outside of my committee, discussions with Alan Wells (University of Pittsburgh) were integral for helping me place my work within the wider context of cell migration research.

Past and present members of the Lauffenburger, Griffith, and Horwitz laboratories have provided essential research and personal support during my time at MIT. They are a fantastic group of people both scientifically and socially! In particular, Wendy Prudhomme and Lily Koo always lent welcome ears, wise counsel, and sincere friendship in all aspects of my life.

I had the privilege to work with two talented undergraduates during my thesis: Gina Bassi and Alia Burton. I thank them for both assisting me with many experiments and giving me the opportunity to be a mentor in their own career paths. Sincere appreciation is also due to JoAnn Sorrento, Doug's administrative assistant. In addition to her ever-filled basket of candy and ever-sunny demeanor, JoAnn went far beyond the call of duty in helping to navigate me through the MIT research bureaucracy.

Now that I'm done with my formal education, my parents can relax knowing that I really do have a career path in mind beyond permanent schooling. They probably never imagined that the simple math problems they put on a blackboard for me when I was in elementary school would prove so alluring that I'd stay in school until nearly 30. I know it was sometimes difficult for them to understand the Ph.D. process, but they have always given me their unwavering love and support.

Beyond the research excellence of MIT and the allure of rowing on the Charles, my brother's presence in Boston was a primary reason for my choosing MIT for graduate school. I was very blessed to get to know Mike better while we were here together, and also to watch him date and marry Nicole, the best sister-in-law you could hope for. In closing, I say: it's your turn for graduate school now, Erin! Hopefully I can be a source of care and support for you like you were for me during my time at MIT.

Soli Deo Gloria,
Brian Harms
July 12, 2004

Financial support for this work was provided by the both the National Institutes of Health and a graduate fellowship from the Whitaker Foundation.

The fear of the LORD is the beginning of wisdom, and knowledge of the Holy One is understanding.

Proverbs 9:10

In his heart a man plans his course, but the LORD determines his steps.

Proverbs 16:9

TABLE OF CONTENTS

CHAPTER 1

INTRODUCTION AND OVERVIEW

1.1 Motivation: developing design principles for cell migration

Cell motility is integral to a host of biological processes. The proper regulation of migration undergirds the development of embryos, the growth of blood vessels, the healing of wounds, and the body's ability to fight off pathogens. Conversely, aberrant regulation of migration contributes to diverse diseases including metastatic cancer, rheumatoid arthritis, and vascular disease (Hart, 2002; Kassis et al., 2001; Keller, 2002; Kraemer, 2000; Martin, 1997; Szekanecz and Koch, 2000).

Despite this manifest importance of migration in human biology and pathology, there is a notable lack of medical pharmaceutics and biologics designed to modulate in vivo cell motility (Fenteany and Zhu, 2003). A primary example of this deficiency occurs in the treatment of human cancer, where radiation and chemotherapy protocols are largely intended to disrupt the proliferation of tumor cells. While this approach has reasonable success in localized tumors, metastatic cells - which acquire a migratory phenotype, invade the circulatory system, and are subsequently transported to secondary locations in the body - result in a much poorer patient prognosis. Treatment options specifically designed to disrupt tumor cell motility and prevent secondary tumor formation would thus be a major advance in cancer therapy.

The lack of therapeutics directed towards cell migration is not due to a lack of historical interest in cell motility, for the study of migration dates back to the 17th century and the observational studies of van Leeuwenhook (Chicurel, 2002). Rather, after more than

300 years of subsequent study, a detailed understanding of the mechanisms of migration still eludes researchers. The research presented in this thesis was motivated by the desire to increase the mechanistic understanding of cell motility for the development of improved treatments for human disease.

The backbone of modern biomedical science is molecular-scale research. Qualitative techniques of gene overexpression and deletion, along with pharmacologic approaches, have been used to great advantage for the discovery of molecules and proteins involved in cellular processes like migration. However, our knowledge of the massive numbers of intracellular proteins implicated in motility, such as surface receptors for directional sensing, signaling network enzymes for information flow, and cytoskeletal components for force generation, does not translate to a detailed understanding of the cellular control mechanisms governing motility. The fundamental reason behind this dilemma lies in the complexity of intracellular molecular interactions—it is immensely difficult to predict how qualitative changes in the activity and function of molecular components integrate to affect such a complex cell response as migration (Maheshwari and Lauffenburger, 1998).

As engineers, our approach to parsing the complexity of migration is a search for predictive "design principles" governing how alteration of the molecular properties of subcellular components can elicit useful responses of cell migration. To construct migration design principles, the engineering perspective relies on the testing and application of parameterized, quantitative models of migratory behavior across multiple levels of scale ranging from molecular to macroscopic. These models should be self-consistent, in that parameters describing motility on a less detailed scale should be predictably related to parameters describing motility on a more detailed scale. The adequacy of these hierarchical models will be defined by a sufficient level of detail to make accurate predictions about how changing molecular properties will affect the bulk migration of a cell or population of cells. With knowledge of this type, therapeutic genetic or pharmacological interventions could be rationally targeted towards appropriate molecular targets governing motility.

Integral to this sort of hierarchical model development is the rigorous application of quantitative assays under well-controlled, systematically altered experimental conditions, as quantitative experiments are useful for both hypothesis-driven testing and data-driven development of proposed relationships between parameters on different levels of scale. The work presented in this thesis addresses this crucial part of the engineering approach to migration by using quantitative experimentation to explore relationships between three levels of scale used to describe motility. Specifically, the research reported herein sought to establish mechanistic correlations between systematic alteration of the level of activation of key intracellular signaling proteins and the effects of this alteration on both the biophysical processes comprising motility and parameters describing the paths of translocating cells. We believe in the future this quantitative, hierarchical form of analysis will become an increasingly important research tool for deconvolving the molecular regulatory mechanisms underlying motility, because it allows the systematic, combinatorial evaluation of the effects of molecular components on the macroscopic properties ultimately observable as cell motion.

1.2 Chapter overview

This thesis is composed of three chapters addressing complementary aspects of migration behavior as defined by different levels of system abstraction and detail (phenomenological, biophysical, and biochemical). The migratory cell system of interest consists of Chinese Hamster Ovary cells transfected with the epidermal growth factor (EGF) receptor (CHO-EGFR cells) and separated into two subpopulations of differing receptor expression level.

In Chapter 3 we report the combined regulation of CHO-EGFR translocation by EGF and varying surface densities of the extracellular matrix protein fibronectin (Fn). We find that directional persistence, but not cell speed, is strongly dependent on Fn surface density in the presence of EGF. Specifically, EGF-induced persistence increases monotonically with

increasing levels of Fn. We account for this result via an examination of the biophysical processes of cell adhesion and membrane extension activity, showing that the adhesion-mediated stabilization of lamellipodial protrusions can govern the magnitude of directional persistence in migration.

Given the elucidation in Chapter 3 of a biophysical mechanism for regulating direction persistence, an attractive course of action was the study of signaling molecules possibly governing the regulation of directional persistence in isotropic cell migration. The extracellular signal-regulated kinase (ERK) and the phosphotidylinositol 3-kinase (PI3K) were identified as likely candidates, the former due to its established role in modulating cell adhesion to substrate (Glading et al., 2001; Xie et al., 1998), and the latter due to its necessity for effective chemotaxis (Funamoto et al., 2002; Weiner, 2002). In Chapter 4, we examine EGF-induced cell migration as a function of graded amounts of pharmacological inhibitors of ERK and PI3K signaling. Significantly, both molecules control directional persistence in a biphasic manner, with maximal persistence occurring at intermediate levels of signal. For ERK, studies of lamellipodial protrusion results indicate that the biphasic curve is at least partially explained by the adhesive regulation of persistence described in Chapter 3. For PI3K, a different but poorly defined biophysical mechanism appears to be responsible for persistence modulation.

Chapters 3 and 4 highlight how quantifying cell speed and persistence time provides information useful for discerning the biochemical and biophysical mechanisms governing motility. However, speed and persistence are time-averaged summaries of cell motility that mask the more detailed displacement information inherent in the local structure of cell paths. In Chapter 5 we utilize two "2nd-order" tools—turn angle distribution plots and time series analysis—to study this local structure in CHO-EGFR cell tracks. We find that increased local cell speed correlates with increased likelihood of local persistence in direction of motion. Moreover, we find that time autocorrelations exist for cell directionality

but not speed, and that some evidence exists for an unusual non-Markov cell behavior in CHO-EGFR migration.

Overall, we believe that the primary advance described in this thesis is the novel biphasic relationships developed between intracellular signaling and directional persistence. These results are two-fold interesting given the general assumption that the effects of signaling proteins on migration are monotonic, along with the relative lack of attention paid to the regulation of directional migration in isotropic as opposed to gradient extracellular environments. With some success, we have sought to deconstruct these relationships using a quantitative approach emphasizing the biophysical processes underlying motility. In using this approach, this thesis demonstrates that insights into complex biological events like migration may be gained through quantitative combinatorial experimentation on multiple levels of detail. This integrated "systems approach" has generated numerous avenues for further research.

1.3 References

Chicurel, M. 2002. Cell migration research is on the move. *Science.* 295:606-609.

Fenteany, G., and S. Zhu. 2003. Small-molecule inhibitors of actin dynamics and cell motility. *Curr. Top. Med. Chem.* 3:593-616.

Funamoto, S., R. Meili, S. Lee, L. Parry, and R.A. Firtel. 2002. Spatial and temporal regulation of 3-phosphoinositides by PI 3-kinase and PTEN mediates chemotaxis. *Cell.* 109:611-623.

Glading, A., F. Überall, S.M. Keyse, D.A. Lauffenburger, and A. Wells. 2001. Membrane proximal ERK signaling is required for M-calpain activation downstream of epidermal growth factor receptor signaling. *J. Biol. Chem.* 276:23341-23348.

Hart, J. 2002. Inflammation. 1: Its role in the healing of acute wounds. *J. Wound Care.* 11:205-209.

Kassis, J., D.A. Lauffenburger, T. Turner, and A. Wells. 2001. Tumor invasion as dysregulated cell motility. *Semin. Cancer Biol.* 11:105-117.

Keller, R. 2002. Shaping the vertebrate body plan by polarized embryonic cell movements. *Science.* 298:1950-1954.

Kraemer, R. 2000. Regulation of cell migration in atherosclerosis. *Curr. Atheroscler. Rep.* 2:445-452.

Maheshwari, G., and D.A. Lauffenburger. 1998. Deconstructing (and reconstructing) cell migration. *Microsc. Res. Techniq.* 43:358-368.

Martin, P. 1997. Wound healing: aiming for perfect regeneration. *Science.* 275:75-81.

Szekanecz, Z., and A.E. Koch. 2000. Endothelial cells and immune cell migration. *Arthritis Res.* 2:368-373.

Weiner, O.D. 2002. Regulation of cell polarity during eukaryotic chemotaxis: the chemotactic compass. *Curr. Opin. Cell Biol.* 14:196-202.

Xie, H., M.A. Pallero, D. Gupta, P. Chang, M.F. Ware, W. Witke, D.J. Kwiatkowski, D.A. Lauffenburger, J.E. Murphy-Ullrich, and A. Wells. 1998. EGF receptor regulation of cell motility: EGF induces disassembly of focal adhesions independently of the motility-associated PLCg signaling pathway. *J. Cell Sci.* 111:615-624.

CHAPTER 2

BACKGROUND

2.1 Cell migration in physiology and pathology

Cell migration is an important component of many normal physiological processes along with several pathologies. In the developing embryo, properly regulated migration over large spatial distances is essential for body segmentation and neuronal development (Keller, 2002). In the adult organism, leukocytes migrate to areas of infection or damage and help mediate the inflammatory and immune response (Hart, 2002). Wound healing requires the directed migration of fibroblasts with subsequent wound closure occurring due to cell-mediated contraction of extracellular matrix (Lawrence, 1998; Martin, 1997; Sethi et al., 2002). The movement of vascular endothelial and smooth muscle cells is essential for angiogenesis (Patan, 2004). Conversely, dysregulated motility underlies pathologies including rheumatoid arthritis (Szekanecz and Koch, 2000), atherosclerosis (Kraemer, 2000; Schwartz, 1997), and cancer (Kassis et al., 2001). In cancer, local tumor growth relies on the stimulation of neovascularization and endothelial cell migration for creation of tumor blood supply, while metastatic tumor spreading occurs when localized cancer cells acquire a migratory phenotype, penetrate into the vascular system, and are transported throughout the body.

Given its importance in physiology and pathology, motility has been studied extensively in recent decades, with a great deal of knowledge gained of the molecular regulatory mechanisms governing it. A detailed, predictive understanding of this regulation would lead to new insights for therapeutic interventions; yet in most cases such a

detailed understanding of migration is still elusive, as new discoveries continually indicate increasing complexity in the molecular components regulating the behavior of a migrating cell. Moreover, it is quite difficult to predict how altering specific molecular properties will affect the overall migration behavior of a cell.

As engineers, we believe that systematic study of the quantitative relationships between the alteration of subcellular molecular properties and resulting effects on macroscopic migratory responses is necessary to fully parse the complex cellular regulation of motility. Yet to date, the possible existence of these quantitative relationships remains largely unexplored. In this thesis, we focused on the quantitative effects on motility that result from modulation of the activation of intracellular signaling pathways identified as critical for migration. The next section contains a brief overview of the three hierarchical levels of scale at which the study of motility in this thesis proceeded (Fig. 2.5.1).

2.2 Hierarchical descriptions of motility

The most detailed scale of study concerns the molecular regulation of motility. At this level, two categories of extracellular molecules are known to affect cell migration. These migration-regulating agents are classified as either extracellular matrix molecules that comprise the surface over which cells migrate, or soluble molecules present in the extracellular milieu such as growth factors or cytokines. Transmembrane cell-surface receptors transmit information about these extracellular motility cues to the cell interior by activating multiple intracellular signal transduction pathways. Ultimately, it is the integrated effects of these signaling pathways, in response to extracellular cues, that govern cell motion. Molecular studies of motility employing genetic or pharmacological approaches to deconstruct these signaling pathways have been remarkably successful in developing a qualitative picture of how cells control migration through the identification of relevant intracellular signaling proteins and their functions (Ridley et al., 2003); an overview of several key signaling proteins and their putative roles in regulating motility can be found

in the next section of this chapter. Yet the functional forms of quantitative relationships between intracellular signaling and other more macroscopic descriptions of motility remain largely unexplored (Fig. 2.5.2).

At the next increasing scale of detail, cell migration can be viewed as a cyclical process with distinct biophysical components activated and controlled by intracellular signaling pathways (Fig. 2.5.3). At the beginning of a cycle, the cell body polarizes and protrudes at its lamellipodium, and this protrusion adheres itself to the substrate over which the cell is moving. Subsequent to attachment, a cell generates motive force by actomyosin-based contraction that moves the cell body forward. The end of the cycle occurs when cell-substrate attachments at the rear of the cell detach, allowing uropodial retraction and the "crawling" cycle to begin again (Lauffenburger and Horwitz, 1996; Mitchison and Cramer, 1996). Repeated cycles of these biophysical components result in sustained motility.

At the broadest level of detail, phenomenological observation of migrating cells indicates that over short time periods cells move in a constant direction, while over longer time periods the direction of cell migration changes randomly (Fig. 2.5.4). This path behavior can be described as a persistent random walk where the expected mean-square displacement of a cell at time Δt is governed by two fundamental cell parameters, cell speed (S) and persistence time (P) (Dunn, 1983; Othmer et al., 1988).

$$\left\langle (\Delta \mathbf{x})^2 \right\rangle = 2S^2 P[(\Delta t) - P(1 - exp\{-(\Delta t)/P\})], \quad \mathbf{x} \in \Re^n$$

$$S = \lim_{(\Delta t)\to 0} \frac{\left\langle (\Delta \mathbf{x})^2 \right\rangle^{1/2}}{(\Delta t)}$$

$$P = \lim_{(\Delta t)\to 0} \frac{2(\Delta t)}{\left\langle \varphi^2 \right\rangle}$$

Speed describes the scalar velocity of cell centroid movement, while persistence represents the length of time over which a cell's direction of motion remains relatively constant. A third parameter, chemotactic index, may be used to quantify a cell's ability to bias its migration in a gradient of soluble or adhesive ligand (Maheshwari and Lauffenburger, 1998; Othmer et al., 1988), but this parameter does not enter into the experiments of this thesis, which were conducted in uniform extracellular environments.

Ideally, we desire our understanding of how these three levels of scale affect motility to be self-consistent. In this circumstance, altering key parameters governing motility at each level of scale would result in predictable effects on motility at the next larger level of scale. Within this thesis, this hierarchical result is sought in the context of the quantitative study of how the magnitude of signal flux through key intracellular biochemical signaling targets controls biophysical parameters like cell-substratum adhesion and lamellipodial protrusion that in turn govern cell speed and persistence.

It should be noted that experimental protocols most often used to study how intracellular signaling governs motility (Boyden chamber, Transwell, or wound scrape assays) are population-level assays that count the number of migratory cells or measure the movement of a cell front. While these assays are useful for qualitative examinations of how signaling proteins affect migratory potential, it is clear that experiments using individual cell tracking methods allow a more nuanced and informative readout of the regulatory effects of intracellular signaling on cell motility. Unfortunately, very few published studies systematically examine the effects of signaling on speed and directionality as separable properties of cell migration (for two examples, see Gu et al., 1999, and Lokuta et al., 2003).

In contrast, much information exists deconstructing how biophysical processes govern phenomenological migration parameters, in particular cell speed. Both theoretical models (DiMilla et al., 1991; Lauffenburger, 1989) and experiments in multiple cell types have demonstrated that cell-substratum adhesion strength regulates cell speed biphasically, with maximal speed of translocation occurring at intermediate levels of adhesion as

governed by the amount of adhesion ligand on the substratum (DiMilla et al., 1993; Goodman et al., 1989; Maheshwari et al., 1999; Palecek et al., 1997), the expression level of integrin cell adhesion receptors (Keely et al., 1995; Palecek et al., 1997), and integrin-ligand affinity (Palecek et al., 1997; Palecek et al., 1998). On weakly adhesive surfaces, insufficient adhesion formation and low rates of lamellipodial protrusion limit the generation of traction for cell locomotion, whereas highly adhesive surfaces limit cell speed by preventing the disruption of cell-substratum attachments at the cell rear and reducing uropodial detachment rates (Maheshwari et al., 1999; Palecek et al., 1998; Ware et al., 1998). Variations in front-rear adhesive asymmetry and the magnitude of contractile force are also predicted to alter cell speed (DiMilla et al., 1991), but developing adequate experimental tests for testing these predictions has proven intractable.

While the regulation of speed by biophysical parameters like adhesion strength or lamellipodial protrusion rate is somewhat intuitive, it is less obvious how biophysical processes might affect directional persistence in cell migration. Perhaps for this reason, the simultaneous analysis of changes in directional persistence and underlying biophysical processes has remained largely unexplored in the literature. Two models exist proposing stochastic fluctuations in receptor-ligand binding as a basis for directional persistence in uniform adhesive and soluble environments (Dickinson and Tranquillo, 1993; Tranquillo and Lauffenburger, 1987). These models link the stochastic fluctuations to variations in short-timescale spatiotemporal forces that affect the direction of cell migration over longer timescales. One of the models, which describes the regulation of persistence by adhesion, predicts an inverted biphasic dependence of persistence time to cell-substratum adhesion strength. However, previous studies of the correlation between cell adhesion and persistence are contradictory, with both biphasic and inverted biphasic relationships having been reported (DiMilla et al., 1993; Ware et al., 1998). To our knowledge, the other stochastic model has not been experimentally tested to date.

2.3 Overview of signaling linked to cell motility

Studies elucidating the role of signaling pathways in the control of motility have proceeded in a variety of cell types appropriate to the question of interest. Thus leukocytes, whose ability to migrate efficiently towards pathogens is essential for the immune response, are widely studied to ascertain how cells establish and maintain their direction of migration. Similarly fibroblasts, important for wound repopulation and matrix remodeling, are often utilized in research addressing how cells generate contractile force. The current picture of signaling pathway regulation of migration is a composite of studies using these different cell types and environments (Ridley et al., 2003).

A full review of the major molecular effectors of motility signaling is beyond the scope of this thesis (for a comprehensive overview see Ridley et al., 2003, and the references therein). What follows is a selective discussion of some key signaling pathways focused on the control of three aspects of higher scale migration particularly relevant to this thesis: modulation of cell-substratum adhesion, directional orientation and sensing, and lamellipodial protrusion and actin polymerization.

2.3.1 Modulation of cell adhesion

Effective migration is dependent on the coordinated formation and dissolution of cell adhesions to substrate. The primary class of receptors mediating cell-substratum adhesion are the integrins, a large group of heterodimeric proteins with matrix-binding extracellular domains (Hynes, 2002). Though devoid of enzymatic activity, integrins act not only as passive linkages between the substrate and cytoskeleton, but also as cytoplasmic nuclei for intracellular signaling in response to integrin binding and clustering (Giancotti and Ruoslahti, 1999; Miranti and Brugge, 2002). Often, integrin signaling synergistically regulates cell responses in concert with signaling downstream of soluble extracellular factors (Hauck et al., 2000; Kawahara et al., 2002; Renshaw et al., 1999; Sakai et al., 1999; Sieg et al., 2000; Woodard et al., 1998).

Focal adhesion kinase (FAK) is one key signaling protein that affects migration through modulation of cell-substratum adhesion (Parsons, 2003). A tyrosine kinase, FAK autophosphorylates upon integrin binding to substrate, and subsequently associates within focal adhesions with a number of signaling and cytoskeletal proteins that mediate its signaling effects. FAK constructs with phosphorylation site mutations or lacking a kinase domain show reduced motility (Cary et al., 1996; Gilmore and Romer, 1996; Sieg et al., 1999), and while the precise role FAK signaling plays in allowing cell migration is unclear, the bulk of the evidence suggests that it regulates the turnover of cell-substratum adhesions. FAK-null mouse fibroblasts show increased numbers of focal adhesions and greatly reduced motility (Ilic et al., 1995), and recent quantitative measurements of rate constants for the formation and disassembly of dynamic adhesions within lamellipodia showed that the presence of active FAK phosphorylated at Tyr-397 is a requirement for efficient adhesion turnover at the cell front (Webb et al., 2004). Consistent with these results is a report of FAK-mediated recruitment of the cytoskeletal protease calpain to focal adhesions; calpain subsequently cleaves FAK to potentiate focal complex turnover (Carragher et al., 2003).

Another key signaling target in motility is the extracellular signal-regulated kinase (ERK) cascade. Extensive evidence links its activation by both integrins and soluble factors to increased cell migration (Ho et al., 2001; Kawahara et al., 2002; Klemke et al., 1997; Krueger et al., 2001; Vial et al., 2003). ERK regulation of motility seems to extend to all aspects of the lifetime of a cell-substratum adhesion—formation, maturation, and release. Active, phosphorylated ERK colocalizes with focal adhesions in spreading and migrating cells; this effect occurs primarily at newly forming adhesions and is dependent on ERK-mediated myosin light chain kinase activation (Fincham et al., 2000; Shono et al., 2001; Stähle et al., 2003). This suggests that active ERK potentiates adhesion maturation within lamellipodia via a myosin-based contractility effect (Fincham et al., 2000). Indeed, integrin-mediated ERK signaling, via activation of myosin light chain kinase, phosphorylates myosin light chains to promote assembly of active actin-myosin motors able to generate contractile

force (Cheresh et al., 1999; Klemke et al., 1997). Counter-intuitively based on the above, growth factor-mediated ERK signaling also appears to play a role in the overall reduction of cell-substratum adhesion strength (Xie et al., 1998). This effect results from the dissolution of uropodial cell adhesions through the ERK-mediated activation of calpain and the subsequent cleavage of focal adhesion and cytoskeleton proteins (Cuevas et al., 2003; Glading et al., 2000; Glading et al., 2001).

The GTPase RhoA has a similar ability as ERK to generate contractility. Rho activity promotes cell adhesion and the formation of stress fibers and focal adhesions (Nobes and Hall, 1999; Ridley and Hall, 1992); this appears to occur through Rho activation of Rho-kinase (ROCK), which then upregulates MLC phosphorylation and cell contractility (Ridley, 2001). Though the ERK and Rho effects on MLC phosphorylation are biochemically parallel, their contractility effects seem to be localized to different regions of the cell, with MLCK acting in adhesion assembly at the cell periphery (see above) and ROCK acting in stress fiber formation in the cell body (Totsukawa et al., 2004; Totsukawa et al., 2000).

2.3.2 Directional orientation and sensing

Recent years have witnessed an explosion of knowledge regarding how cells generate biochemical and morphological polarity for directional migration. The production of the 3′-phosphotidylinositols PtdIns(3,4,5)P_3 (PIP_3) and PtdIns(3,4)P_2 (PI(3,4)P_2), as regulated by the opposing activities of the lipid kinase phosphotidylinositol 3-kinase (PI3K) and the 3′ lipid phosphatase PTEN, has emerged as a critical regulatory system for directional migration.

The first indications of the role of 3′-PtdIns lipids in directional orientation were observations of the sharply asymmetric localization of PI3K lipid products to the area of plasma membrane facing a chemoattractant source despite uniform membrane distribution of chemoreceptors and only a moderate gradient of receptor occupany (Devreotes and Janetopoulos, 2003). Originally noted downstream of G protein receptors in *Dictyostelium*

discoideum and neutrophils (Parent et al., 1998; Servant et al., 2000), this phenomenon also occurs downstream of receptor tyrosine kinases in fibroblasts (Haugh et al., 2000). Genetic or pharmacological disruption of PI3K isoforms results in both the abrogation of these lipid gradients and a reduced chemotactic and migratory ability due to the presence of multiple competing lamellipodia (Funamoto et al., 2002; Iijima and Devreotes, 2002). Such evidence suggests that PI3K serves only a directional orientation and sensing function, but other data indicate that localized PI3K activity can initiate membrane extension directly, as localization correlates to areas of membrane protrusion (Devreotes and Janetopoulos, 2003; Funamoto et al., 2002; Hill et al., 2000; Insall and Weiner, 2001; Qian et al., 2004). This correlation appears to derive from a positive feedback loop containing PIP_3 and Rac that creates actin polymers at the leading edge (see Chapter 2.3.3 for the role of Rac in lamellipodial protrusion) (Srinivasan et al., 2003; Wang et al., 2002; Weiner et al., 2002). Overall then, the effects of PI3K-derived 3'-PtdIns lipids seem to affect directionality in migration by both amplifying external gradients and aiding in the polarized reorganization of cell morphology and cytoplasm (Devreotes and Janetopoulos, 2003).

The lipid phosphatase PTEN also regulates 3'-PtdIns gradients in concert with PI3K, as cells lacking PTEN have elevated levels of 3'-PtdIns lipids (Comer and Parent, 2002; Sulis and Parsons, 2003). PTEN localizes to surface membranes at the rear of chemotaxing cells, showing reciprocal localization to the leading edge translocation of PI3K (Funamoto et al., 2002; Iijima and Devreotes, 2002), and PTEN gene disruption in *Dictyostelium* results in a similar phenotype as PI3K-null cells in that they are unable to efficiently move up chemattractant gradients (Funamoto et al., 2002; Iijima and Devreotes, 2002).

Interestingly, no evidence currently exists regarding the potential of the PIP_3/PI3K/PTEN signaling module to affect directional persistence in uniform extracellular environments, though it has been shown that PI3K localizes to the ends of lamellipodia in randomly migrating cells in uniform environments (Funamoto et al., 2002).

2.3.3 Lamellipodial protrusion

Lamellipodial protrusion is the result of the creation of a branched, "dendritic" F-actin network through activation of the Arp2/3 complex. The Arp2/3 complex mediates lamellipodial actin polymerization by binding to an existing F-actin filament and nucleating a new filament that branches off the mother filament (Mullins, 2000). The Rho-family GTPases Rac and Cdc42 have emerged as critical regulators of leading edge formation through their control over this polymerization process (Ridley, 2001). Both extracellular matrix and soluble stimuli activate Rac and Cdc42 (Clark et al., 1998; Price et al., 1998; Ridley et al., 1992; Srinivasan et al., 2003).

While both Rac and Cdc42 have defined pathways linking them to Arp2/3 complex activation and the dendritic actin polymerization characteristic of lamellipodia (Pollard and Borisy, 2003), evidence indicates that these GTPases have separable functions in cells. As stated earlier, Rac activity mediates membrane ruffling and lamellipodial protrusion through a positive feedback loop involving PIP_3 (Ridley et al., 2003; Srinivasan et al., 2003). In contrast, cells whose Cdc42 activity is inhibited form multiple competing lamellipodia that prevent effective cell polarization (Ridley et al., 2003; Srinivasan et al., 2003). Thus Cdc42 activity appears to restrict polymerization to one region of the cell membrane rather than controlling lamellipodial protrusion *per se*, thereby helping to establish the leading edge and cytoskeletal polarity (Nobes and Hall, 1999; Ridley, 2001). Along these lines, Cdc42 inhibition abrogates the chemotactic directional sensitivity of macrophage migration but does not decrease the absolute speed of cell movement (Allen et al., 1998). Interestingly, a recent report suggests that PIP_3 is required for Cdc42 localization to the leading edge without being necessary for its activity, thus giving both Cdc42 and PIP_3 concurrent regulatory roles in coordinating protrusion directionality (Li et al., 2003).

Lamellipodial protrusion and actin polymerization are also regulated by several actin-modifying proteins, including cofilin, profilin, and gelsolin, that control the concentration and availability of actin monomers and polymers for Arp2/3 nucleation

(Ridley et al., 2003). One signaling protein connected to the action of these actin-binding proteins is phospholipase C-gamma (PLCγ). Current evidence indicates that PLCγ acts by mobilizing actin-modifying proteins at the leading edge, in particular gelsolin, to help the cell transition from a non-polarized to an asymmetric motile morphology (Chen et al., 1996; Piccolo et al., 2002; Wells et al., 1999). PLCγ also appears to mediate at least part of the effects of Rac and Cdc42 on lamellipodial protrusion (Chou et al., 2003; Nogami et al., 2003).

2.4 EGF and EGFR in cell motility

The wealth of information available about the epidermal growth factor (EGF) and its receptor (EGFR), coupled with their clinical and experimental relevance to cell migration, make the EGF/EGFR system an ideal choice for the studies conducted in this thesis. EGFR is the most thoroughly studied member of the ErbB class of receptor tyrosine kinases (for an extensive review of the biology of both the EGFR and other ErbB receptors, please refer to *Experimental Cell Research*, 284 (1), 2003). The structure of the EGFR consists of a ligand-binding extracellular domain consisting of four subdomains, a short transmembrane domain, and a cytoplasmic region consisting of a small juxtamembrane region, a tyrosine kinase domain, and a C-terminal regulatory domain (Fig. 2.5.5) (Jorissen et al., 2003).

EGFR binds several related ligands including epidermal growth factor (EGF), transforming growth factor-α, heparin-binding EGF-like growth factor, amphiregulin, β-cellulin, epiregulin, and epigen (Harris et al., 2003). EGF, the most widely-studied EGFR ligand, was first discovered in 1962 as a protein that accelerated tooth eruption and eyelid opening in newborn mice (Cohen, 1962). It is a 6 kilodalton, 53 amino acid soluble polypeptide derived from proteolytic cleavage of a transmembrane precursor and stabilized by three disulfide bonds (Harris et al., 2003; Massague and Pandiella, 1993).

EGFR is expressed by normal cell types including epithelial cells and fibroblasts, and its overexpression in cancer tumors correlates to poorer patient prognosis (Arteaga, 2003). Significantly, this prognosis may be due to a correlation between the overexpression and

ligand-induced activation of EGFR and increased invasiveness of tumors *in vivo* (Fontanini et al., 1995; Jorissen et al., 2003; Schlessinger, 2000; Turner et al., 1996). This invasiveness likely relates to the observation that EGF-induced activation of EGFR also increases motility in numerous cell lines *in vitro* (Blay and Brown, 1985; Cha et al., 1996; Chen et al., 1994a; McCrawley et al., 1997; Verbeek et al., 1998; Westermark et al., 1991).

The intracellular signaling pathways leading to EGF-induced cell motility begin at five tyrosine residues in the EGFR C-terminal regulatory domain that become trans-autophosphorylated upon the dimerization of ligand-bound receptors (Downward et al., 1984; Jorissen et al., 2003). Once phosphorylated, the tyrosines are docking sites that recruit and activate a host of signaling and adaptor molecules including Grb2, Nck, Crk, Shc, PLCγ, Src, Abl, and Shp1 (Jorissen et al., 2003). These receptor-docking molecules serve as entry points into intracellular signaling cascades that ultimately mediate the effects of EGFR signaling on cell functions including proliferation (Jorissen et al., 2003; Wells et al., 1990) and differentiation (Jost et al., 2000; Shvartsman et al., 2002; Troyer and Lee, 2001) as well as migration.

EGF-induced migratory responses involve many of the same signaling effectors described previously. In particular, EGFR signaling recruits and activates the ERK pathway (Brock and Jovin, 2001; Glading et al., 2000; Glading et al., 2001; Ho et al., 2001; Kawahara et al., 2002; Kempiak et al., 2003; Pederson et al., 2004; Sawano et al., 2002; Xie et al., 1998), FAK (Tapia et al., 1999), calpain (Glading et al., 2000; Glading et al., 2001), PI3K (Gillham et al., 1999; Hill et al., 2000; Lee and Juliano, 2002; Piccolo et al., 2002), Rac and Cdc42 (Chou et al., 2003; Kurokawa et al., 2004; Nogami et al., 2003), and PLCγ (Chen et al., 1994b; Nogami et al., 2003; Piccolo et al., 2002).

EGF is also known to have effects on multiple biophysical aspects of cell migration. Many of these effects have been connected to specific signaling pathways. At the cell front, EGFR activation upregulates actin polymerization leading to lamellipodial extension and membrane ruffling (Bailly et al., 1998a; Bailly et al., 1998b; Kurokawa et al., 2004; Nogami et

al., 2003; Ridley, 1995; Segall et al., 1996; Wells et al., 1999). These lamellipodial effects have been linked qualitatively to a wealth of signaling targets in a variety of cells, including PLCγ signaling in fibroblasts (Chen et al., 1994b), a PLCγ/Rac pathway in Chinese Hamster Ovary cells (Nogami et al., 2003), both Rac and Cdc42 activation in Cos1 and A431 cells (Kurokawa et al., 2004), and both PI3K and PLCγ pathways in breast cancer cells (Hill et al., 2000; Piccolo et al., 2002). EGFR signaling also induces both acute and long-term cell de-adhesion and the disassembly of substrate-binding focal adhesions through ERK signaling leading to M-calpain activation (Glading et al., 2000; Glading et al., 2001; Maheshwari et al., 1999; Xie et al., 1998); this M-calpain activity appears to play a role in potentiating the effective release of fibroblast uropodia (Cuevas et al., 2003; Glading et al., 2002). Finally, EGF stimulates the generation of motile force and contractility (Allen et al., 2002; Iwabu et al., 2004). Overall, these qualitative studies demonstrate that EGF-induced motility results from the coordination of multiple biochemical and biophysical mechanisms, making it a rich, largely untapped subject for quantitative study of the relationships between biochemical signal activation and biophysical processes.

At the phenomenological level of scale, single-cell tracking studies of EGF-induced motility have shown that fibroblast speed in the presence of EGF varies biphasically with cell-substratum adhesion to Amgel (a biologically-active extracellular matrix derived from human placental amniotic membranes) and fibronectin (Maheshwari et al., 1999; Ware et al., 1998). Ware et al. further reported an inverse relationship between EGF-induced speed and persistence, where increases in speed correlated with decreases in persistence. However, this thesis presents the first studies examining how activation of the specific signaling pathways detailed above affect speed and directional persistence as separable parameters in EGF-induced motility.

2.5 Figures

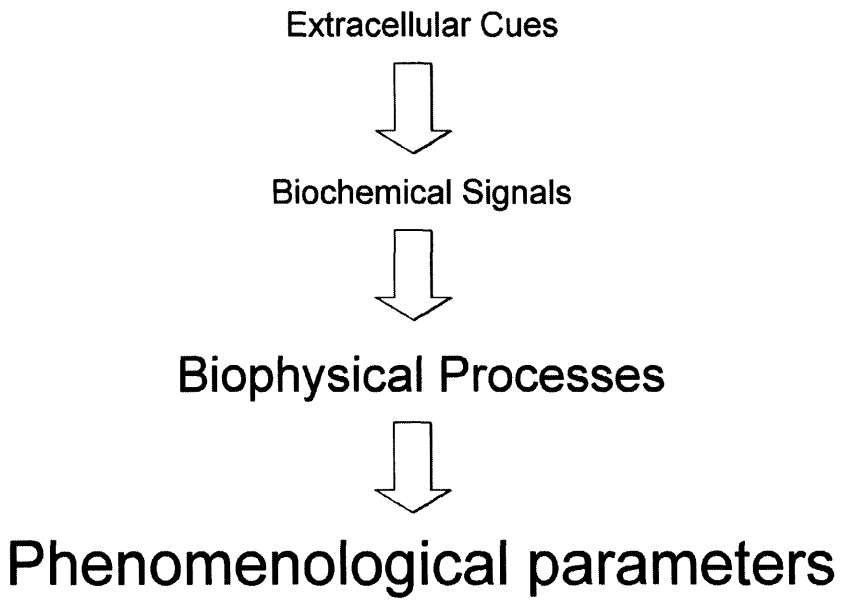

Figure 2.5.1 Hierarchical levels of scale in the study of cell motility.
Insights into cell migration can be gained from studying motility at any of three levels of scale. At the molecular level, extracellular cues are transduced by cell surface receptors and activate intracellular biochemical signaling pathways. The coordinated activation of these signaling pathways governs a set of biophysical processes that cells must integrate together to create motion. Over time, repeated cycles of these biophysical processes result in cell translocation, the largest scale of study of motility. At this level, the paths of motile cells obey a persistent random walk. Ideally, parameters governing larger levels of scale can be related quantitatively to parameters governing smaller levels of scale, leading to an integrated hierachical description of cell motility.

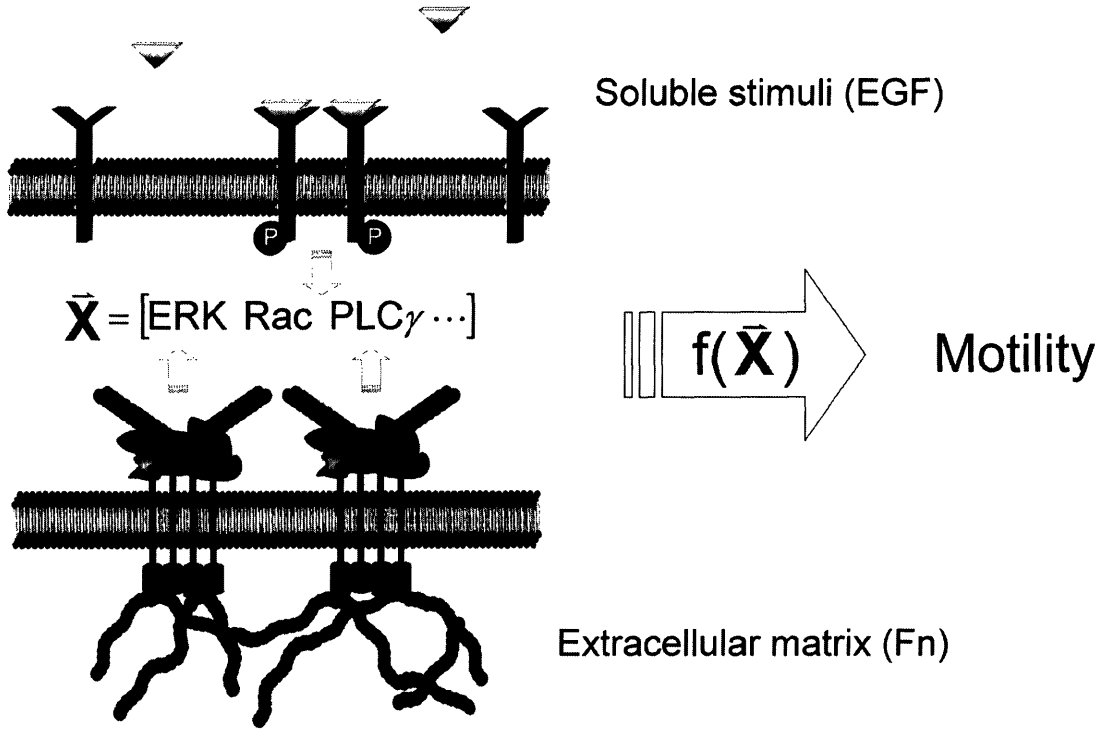

Figure 2.5.2 Extracellular cues activate signaling pathways governing cell motility.
Two categories of extracellular molecules affect cell migration, extracellular matrix molecules (typified by fibronectin) and soluble factors (typified by epidermal growth factor). Transmembrane receptors transmit information about these extracellular motility cues to the cell interior by activating multiple intracellular signal transduction pathways. This multidimensional intracellular signaling "vector" serves as the input to a complex motility output "function." Currently, the quantitative forms of this "function" relating intracellular signaling to other more macroscopic descriptions of motility remain largely unexplored.

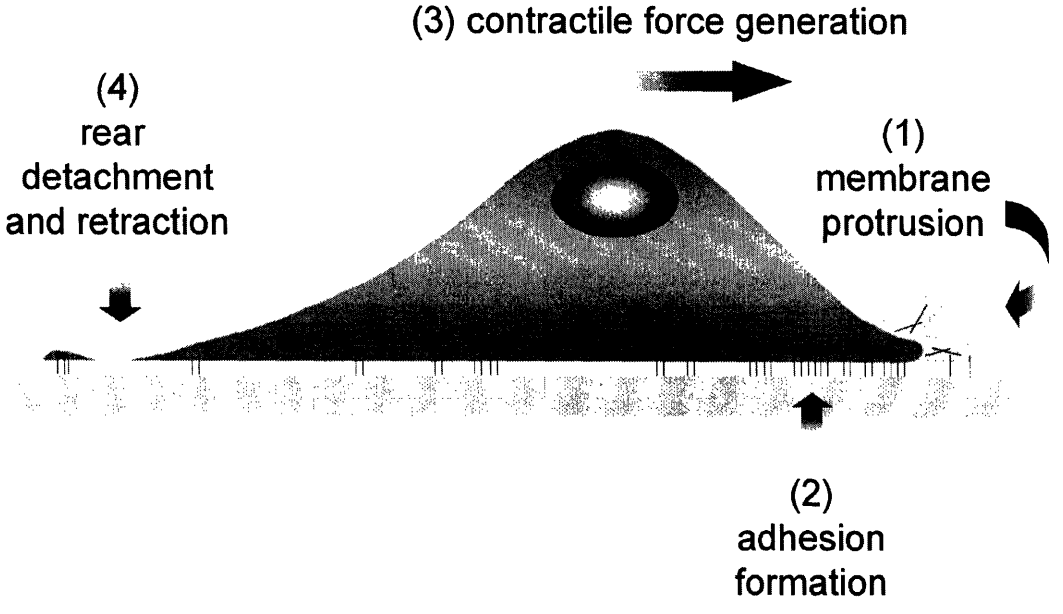

Figure 2.5.3 The biophysical migration cycle.
Cell migration can be viewed as a cyclical process with distinct biophysical components. Initially, the cell polarizes and protrudes at its lamellipodium. Protrusions are stabilized by the formation of adhesions to the substrate over which the cell is moving. Subsequent to attachment, a cell generates motive force able to move the main cell body forward. The end of the cycle occurs when cell-substrate attachments at the rear of the cell detach, allowing uropodial retraction and the biophysical cycle to begin again.

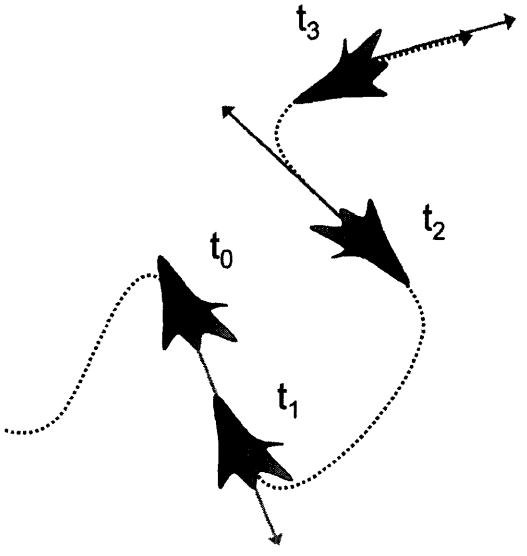

$$\left\langle (\Delta x)^2 \right\rangle = 2S^2P\left[(\Delta t) - P\left(1 - e^{-\Delta t/P}\right)\right]$$

Figure 2.5.4 The persistent random walk.
Over short periods of time, migrating cells maintain a roughly constant direction of motion (time period $t_0 \rightarrow t_1$). Over longer periods of time (time periods $t_0 \rightarrow t_2$ and $t_0 \rightarrow t_3$), this directional correlation is gradually lost. This path behavior of motile cells is called a persistent random walk and is characterized by speed (S) and persistence time (P).

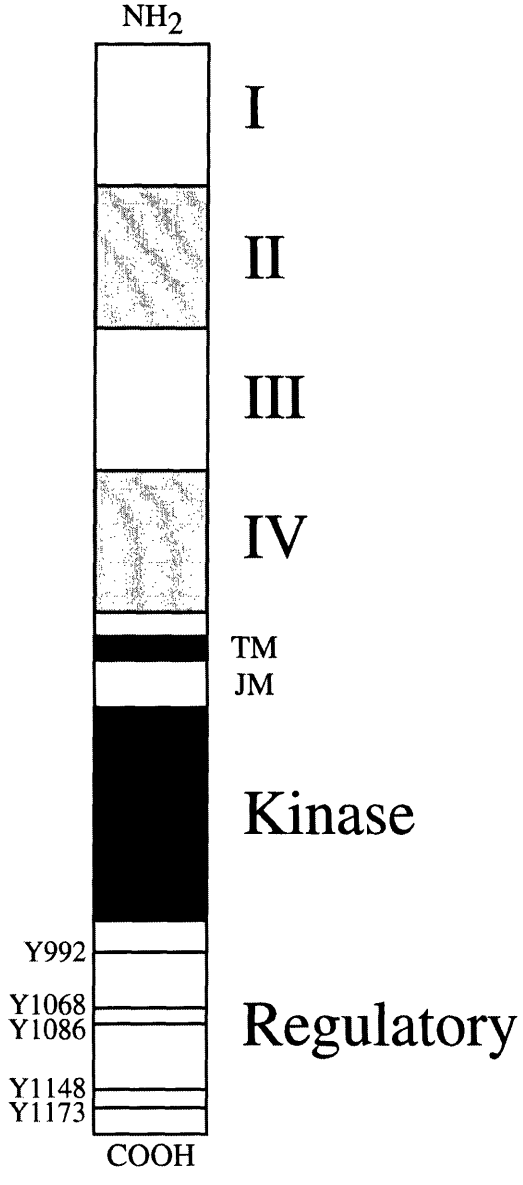

Figure 2.5.5 Schematic structure of EGF receptor.
The EGF receptor is an 1186-residue transmembrane receptor tyrosine kinase. Its extracellular ligand binding domain contains four subdomains, subdomains II and IV being cysteine-rich. Major intracellular segments include a short juxtamembrane region (JM), a kinase domain activated by ligand-induced receptor dimerization, and a regulatory domain containing five tyrosine autophosphorylation sites. TM = transmembrane region.

2.6 References

Allen, F.D., C.F. Asnes, P. Chang, E.L. Elson, D.A. Lauffenburger, and A. Wells. 2002. Epidermal growth factor induces acute matrix contraction and subsequent calpain-modulated relaxation. *Wound Repair Regen.* 10:67-76.

Allen, W.E., D. Zicha, A.J. Ridley, and G.E. Jones. 1998. A role for Cdc42 in macrophage chemotaxis. *J. Cell Biol.* 141:1147-1157.

Arteaga, C.L. 2003. ErbB-targeted therapeutic approaches in human cancer. *Exp. Cell Res.* 284:122-130.

Bailly, M., J.S. Condeelis, and J.E. Segall. 1998a. Chemoattractant-induced lamellipod extension. *Microsc. Res. Techniq.* 43:433-443.

Bailly, M., L. Yan, G.M. Whitesides, J.S. Condeelis, and J.E. Segall. 1998b. Regulation of protrusion shape and adhesion to the substratum during chemotactic responses of mammalian carcinoma cells. *Exp. Cell Res.* 241:285-299.

Blay, J., and K.D. Brown. 1985. Epidermal growth factor promotes the chemotactic migration of cultured rat intestinal epithelial cells. *J. Cell. Physiol.* 124:107-112.

Brock, R., and T.M. Jovin. 2001. Heterogeneity of signal transduction at the subcellular level: microsphere-based focal EGF receptor activation and stimulation of Shc translocation. *J. Cell. Sci.* 114:2437-2447.

Carragher, N.O., M.A. Westhoff, V.J. Fincham, M.D. Schaller, and M.C. Frame. 2003. A novel role for FAK as a protease-targeting adaptor protein: regulation by p42 ERK and Src. *Curr. Biol.* 13:1442-1450.

Cary, L.A., J.F. Chang, and J.-L. Guan. 1996. Stimulation of cell migration by overexpression of focal adhesion kinase and its association with Src and Fyn. *J. Cell Biol.* 109:1787-1794.

Cha, D.P., E.A. O'Brien, E.A. O'Toole, D.T. Woodley, and L.G. Hudson. 1996. Enhanced modulation of keratinocyte motility by transforming growth factor-alpha (TGF-alpha) relative to epidermal growth factor (EGF). *J. Invest. Dermatol.* 106:590-597.

Chen, P., K. Gupta, and A. Wells. 1994a. Cell movement elicited by epidermal growth factor receptor requires kinase and autophosphorylation but is separable from mitogenesis. *J. Cell Biol.* 124:547-555.

Chen, P., J. Murphy-Ullrich, and A. Wells. 1996. A role for gelsolin in actuating epidermal growth factor receptor-mediated cell motility. *J. Cell Biol.*134:689-698.

Chen, P., H. Xie, M.C. Sekar, K.B. Gupta, and A. Wells. 1994b. Epidermal growth factor-mediated cell motility: phospholipase C activity is required, but mitogen-activated protein kinase activity is not sufficient for induced cell movement. *J. Cell Biol.* 127:847-857.

Cheresh, D.A., J. Leng, and R.L. Klemke. 1999. Regulation of cell contraction and membrane ruffling by distinct signals in migratory cells. *J. Cell Biol.* 146:1107-1116.

Chou, J., N.A. Burke, A. Iwabu, S.C. Watkins, and A. Wells. 2003. Directional motility induced by epidermal growth factor requires Cdc42. *Exp. Cell Res.* 287:47-56.

Clark, E.A., W.G. King, J.S. Brugge, M. Symons, and R.O. Hynes. 1998. Integrin-mediated signals regulated by members of the rho family of GTPases. *J. Cell Biol.* 142:573-586.

Cohen, S. 1962. Isolation of a mouse submaxillary gland protein accelerating incisor eruption and eyelid opening in the new-born animal. *J. Biol. Chem.* 237:1555-1562.

Comer, F.I., and C.A. Parent. 2002. PI 3-kinases and PTEN: how opposites chemoattract. *Cell.* 109:541-544.

Cuevas, B.D., A.N. Abell, J.A. Witowsky, T. Yujiri, K. Kesavan, M. Ware, P.L. Jones, S.A. Weed, R.L. DeBiasi, Y. Oka, K.L. Tyler, and G.L. Johnson. 2003. MEKK1 regulates calpain-independent proteolysis of focal adhesion proteins for rear-end detachment of migrating fibroblasts. *EMBO. J.* 22:3346-3355.

Devreotes, P., and C. Janetopoulos. 2003. Eukaryotic chemotaxis: distinctions between directional sensing and polarization. *J. Biol. Chem.* 278:20445-20448.

Dickinson, R.B., and R.T. Tranquillo. 1993. A stochastic model for adhesion-mediated cell random motility and haptotaxis. *J. Math. Biol.* 31:563-600.

DiMilla, P.A., K. Barbee, and D.A. Lauffenburger. 1991. Mathematical model for the effects of adhesion and mechanics on cell migration speed. *Biophys. J.* 60:15-37.

DiMilla, P.A., J.A. Stone, J.A. Quinn, S.M. Albelda, and D.A. Lauffenburger. 1993. Maximal migration of human smooth muscle cells on fibronectin and Type IV collagen occurs at an intermediate attachment strength. *J. Cell Biol.* 122:729-737.

Downward, J., P. Parker, and M.D. Waterfield. 1984. Autophosphorylation sites on the epidermal growth factor receptor. *Nature.* 311:483-485.

Dunn, G.A. 1983. Characterizing a kinesis response; time averaged measures of cell speed and directional persistance. *Agents Actions [Suppl.].* 12:14-33.

Fincham, V.J., M. James, M.C. Frame, and S.J. Winder. 2000. Active ERK/MAP kinase is targeted to newly forming cell-matrix adhesions by integrin engagement and v-Src. *EMBO J.* 19:2911-2923.

Fontanini, G., S. Vignati, D. Bigini, A. Mussi, H. Lucchi, C.A. Angeletti, R. Pingitore, S. Pepe, F. Basolo, and G. Bevilacqua. 1995. Epidermal growth factor receptor (EGFr) expression in non-small cell lung carcinomas correlates with metastatic involvement of hilar and mediastinal lymph nodes in the squamous subtype. *Eur. J. Cancer.* 31A:178-183.

Funamoto, S., R. Meili, S. Lee, L. Parry, and R.A. Firtel. 2002. Spatial and temporal regulation of 3-phosphoinositides by PI 3-kinase and PTEN mediates chemotaxis. *Cell.* 109:611-623.

Giancotti, F.G., and E. Ruoslahti. 1999. Integrin Signaling. *Science.* 285:1028-1033.

Gillham, H., M.C.H.M. Golding, R. Pepperkok, and W.J. Gullick. 1999. Intracellular movement of green fluorescent protein-tagged phosphatidylinositol 3-kinase in response to growth factor receptor signaling. *J. Cell Biol.* 146:869-880.

Gilmore, A., and L. Romer. 1996. Inhibition of focal adhesion kinase (FAK) signaling in focal adhesions decreases cell motility and proliferation. *Molec. Biol. Cell.* 7:1209-1224.

Glading, A., P. Chang, D.A. Lauffenburger, and A. Wells. 2000. Epidermal growth factor receptor activation of calpain is required for fibroblast motility and occurs via an ERK/MAP kinase signaling pathway. *J. Biol. Chem.* 275:2390-2398.

Glading, A., D.A. Lauffenburger, and A. Wells. 2002. Cutting to the chase: calpain proteases in cell motility. *Trends Cell Biol.* 12:46-54.

Glading, A., F. Überall, S.M. Keyse, D.A. Lauffenburger, and A. Wells. 2001. Membrane proximal ERK signaling is required for M-calpain activation downstream of epidermal growth factor receptor signaling. *J. Biol. Chem.* 276:23341-23348.

Goodman, S.L., G. Risse, and K.v.d. Mark. 1989. The E8 subfragment of laminin promotes locomotion of myoblasts over extracellular matrix. *J. Cell Biol.* 109:799-809.

Gu, J., M. Tamura, R. Pankov, E.H.J. Danen, T. Takino, K. Matsumoto, and K.M. Yamada. 1999. Shc and FAK differentially regulate cell motility and directionality modulated by PTEN. *J. Cell Biol.* 146:389-403.

Harris, R.C., E. Chung, and R.J. Coffey. 2003. EGF receptor ligands. *Exp. Cell Res.* 284:2-13.

Hart, J. 2002. Inflammation. 1: Its role in the healing of acute wounds. *J. Wound Care.* 11:205-209.

Hauck, C.R., D.A. Hsia, and D.D. Schlaepfer. 2000. Focal adhesion kinase facilitates platelet-derived growth factor-BB-stimulated ERK2 activation required for chemotaxis migration of vascular smooth muscle cells. *J. Biol. Chem.* 275:41092-41099.

Haugh, J.M., F. Codazzi, M. Teruel, and T. Meyer. 2000. Spatial sensing in fibroblasts mediated by 3' phosphoinositides. *J. Cell Biol.* 151:1269-1279.

Hill, K., S. Welti, J. Yu, J.T. Murray, S.-C. Yip, J.S. Condeelis, J.E. Segall, and J.M. Backer. 2000. Specific requirement for the p85-p110α phosphatidylinositol 3-kinase during epidermal growth factor-stimulated actin nucleation in breast cancer cells. *J. Biol. Chem.* 275:3741-3744.

Ho, W.-c., S. Uniyal, S.O. Meakin, V.L. Morris, and B.M.C. Chan. 2001. A differential role of extracellular signal-related kinase in stimulated PC12 pheochromocytoma cell movement. *Exp. Cell Res.* 263:254-264.

Hynes, R. 2002. Integrins. Bidirectional, allosteric signaling machines. *Cell.* 110:673-687.

Iijima, M., and P. Devreotes. 2002. Tumor suppressor PTEN mediates sensing of chemoattractant gradients. *Cell.* 109:599-610.

Ilic, D., Y. Furuta, S. Kanazawa, N. Takeda, K. Sobue, N. Nakatsuji, S. Nomura, J. Fujimoto, M. Okada, T. Yamamoto, and S. Aizawa. 1995. Reduced cell motility and enhanced focal adhesion contact formation in cells from FAK-deficient mice. *Nature.* 377:539-544.

Insall, R.H., and O.D. Weiner. 2001. PIP3, PIP2, and cell movement - similar messages, different meanings? *Dev. Cell.* 1:743-747.

Iwabu, A., K. Smith, F.D. Allen, D.A. Lauffenburger, and A. Wells. 2004. Epidermal growth factor induces fibroblast contractility and motility via a protein kinase C delta-dependent pathway. *J. Biol. Chem.* 279:14551-14560.

Jorissen, R.N., F.W. Walker, N. Pouliot, T.P.J. Garrett, C.W. Ward, and A.W. Burgess. 2003. Epidermal growth factor receptor: mechanisms of activation and signaling. *Exp. Cell Res.* 284:31-53.

Jost, M., C. Kari, and U. Rodeck. 2000. The EGF receptor - an essential regulator of multiple epidermal functions. *Eur. J. Dermatol.* 10:505-510.

Kassis, J., D.A. Lauffenburger, T. Turner, and A. Wells. 2001. Tumor invasion as dysregulated cell motility. *Semin. Cancer Biol.* 11:105-117.

Kawahara, E., N. Nakada, T. Hikichi, J. Kobayashi, and I. Nakanishi. 2002. EGF and β1 integrin convergently regulate migration of A431 carcinoma cells through MAP kinase activation. *Exp. Cell Res.* 272:84-91.

Keely, P.J., A.M. Fong, M.M. Zutter, and S.A. Santoro. 1995. Alteration of collagen-dependent adhesion, motility, and morphogenesis by the expression of antisense alpha 2 integrin mRNA in mammary cells. *J. Cell Sci.* 108:595-607.

Keller, R. 2002. Shaping the vertebrate body plan by polarized embryonic cell movements. *Science.* 298:1950-1954.

Kempiak, S.J., S.-C. Yip, J.M. Backer, and J.E. Segall. 2003. Local signaling by the EGF receptor. *J. Cell. Biol.* 162:781-787.

Klemke, R.S., S. Kai, A. Giannini, P. Gallagher, P.d. Lanerolle, and D. Cheresh. 1997. Regulation of cell motility by mitogen-activated protein kinase. *J. Cell Biol.* 137:481-492.

Kraemer, R. 2000. Regulation of cell migration in atherosclerosis. *Curr. Atheroscler. Rep.* 2:445-452.

Krueger, J.S., V.G. Keshamouni, N. Atanaskova, and K.B. Reddy. 2001. Temporal and quantitative regulation of mitogen-activated protein kinase (MAPK) regulates cell motility and invasion. *Oncogene.* 20:4209-4218.

Kurokawa, K., R.E. Itoh, H. Yoshizaki, Y. Ohba, T. Nakamura, and M. Matsuda. 2004. Coactivation of Rac1 and Cdc42 at lamellipodia and membrane ruffles induced by epidermal growth factor. *Mol. Biol. Cell.* 15:1003-1010.

Lauffenburger, D.A. 1989. A simple model for the effects of receptor-mediated cell-substratum adhesion on cell migration. *Chem. Eng. Sci.* 44:1903-1914.

Lauffenburger, D.A., and A.F. Horwitz. 1996. Cell migration: a physically integrated molecular process. *Cell.* 84:359-369.

Lawrence, W.T. 1998. Physiology of the acute wound. *Clin. Plast. Surg.* 25:321-340.

Lee, J.W., and R.L. Juliano. 2002. The alpha5beta1 integrin selectively enhances epidermal growth factor signaling to the phosphatidylinositol-3-kinase/Akt pathway in intestinal epithelial cells. *Biochim Biophys Acta.* 1542:23-31.

Li, Z., M. Hannigan, Z. Mo, B. Liu, W. Lu, Y. Wu, A.V. Smrcka, G. Wu, L. Li, and M. Liu. 2003. Directional Sensing Requires G[beta][gamma]-Mediated PAK1 and PIX[alpha]-Dependent Activation of Cdc42. *Cell.* 114:215-227.

Lokuta, M.A., P.A. Nuzzi, and A. Huttenlocher. 2003. Calpain regulates neutrophil chemotaxis. *Proc. Natl. Acad.. Sci. USA.* 100:4006-4011.

Maheshwari, G., and D.A. Lauffenburger. 1998. Deconstructing (and reconstructing) cell migration. *Microsc. Res. Techniq.* 43:358-368.

Maheshwari, G., A. Wells, L.G. Griffith, and D.A. Lauffenburger. 1999. Biophysical integration of effects of epidermal growth factor and fibronectin on fibroblast migration. *Biophys. J.* 76:2814-2823.

Martin, P. 1997. Wound healing: aiming for perfect regeneration. *Science.* 275:75-81.

Massague, J., and A. Pandiella. 1993. Membrane-anchored growth factors. *Ann. Rev. Biochem.* 62:515-541.

McCrawley, I.J., P. O'Brian, and L.G. Hudson. 1997. Overexpression of the epidermal growth factor receptor contributes to enhanced ligand-mediated motility in keratinocyte cell lines. *Endocrinology.* 138:121-127.

Miranti, C., and J. Brugge. 2002. Sensing the environment: a historical perspective on integrin signal transduction. *Nat. Cell Biol.* 4:E83-90.

Mitchison, T.J., and L.P. Cramer. 1996. Actin-based cell motility and cell locomotion. *Cell.* 84:371-379.

Mullins, R.D. 2000. How WASP-family proteins and the Arp2/3 complex convert intracellular signals into cytoskeletal structures. *Curr. Opin. Cell Biol.* 12:91-96.

Nobes, C.D., and A. Hall. 1999. Rho GTPases control polarity, protrusion, and adhesion during cell movement. *J. Cell Biol.* 144:1235-1244.

Nogami, M., M. Yamazaki, H. Watanabe, Y. Okabayashi, Y. Kido, M. Kasuga, T. Sasaki, T. Maehama, and Y. Kanaho. 2003. Requirement of autophosphorylated tyrosine 992 of EGF receptor and its docking protein phospholipase Cγ1 for membrane ruffle formation. *FEBS Lett.* 536:71-76.

Othmer, H.G., S.R. Dunbar, and W. Alt. 1988. Models of dispersal in biological systems. *J. Math. Biol.* 26:263-298.

Palecek, S.E., J.C. Loftus, M.H. Ginsburg, D.A. Lauffenburger, and A.F. Horwitz. 1997. Integrin-ligand binding properties govern cell migration speed through cell-substratum adhesiveness. *Nature.* 385:537-540.

Palecek, S.P., A. Huttenlocher, A.F. Horwitz, and D.A. Lauffenburger. 1998. Physical and biochemical regulation of integrin release during rear detachment of migrating cells. *J. Cell Sci.* 111:929-940.

Parent, C.A., B.J. Blacklock, W.M. Froehlich, D.B. Murphy, and P.N. Devreotes. 1998. G protein signaling events are activated at the leading edge of chemotactic cells. *Cell.* 95:81-91.

Parsons, J.T. 2003. Focal adhesion kinase: the first ten years. *J. Cell Sci.* 116:1409-1416.

Patan, S. 2004. Vasculogenesis and angiogenesis. *Cancer Treat. Res.* 117:3-32.

Pederson, M.W., V. Tkach, N. Pedersen, V. Berezin, and H.S. Poulsen. 2004. Expression of a naturally occurring constitutively active variant of the epidermal growth factor receptor in mouse fibroblasts increases motility. *Int. J. Cancer.* 108:643-653.

Piccolo, E., P.F. Innominato, M.A. Mariggio, T. Maffucci, S. Iacobelli, and M. Falasca. 2002. The mechanism involved in the regulation of phospholipase Cgamma1 activity in cell migration. *Oncogene.* 21:6520-9.

Pollard, T.D., and G.G. Borisy. 2003. Cellular motility driven by assembly and disassembly of actin filaments. *Cell.* 112:453-465.

Price, L.S., J. Leng, M.A. Schwartz, and G.M. Bokoch. 1998. Activation of rac and cdc42 by integrins mediates cell spreading. *Mol. Biol. Cell.* 9:1863-1871.

Qian, Y., L. Corum, Q. Meng, J. Blenis, J.Z. Zheng, X. Shi, D.C. Flynn, and B.-H. Jiang. 2004. PI3K induced actin filament remodeling through Akt and p70S6K1: implication of essential role in cell migration. *Am. J. Physiol. Cell. Physiol.* 286:C153-C163.

Renshaw, M.W., L.S. Price, and M.A. Schwartz. 1999. Focal adhesion kinase mediates the integrin signaling requirement for growth factor activation of MAP kinase. *J. Cell Biol.* 147:611-618.

Ridley, A.J. 1995. Growth factor-induced actin reorganization in Swiss 3T3 cells. *Methods Enzymol.* 256:306-313.

Ridley, A.J. 2001. Rho GTPases and cell migration. *J. Cell Sci.* 114:2713-2722.

Ridley, A.J., and A. Hall. 1992. The small GTP-binding protein Rho regulates the assembly of focal adhesions and actin stress fibers in response to growth factors. *Cell.* 70:389-399.

Ridley, A.J., H.F. Paterson, C.L. Johnston, D. Diekmann, and A. Hall. 1992. The small GTP-binding protein rac regulates growth factor-induced membrane ruffling. *Cell.* 70:401-410.

Ridley, A.J., M.A. Schwartz, K. Burridge, R.A. Firtel, M.H. Ginsberg, G. Borisy, J.T. Parsons, and A.R. Horwitz. 2003. Cell migration: integrating signals from front to back. *Science.* 302:1704-1709.

Sakai, T., J.M.d.l. Pena, and D.F. Mosher. 1999. Synergism among lysophosphatidic acid, β1A integrins, and epidermal growth factor or platelet-derived growth factor in mediation of cell migration. *J. Biol. Chem.* 274:15480-15486.

Sawano, A., S. Takayama, M. Matsuda, and A. Miyakawa. 2002. Lateral propagation of EGF signaling after local stimulation is dependent on receptor density. *Dev. Cell.* 3:245-257.

Schlessinger, J. 2000. Cell signaling by receptor tyrosine kinases. *Cell.* 103:211-225.

Schwartz, S.M. 1997. Smooth muscle migration in atherosclerosis and restenosis. *J. Clin. Invest.* 100:S87-S89.

Segall, J.E., S. Tyerech, L. Boselli, S. Masseling, J. Helft, A. Chan, J. Jones, and J. Condeelis. 1996. EGF stimulates lamellipod extension in metastatic mammary adenocarcinoma cells by an actin-dependent mechanism. *J. Cell Sci.* 14:61-72.

Servant, G., O.D. Weiner, P. Herzmark, T. Balla, J.W. Sedat, and H.R. Bourne. 2000. Polarization of chemoattractant receptor signaling during neutrophil chemotaxis. *Science.* 287:1037-1040.

Sethi, K.K., I.V. Yannas, V. Mudera, M. Eastwood, C. McFarland, and R.A. Brown. 2002. Evidence for sequential utilization of fibronectin, vitronectin, and collagen during fibroblast-mediated collagen contraction. *Wound Rep. Reg.* 10:397-408.

Shono, T., H. Kanetake, and S. Kanda. 2001. The role of mitogen-activated protein kinase activation within focal adhesions in chemotaxis toward FGF-2 by murine brain capillary endothelial cells. *Exp. Cell Res.* 264:275-283.

Shvartsman, S.Y., C.B. Muratov, and D.A. Lauffenburger. 2002. Modeling and computational analysis of EGF receptor-mediated cell communication in Drosophila oogenesis. *Development.* 129:2577-2589.

Sieg, D.J., C.R. Hauck, D. Ilic, C.K. Klingbeil, E. Schaefer, C.H. Damsky, and D.D. Schlaepfer. 2000. FAK integrates growth-factor and integrin signals to promote cell migration. *Nat. Cell Biol.* 2:249-256.

Sieg, D.J., C.R. Hauck, and D.D. Schlaepfer. 1999. Required role of focal adhesion kinase (FAK) for integrin-stimulated migration. *J. Cell Sci.* 112:2677-2691.

Srinivasan, S., F. Wang, S. Glavas, A. Ott, F. Hofmann, K. Aktories, D. Kalman, and H.R. Bourne. 2003. Rac and Cdc42 play distinct roles in regulating PI(3,4,5)P3 and polarity during neutrophil chemotaxis. *J. Cell Biol.* 160:375-385.

Stähle, M., C. Veit, U. Bachfischer, K. Schierling, B. Skripczynski, A. Hall, P. Gierschik, and K. Giehl. 2003. Mechanisms in LPA-induced tumor cell migration: critical role of phosphorylated ERK. *J. Cell. Sci.* 116:3835-3846.

Sulis, M.L., and R. Parsons. 2003. PTEN: from pathology to biology. *Trends Cell Biol.* 13:478-483.

Szekanecz, Z., and A.E. Koch. 2000. Endothelial cells and immune cell migration. *Arthritis Res.* 2:368-373.

Tapia, J.A., C. Camello, R.T. Jensen, and L.J. Garcia. 1999. EGF stimulates tyrosine phosphorylation of focal adhesion kinase (p125FAK) and paxillin in rat pancreatic acini by a phospholipase C-independent process that depends on phosphatidylinositol 3-kinase, the small GTP-binding protein, p21rho, and the integrity of the actin cytoskeleton. *Biochim. Biophys. Acta.* 1448:486-499.

Totsukawa, G., Y. Wu, Y. Sasaki, D.J. Hartshorne, Y. Yamakita, S. Yamashiro, and F. Matsumura. 2004. Distinct roles of MLCK and ROCK in the regulation of membrane protrusions and focal adhesion dynamics during cell migration of fibroblasts. *J. Cell Biol.* 164:427-439.

Totsukawa, G., Y. Yamakita, S. Yamashiro, D.J. Hartshorne, Y. Sasaki, and F. Matsumura. 2000. Distinct roles of ROCK (Rho-kinase) and MLCK in spatial regulation of MLC phosphorylation for assembly of stress fibers and focal adhesions in 3T3 fibroblasts. *J. Cell Biol.* 150:797-806.

Tranquillo, R.T., and D.A. Lauffenburger. 1987. Stochastic model of leukocyte chemosensory movement. *J. Math. Biol.* 25:229-262.

Troyer, K.L., and D.C. Lee. 2001. Regulation of mouse mammary gland development and tumorigenesis by the ERBB signaling network. *J. Mammary Gland Biol.* 6:7021.

Turner, T., P. Chen, L.J. Goodly, and A. Wells. 1996. EGF receptor signaling enhances in vivo invasiveness of DU-145 human prostate carcinoma cells. *Clin. Exp. Metastas.* 14:409-418.

Verbeek, B.S., S.S. Adriaansen-Slot, T.M. Vroom, T. Beckers, and G. Rijksen. 1998. Overexpression of EGFR and c-erbB2 causes enhanced cell migration in human breast cancer cells and NIH3T3 fibroblasts. *FEBS Lett.* 425:145-150.

Vial, E., E. Sahal, and C.J. Marshall. 2003. ERK-MAPK signaling coordinately regulates activity of Rac1 and RhoA for tumor cell motility. *Cancer Cell.* 4:67-79.

Wang, F., P. Herzmark, O.D. Weiner, S. Srinivasan, G. Servant, and H.R. Bourne. 2002. Lipid products of PI(3)Ks maintain persistent cell polarity and directed motility in neutrophils. *Nat. Cell Biol.* 4.

Ware, M.F., A. Wells, and D.A. Lauffenburger. 1998. Epidermal growth factor alters fibroblast migration speed and directional persistence reciprocally and in a matrix-dependent manner. *J. Cell Sci.* 111:2423-2432.

Webb, D.J., K. Donais, L.A. Whitmore, S.M. Thomas, C.E. Turner, J.T. Parsons, and A.F. Horwitz. 2004. FAK-Src signaling through paxillin, ERK, and MLCK regulates adhesion disassembly. *Nat. Cell Biol.* 6:154-161.

Weiner, O.D., P.O. Neilsen, G.D. Prestwich, M.W. Kirschner, L.C. Cantley, and H.R. Bourne. 2002. A PtdInsP3- and Rho GTPase-mediated positive feedback loop regulates neutrophil polarity. *Nat. Cell Biol.* 4:509-512.

Wells, A., M.F. Ware, F.D. Allen, and D.A. Lauffenburger. 1999. Shaping up for shipping out: PLCγ signaling of morphology changes in EGF-stimulated fibroblast migration. *Cell Motil. Cytoskel.* 44:227-233.

Wells, A., J.B. Welsh, C.S. Lazar, H.S. Wiley, G.N. Gill, and M.G. Rosenfeld. 1990. Ligand-induced transformation by a non-internalizing epidermal growth factor receptor. *Science.* 247:962-964.

Westermark, K., M. Nilsson, T. Ebendal, and B. Westermark. 1991. Thryocyte migration and histiotypic follicle regeneration are promoted by epidermal growth factor in primary culture of thyroid follicles in collagen gel. *Endocrinology.* 129:2180-2186.

Woodard, A.S., G. Garcia-Cardena, M. Leong, J.A. Madri, W.C. Sessa, and L.R. Languino. 1998. The synergistic activity of $\alpha_v\beta_3$ integrin and PDGF receptor increases cell migration. *J. Cell Sci.* 111:469-478.

Xie, H., M.A. Pallero, D. Gupta, P. Chang, M.F. Ware, W. Witke, D.J. Kwiatkowski, D.A. Lauffenburger, J.E. Murphy-Ullrich, and A. Wells. 1998. EGF receptor regulation of cell motility: EGF induces dissassembly of focal adhesions independently of the motility-associated PLCγ signaling pathway. *J. Cell Sci.* 111:615-624.

CHAPTER 3

DIRECTIONAL PERSISTENCE OF EGF-INDUCED CELL MIGRATION IS ASSOCIATED WITH STABILIZATION OF LAMELLIPODIAL PROTRUSIONS

Migrating cells can sustain a relatively constant direction of lamellipodial protrusion and locomotion over timescales ranging from minutes to hours. However, individual waves of lamellipodial extension occur over much shorter characteristic times. Little understanding exists regarding how cells might integrate biophysical processes across these disparate timescales to control the directional persistence of locomotion. We address this issue by examining the effects of epidermal growth factor (EGF) stimulation on long-timescale directional persistence and short-timescale lamellipodial dynamics of EGF receptor-transfected Chinese Hamster Ovary cells migrating on fibronectin-coated substrata. Addition of EGF increased persistence, with the magnitude of increase correlating with fibronectin coating concentration. Kymographic analysis of EGF-stimulated lamellipodial dynamics revealed that the temporal stability of lamellipodial protrusions similarly increased with fibronectin concentration. A soluble RGD peptide competitor reduced both the persistence of long-timescale cell paths and the stability of short-timescale membrane protrusions, indicating that cell-substratum adhesion concomitantly influences lamellipodial dynamics and directional persistence. These results reveal the importance of adhesion strength in regulating the directional motility of cells and suggest that the short-timescale kinetics of adhesion complex formation may play a key role in modulating directional persistence over much longer timescales.

3.1 Introduction

Cell migration plays an essential role in normal and pathological processes such as embryonic morphogenesis (Keller, 2002), inflammation and the immune response (Hart, 2002), wound healing (Martin, 1997), metastatic cancer (Kassis et al., 2001), rheumatoid arthritis (Szekanecz and Koch, 2000), and atherosclerosis (Kraemer, 2000). Critical to both normal and dysregulated motility is the adhesive interaction between cells and substratum. Formation of adhesions at the leading edge of migrating cells stabilizes lamellipodial protrusions, while movement of the cell body requires both generation of traction force against the substratum and the regulated release of adhesions at the cell rear (Lauffenburger and Horwitz, 1996; Mitchison and Cramer, 1996).

Migrating cells follow a persistent random walk model parameterized by both cell speed (S) and directional persistence time (P). Persistence characterizes the average time between significant changes in the direction of a cell's translocation (Dunn, 1983; Gail and Boone, 1970; Othmer et al., 1988). The existence of a biphasic relationship between cell adhesion strength and speed is well-established, with maximal speed occurring at intermediate levels of adhesion (DiMilla et al., 1993; Goodman et al., 1989; Maheshwari et al., 1999; Palecek et al., 1997). In contrast, previous studies of the correlation between cell adhesion and persistence are contradictory, with both biphasic and inverted biphasic relationships having been reported (DiMilla et al., 1993; Ware et al., 1998). As such, the adhesive regulation of directional persistence is poorly understood and requires further study.

Because a cell must extend an adherent new leading lamellipod to change its direction of locomotion, the relationship between cell-substratum adhesion and lamellipodial protrusion dynamics is expected to play an important role in the adhesion-based modulation of directional persistence. Lamellipodial protrusion in migrating cells occurs via repeating waves of actin polymerization and membrane ruffling (Bailly et al., 1998b; Bear et al., 2002; Hinz et al., 1999). It has been reported that these waves of

membrane extension do not require adhesion to occur, but that cell-substratum adhesion conditions the shape and stability of the protrusions (Bailly et al., 1998b). Importantly, while the extension and retraction of an individual lamellipodial wave occurs on the order of seconds to minutes (Bear et al., 2002; Hinz et al., 1999), the random directional behavior of a cell manifests at much longer timescales. Thus, a crucial part of understanding adhesion-mediated directional persistence is deconstructing whether adhesion-mediated variations in short-timescale spatial and temporal lamellipodial dynamics can control changes in long-timescale persistence time.

This chapter describes how variations in fibronectin-mediated cell-substratum adhesion affect both the long-timescale directional persistence and short-timescale membrane dynamics of migrating cells stimulated by the epidermal growth factor (EGF). The overexpression and ligand-induced activation of EGF receptor (EGFR), a prototypic receptor tyrosine kinase, correlates with increased invasiveness of tumors in vivo and increased migration of cell lines in vitro (Fontanini et al., 1995; Jorissen et al., 2003; McCrawley et al., 1997; Schlessinger, 2000; Turner et al., 1996; Verbeek et al., 1998). EGF is also known to stimulate both actin polymerization and lamellipodial extension (Kurokawa et al., 2004; Nogami et al., 2003; Segall et al., 1996; Wells et al., 1999). Our model system consisted of Chinese Hamster Ovary (CHO) cells transfected with an EGFR-GFP fusion protein. Our choice of this system derived from the weakly adhesive nature of CHO cells. In weakly adherent cells, lamellipodial extension rate has been shown to limit EGF-mediated cell speed (Maheshwari et al., 1999). Also, unlike other weakly adherent cells like neutrophils and keratocytes that "glide" smoothly, CHO cells exhibit membrane extension steps that are relatively distinct from actual cell translocation. Together these traits made CHO cells an attractive model system for studying the relationships between cell-substratum adhesion, lamellipodial protrusion, and the directional persistence of cell locomotion.

We find that EGF stimulation increases CHO cell motility, with the magnitude of increase correlating monotonically with increasing fibronectin (Fn) surface concentration. This increased motility results entirely from a Fn-dependent upregulation of persistence time in the presence of EGF, and actually conceals a decrease in cell speed. Both the overall increase in persistence due to EGF stimulation and the Fn-dependence of the magnitude of increase correlate with the temporal stability of individual waves of lamellipodial protrusion and retraction. Addition of soluble GRGDSP peptide, a competitive inhibitor of cell adhesion, decreases both persistence time and lamellipodial stability, indicating that directional migration is enhanced by adhesion-mediated protrusive stabilization. Our findings suggest that the short-timescale kinetics of adhesion complex formation may play a key role in modulating directional persistence over much longer timescales.

3.2 Experimental methods

3.2.1 Reagents and materials

Dulbecco's Modified Eagle's Medium (DMEM), OptiMEM, fetal bovine serum (FBS), L-glutamine, sodium pyruvate, non-essential amino acids, penicillin, streptomycin, geneticin/G418 sulfate, HEPES, trypsin, Versene (EDTA) and phosphate-buffered saline (PBS) were purchased from Life Technologies (Carlsbad, CA). Bovine serum albumin (BSA), human fibronectin (Fn) and recombinant human epidermal growth factor (EGF) were purchased from Sigma Chemical (St. Louis, MO). Tissue culture flasks were purchased from Corning (Acton, MA). Unless noted, all other reagents were purchased from Sigma.

3.2.2 Construction of EGFR-pEGFP-N1 expression plasmid

The EGFR cDNA in pRC CMV2 vector (Invitrogen, Carlsbad, CA) was kindly provided by Dr. Steven Wiley (Pacific Northwest National Laboratories, Richland, WA). Using *Xba*I and *Hind*III sites the cDNA was excised and cloned into PCR 2.1 TOPO

(Invitrogen) which was used as an intermediate cloning vector. The 5' terminus of the cDNA was then PCR-amplified using the following sets of primers:

Sense: 5'-GAGACCCACACTACCAG-3'

Antisense 5'-TAAAGCTTAAGTGCTCCAATAAATTCACTG-3'

The antisense primer was designed to introduce a *Hind*III site (underlined) and disrupt the stop codon.

The PCR product was ligated into pCR 2.1 TOPO, subsequently digested with *Hinc*II/*Hind*III and cloned into the same sites on the full length EGFR cDNA in PCR2.1 TOPO. The full length EGFR cDNA (with the stop codon disrupted) was then removed from PCR2.1 TOPO using *Xba*I/*Hind*III sites and cloned into *Nhe*I/*Hind*III sites (*Xba*I and *Nhe*I produce compatible ends) on pEGFP-N1 (Clontech, Palo Alto, CA) for expression in mammalian cells.

3.2.3 Creation of and maintenance of cell lines

Lipofectamine (Life Technologies) was used to transfect CHO K1 cells with EGFR-GFP according to manufacturer's protocols. Briefly, 10^5 cells were plated in 35-mm culture dishes 18-24 hours before transfection. DNA (2.7 μg premixed in 50 μl DMEM) was complexed with Lipofectamine (8.5 μl premixed in 50 μl DMEM) for 45 minutes at room temperature. The DNA complexes were combined with 1 ml cell growth medium and the mixture added to the cell plate. After incubation for 12 hours, the complexes were removed and the cells grown in selection medium (normal growth medium containing 1 mg/ml G418; see below) for 10 days. Fluorescence-activated cell sorting separated cells into subpopulations of differing EGFR-GFP expression (FACStar Plus, Becton Dickinson, San Jose, CA). Sorted cells were grown for 1 passage and frozen for future use.

Transfected cells were grown in high-glucose DMEM containing 10% FBS (v/v), 2 mM glutamine, 1 mM sodium pyruvate, 1 mM non-essential amino acids, 100 U/ml penicillin and 100 μg/ml streptomycin, along with 500 μg/ml G418 for plasmid expression maintenance. All cells were passaged at sub-confluence and maintained in a 5% CO_2 environment. Cells were used for a limited time such that mean EGFR-GFP expression level did not drop more than 50% relative to the initially sorted population.

3.2.4 Preparation of surfaces for experiments

Glass-bottomed migration culture dishes (Bioptechs, Butler, PA) were sterilized using UV light and incubated overnight at 4 °C with 1-30 μg/ml Fn dissolved in 0.5 ml PBS. The Fn solution was aspirated and the dishes rinsed twice with PBS. Dishes were then incubated for 1 hour at 37 °C with 0.5 ml 1% BSA in PBS. The BSA solution was aspirated and the dishes rinsed twice with PBS. All prepared dishes were stored under PBS at 37 °C until ready for use (less than 30 minutes in all cases).

3.2.5 Cell pre-treatment for experiments

While in mid-exponential growth, cells were starved for 18 hours in serum-free medium containing DMEM, 2 mg/ml BSA, 2 mM glutamine, 1 mM sodium pyruvate, 1 mM non-essential amino acids, 100 U/ml penicillin and 100 μg/ml streptomycin, and 500 μg/ml G418. Starved cells were lifted from culture plates using Versene, then pelleted and resuspended for one hour in serum-free medium buffered with 15 mM HEPES rather than sodium bicarbonate. After cell suspension, cells were pelleted and resuspended in assay medium consisting of OptiMEM supplemented with penicillin (100 U/ml) and streptomycin (100 μg/ml), as well as 25 nM EGF and GRGDSP/GRADSP peptide (Calbiochem, San Diego, CA) as appropriate.

3.2.6 Long-timescale migration assay

Cell motility data was generated using a single-cell time-lapse videomicroscopy system consisting of an inverted microscope with 10×-magnification differential interference contrast objective (Carl Zeiss Microimaging, Thornwood, NY); motorized *xy*-stage, *z*-focus drive, and shutter (Ludl Electronic Products, Hawthorne, NY); CCD camera (Hamamatsu Photonics, Bridgewater, NJ); and automated data acquisition software (Improvision, Lexington, MA). For maintenance of cell viability, a temperature control system was used that electrically heats the underside of the migration assay dish (Bioptechs). Additionally, a metal lid with glass aperture was placed on top of the assay dish such that no air pocket remained above the medium.

Cells suspended in assay medium (17500 total) were plated onto Fn-coated assay dishes and allowed to adhere for 3 hours in order for steady-state cell translocation behavior to develop (data not shown). Twenty separate fields containing 80-100 total cells were digitally imaged every 15 minutes for 6 hours. Cell outlines and *xy*-centroids were determined using commercial image processing software (DIAS, Solltech, Inc., Oakdale, IA). Only cells that did not divide, touch other cells, or leave the image field during the experiment were used for data analysis; this restriction eliminated up to 25% of the cells initially tracked but did not affect any experimental conclusions.

3.2.7 Speed and persistence data analysis

Mean-squared displacements for the centroid path of each cell were calculated using the method of non-overlapping intervals (Dickinson and Tranquillo, 1993a). In this method, a cell tracked for N sequential positions with constant time interval Δt has mean-squared displacement for time interval $t_i = i\,\Delta t$ of:

$$\langle d \cdot d(t_i) \rangle = \frac{1}{n_i} \sum_{j=1}^{n_i} d \cdot d_{(1+i(j-1))\Delta) \to (1+ij)\Delta j}$$

$$i = [1,2,\ldots,N-1]$$

$$n_i = floor\left\{\frac{N-1}{i}\right\}$$

where "floor" represents the largest integer less than or equal to the bracketed quotient. Each cell's speed was determined by dividing the root-mean-square displacement when i=1 by the tracking interval Δt =15 minutes. Each cell's persistence time was fit using a non-linear least-squares regression by inserting its speed into a persistent random walk model for cell migration (Dunn, 1983; Othmer et al., 1988):

$$\langle d \cdot d(t_i) \rangle = 2S^2 P[t_i - P(1 - exp\{-t_i/P\})] \ .$$

Individual cell speeds and persistence times from each experiment were averaged to obtain a single experiment's parameter means and the associated standard errors. Each experiment was repeated at least 3 times; the reported S and P data are non-weighted averages across these separate experiments. Associated error bars represent ±2 SEM and were derived using standard propagation of error techniques. ANOVA results were derived using the experimental means for S and P. All computational routines were implemented in MATLAB 5.3 (The MathWorks, Inc., Natick, MA).

3.2.8 Kymography

To generate kymographs, cells were plated as in the long-timescale migration experiments. Time-lapse movies were obtained using a 40× phase-contrast objective; each movie consisted of 2-3 cells observed over 25 minutes with an image capture interval of 5 seconds. Kymographs were produced using Metamorph software (Universal Imaging

Corp., Downington, PA). Briefly, a one-pixel wide line was drawn perpendicular to the cell membrane at the location of an active protrusion event; image information along this line was compiled sequentially from each movie frame and pasted into a composite image. The resulting image records membrane dynamics at a single region of the cell perimeter. Kymographs were analyzed by drawing straight lines from the beginning of each protrusion event to its peak, neglecting protrusion heights of less than 3 pixels (0.5 μm). The slopes of these lines represent protrusion velocity, and the *x*-axis projection distance of these lines protrusion stability (Bear et al., 2002; Hinz et al., 1999). Reported data ±2 SEM represent the mean of two independent experiments per condition with 15-20 cells and 150-200 individual protrusion events per experiment.

3.3 Results

3.3.1 EGF increases cell motility in CHO-EGFR cells in a manner dependent on Fn coating concentration

EGF receptor expression and ligation stimulate migration in many cell lines, including keratinocytes, epithelial cells, and fibroblasts (McCrawley et al., 1997; Verbeek et al., 1998; Wells et al., 1998). Previous studies have demonstrated that EGF activates actin polymerization and lamellipodial protrusion (Bailly et al., 1998b; Segall et al., 1996), and that at low levels of adhesiveness lamellipodial protrusion rate limits overall EGF-stimulated motility (Maheshwari et al., 1999; Ware et al., 1998). Taking these facts together, we elected to use Chinese Hamster Ovary cells for our motility experiments because they are weakly adhesive yet exhibit easily observable membrane protrusions.

However, as CHO cells do not express endogenous EGFR, we first examined whether exogenous EGFR expression and subsequent EGF stimulation influenced CHO cell motility. We created a plasmid vector linking GFP to the C-terminus of EGFR and stably transfected it in CHO cells. Fluorescence-activated cell sorting was then used to create two

subpopulations of 1- and 4-fold relative EGFR expression level (1×-CHO and 4×-CHO; Fig. 3.5.1). Time-lapse single-cell videomicroscopy experiments were then used to track the migration of these transfected cells on glass surfaces adsorbed with the extracellular matrix protein Fn, which binds to $\alpha_5\beta_1$ integrins expressed by the CHO cells. A broad range of Fn coating concentrations (1, 3, 10, and 30 μg/ml) was employed to accurately assess the role of cell-substratum adhesion in modulating EGF-dependent CHO cell migration.

Using wind-rose plots, Fig. 3.5.2 depicts the qualitative changes in 1×-CHO and 4×-CHO motility resulting from variations in Fn coating concentration in both the presence and absence of EGF. To more clearly reveal the results we have plotted cell tracks from only the two extremes of Fn coating concentration (1 and 30 μg/ml). EGF stimulation augmented cell motility at all Fn coating concentrations; however, the level of increase in motility was higher in the 4×-CHO subpopulation. Also, the level of EGF-mediated motility rose as Fn coating concentration increased. Again, this EGF-mediated Fn effect on motility was stronger in the 4×-CHO subpopulation than in the 1×-CHO cells. In the absence of EGF, cell motility was low and showed no qualitative dependence on Fn concentration in either cell type. Taking these results together, the CHO-EGFR cell system exhibits the expected upregulation of migration in response to EGF stimulation, but the migration response is a complex output resulting from variations in Fn coating concentration, EGF stimulation, and EGFR expression level.

3.3.2 Fn and EGF effects on speed and persistence time

The paths of individual migrating cells can be described using a persistent random walk model characterized by two phenomenological parameters: cell speed (*S*) and persistence time (*P*) (Dunn, 1983; Gail and Boone, 1970; Othmer et al., 1988). Use of these parameters permits a quantitative analysis of the qualitative differences in migration behavior observed in the wind-rose diagrams. By fitting cell path mean-squared

displacement data to the persistent random walk model, we obtained S and P data characterizing CHO-EGFR migration responses to Fn and EGF. (Fig. 3.5.3 and 3.5.4).

The average speed of cells in the 1×-CHO subpopulation was roughly constant, at ~17 μm/hr (Fig. 3.5.3). This speed did not significantly vary due to either changes in Fn coating concentration or the addition of EGF. Similarly, the average speed of cells in the 4×-CHO subpopulation did not vary with changes in Fn coating concentration. However, this subpopulation demonstrated an unexpected but consistent decrease in cell speed in experiments containing EGF, from ~16 μm/hr to ~13 μm/hr.

Directional persistence in the absence of EGF is uniformly low across both CHO subpopulations and all Fn coating concentrations, ~10 minutes or less (Fig. 3.5.4). EGF ligation results in an increase in persistence time, although this effect is much stronger in the 4×-CHO cells. Moreover, persistence time in the presence of EGF rises as Fn concentration increases from 1 μg/ml to 30 μg/ml. In the 1×-CHO subpopulation, the change of persistence across rising Fn concentrations is moderate, increasing from 13 minutes to 20 minutes; the change in the 4×-CHO subpopulation is more dramatic, increasing from 22 minutes to 43 minutes.

Overall, we conclude that our qualitative observations showing a Fn-dependent increase in EGF-stimulated cell migration (Fig. 3.5.2) result from concomitant increases in directional persistence time but not an increase in cell speed. Because the magnitudes of the EGF-mediated persistence effects were substantially greater in the 4×-CHO subpopulation, we chose to use those cells only for further studies.

3.3.3 CHO-EGFR cells are weakly adhesive

Previous investigations of the combined effects of EGF stimulation and extracellular matrix surface density on fibroblast migration indicate that EGF upregulates cell speed at medium and high matrix surface densities, but reduces speed under conditions of weak cell-substratum adhesion (Maheshwari et al., 1999; Ware et al., 1998). We reasoned that our

observed reduction in cell speed upon EGF stimulation indicated that the CHO-EGFR cells were weakly adhesive across all tested Fn coating concentrations.

To more directly ascertain the adhesive state of the CHO-EGFR cells, we studied the role of M-calpain activity in modulating 4×-CHO cell speed. M-calpain acts downstream of EGF receptor signaling to cleave cytoskeletal linkages and reduce cell adhesion (Cuevas et al., 2003; Glading et al., 2000; Xie et al., 1998). In particular, M-calpain acts to potentiate the rate of uropodial membrane retraction (Glading et al., 2002); conversely, M-calpain inhibition restricts cells' ability to break integrin-substratum bonds and retract their uropods (Huttenlocher et al., 1997; Palecek et al., 1998).

Importantly, however, the rate of rear release is only rate-limiting for cell motility under conditions of medium and high adhesion strength (Glading et al., 2002; Huttenlocher et al., 1997). Thus M-calpain inhibition would not alter 4×-CHO cell speed if they are only weakly adhesive. To directly test the permissive role of calpain signaling in our cells, we performed videotracking experiments in the presence of ALLN, a cell-permeable M-calpain inhibitor. As shown in Fig. 3.5.5, addition of ALLN at 5 μg/ml, a level known to reduce cell speed (Glading et al., 2000; Huttenlocher et al., 1997), did not affect cell speed in the 4×-CHO cells. This result provided further evidence of the weakly adhesive state of CHO-EGFR cells.

3.3.4 Changes in the temporal stability of lamellipodial protrusions correlate to variations in cell persistence time

The translocation speed of weakly adhesive cells is limited by the rate of lamellipodial protrusion (DiMilla et al., 1991; Lauffenburger, 1989; Maheshwari et al., 1999; Ware et al., 1998). In an analogous fashion, we hypothesized that the stability of membrane protrusions was related to both the EGF-dependent upregulation of directional persistence and the observed linear relationship between EGF-mediated directional persistence and Fn coating concentration. This hypothesis accorded with previous evidence suggesting that

while the initial protrusion of EGF-stimulated lamellipods does not require cell-substratum adhesion, protrusions retract quickly when extended over non-adhesive substrates (Bailly et al., 1998b). To test the hypothesis, we used kymography to analyze lamellipodial dynamics (Hinz et al., 1999). Kymographs are composite time-space images of membrane movement at a single point of an actively protruding leading lamellipod, created by extracting image information from a defined line region in each image of a time-lapse movie and pasting them side-by-side. While cell translocation experiments captured one movie frame every 15 minutes, kymography studies captured one movie frame every 5 seconds. As a result of this high temporal resolution, we were able to observe the local dynamics of individual membrane protrusion and retraction cycles on a much shorter timescale that that required for net CHO-EGFR cell translocation, separating the effects of two related, but not equivalent, aspects of cell motility.

Fig. 3.5.6 contains two representative kymographs showing the qualitative difference in 4×-CHO EGF-stimulated membrane dynamics between 1 μg/ml and 30 μg/ml Fn coating concentration. Lamellipodia at the lower amount of Fn exhibited small, quickly oscillating waves of protrusion and retraction of membrane; lamellipodia at the higher amount exhibited smoother, more sustained protrusion with less frequent retractions. To quantify this observed difference in lamellipodial behavior, we analyzed how the velocity and stability of individual lamellipodial protrusion waves varied with Fn coating concentration. Protrusion velocity represents the average spatial rate of actin polymerization from the beginning of a single protrusion wave to its peak, while protrusion stability measures the time spanned by that wave. As shown in Fig. 3.5.7, protrusion velocity remained constant with variations in EGF stimulation and Fn concentration, at roughly 2.2 μm/min (ANOVA p = 0.86). In contrast, the addition of EGF increases the average stability of individual membrane protrusion waves from 0.55 minutes to 0.72 minutes at 30 μg/ml Fn (p = 0.04). In addition, the temporal stability of EGF-stimulated protrusion waves increased monotonically from approximately 0.44 minutes at 1 μg/ml Fn coating concentration to

approximately 0.72 minutes at 30 μg/ml Fn (ANOVA $p = 0.03$). Comparison with Fig. 3.5.4 indicates that these results occur in parallel with EGF- and Fn-dependent changes in *P*. Hence, a correlation exists between the short-timescale stability of lamellipodial protrusions and long-timescale directional persistence of translocating 4×-CHO cells.

3.3.5 Soluble RGD peptide reduces both long-timescale directional persistence and short-timescale protrusion stability

The Fn-based correlation in Fig. 3.5.7 implies that variations in cell-substratum adhesion strength can affect the long-timescale directional persistence of cell paths through modulation of the stability of short-timescale local membrane protrusion events. To gain better insight into this possibility, we performed both cell translocation and membrane dynamics studies with the 4×-CHO cells in the presence of soluble GRGDSP peptide. Synthetic peptides containing the RGD sequence are competitive inhibitors of fibronectin binding to $\alpha_5\beta_1$ integrin, and have been shown previously to inhibit cell migration (Fujii et al., 1998; Libotte et al., 2001; Shimizu et al., 1997). The response of EGF-stimulated cells to varying concentrations of GRGDSP peptide was tested at 30 μg/ml Fn coating concentration, the condition giving the highest directional persistence time and most stable membrane protrusion events. Average cell area decreased in an RGD-dependent manner (data not shown), indicating that addition of soluble peptide inhibited cell adhesion. We found that the addition of 100 and 300 μM GRGDSP decreased the motility of 4×-CHO cells in a dose-dependent fashion as demonstrated by wind-rose plots (Fig. 3.5.8*A*). Quantification of this RGD-dependent inhibition of cell motility revealed that *P* for 4×-CHO cells decreased to 33 and 29 minutes, respectively, from a baseline of 43 minutes (Fig. 3.5.8*B*). Addition of 300 μM GRADSP control peptide had no effect on persistence (data not shown). Similarly, 300 μM GRGDSP peptide reduced the stability of lamellipodial protrusion events in a statistically significant manner (Fig. 3.5.8C). In contrast, the addition of control GRADSP peptide had no effect on lamellipodial protrusion stability. These

results provide further evidence that adhesion strength modulates persistence time, and show that long-timescale directional migration is enhanced by adhesion-mediated stabilization of short-timescale lamellipodial protrusions.

3.4 Discussion

Individual cell migration exhibits sustained locomotion in the direction of the leading lamellipod over short periods of time and random changing of the directional orientation of lamellipodial protrusion and migration over longer timescales (Dunn, 1983; Maheshwari and Lauffenburger, 1998). This persistent random walk is characterized by both speed and directional persistence time. But though the role of cell-substratum adhesion in modulating S has been characterized extensively (DiMilla et al., 1993; Goodman et al., 1989; Maheshwari et al., 1999; Palecek et al., 1997), it is not well understood how variations in cell-substratum adhesion modulate P. In this chapter we have described how varying the surface coating concentration of Fn substrate modulates P for EGF receptor-transfected CHO cells, and explored how adhesion-dependent changes in lamellipodial protrusion dynamics might explain our results. Our major findings are: *(a)* EGF stimulation increases P across all Fn concentrations but actually reduces S; *(b)* EGF also increases the temporal stability, but not the velocity, of individual lamellipodial protrusion waves; *(c)* in the presence of EGF, both P and protrusion stability increase with higher Fn coating concentration; and *(d)* in the presence of EGF, the addition of GRGDSP peptide, a soluble competitive inhibitor of cell-substratum binding, reduces both P and the stability of lamellipodia.

Stochastic kinetic fluctuations in adhesion receptor binding and transport have been proposed as a mechanistic basis for directional persistence in uniform adhesive environments (Dickinson and Tranquillo, 1993b). This model links these short-timescale fluctuations to variations in spatiotemporal forces that affect the speed and direction of cell migration on longer timescales. The model predicts an inverted biphasic dependence of

persistence time to cell-substratum adhesion strength; however, previous studies of the relationship between substratum coating density and persistence have not confirmed this prediction (DiMilla et al., 1993; Ware et al., 1998). Our observation of a monotonic rather than inverted biphasic curve relating EGF-dependent directional persistence and Fn coating concentration (Fig. 3.5.4) could be reconciled with the stochastic model by postulating a cell type-dependent inability to experimentally access a wide enough dynamic range of adhesion strength. However, a linear correlation between increasing Fn coating concentration and increasing EGF-mediated persistence is consistent with the Dickinson persistence model only if our CHO cells are migrating under conditions of high adhesiveness that limit the ability of stochastic adhesion fluctuations to generate rotational turning force in cells (Dickinson and Tranquillo, 1993b).

In contrast, the CHO-EGFR cells appear to be only weakly adhesive under all the conditions studied. Fn coating concentrations of less than 1 μg/ml were insufficient for the adherence and spreading of both the 1×-CHO and 4×-CHO cells (data not shown). Furthermore, the 4×-CHO subpopulation exhibited decreased cell speed upon EGF stimulation (Fig. 3.5.3), and a previous study of the combined role of EGF and Fn in fibroblast motility has demonstrated that EGF increases S at medium and high levels of cell adhesion while decreasing S at low levels (Maheshwari et al., 1999). This decrease in S at low adhesiveness is caused by an EGF-dependent reduction in cell-substratum adhesivity (Maheshwari et al., 1999; Xie et al., 1998) due to M-calpain activity (Glading et al., 2000; Glading et al., 2002). Inhibition of M-calpain did not affect cell motility (Fig. 3.5.5), a result previously established for weakly adhesive cells (Glading et al., 2002; Huttenlocher et al., 1997). Moreover, that we did not observe a reduction in S in the 1×-CHO cells upon stimulation with EGF can be attributed satisfactorily to an EGFR expression level-dependent quantitative reduction in the magnitude of this deadhesive effect relative to the 4×-CHO cells.

In addition to the EGF-mediated decrease in *S*, another interesting aspect of our results is that CHO-EGFR speed in the presence of EGF is independent of Fn coating concentration while persistence shows substantial Fn-dependent variation (Fig. 3.5.4). One possible explanation involves separating the effects of EGFR signaling on adhesion into separate modules regulating overall adhesion strength and front-rear adhesive asymmetry. These modules would in turn control *S* and *P*, respectively. Mathematical modeling suggests that variations in *S* result from changes in overall adhesion strength relative to the amount of contractile force generated in a cell (DiMilla et al., 1991). The CHO-EGFR cells presumably maintain these in roughly constant balance across all the Fn concentrations studied, with a change in speed only occurring due to the deadhesive effect of EGF (Maheshwari et al., 1999). However, in concert with its overall deadhesive effect, EGF also increases front-rear adhesive asymmetry by accentuating morphological polarization (Wells et al., 1999) and eliciting the creation of new focal complexes at the cell front (Bailly et al., 1998a). Greater adhesive asymmetry could be expected to reinforce a cell's ability to maintain its migration in a constant direction and thus account for the increase in CHO-EGFR persistence when stimulated by exogenous EGF. Interestingly, that the stability of lamellipodial protrusion events also increases upon addition of EGF (Fig. 3.5.7) indirectly supports the idea that EGF actually increases adhesion at the front of cells.

Interestingly, that increasing amounts of surface Fn correlate with increasing EGF-stimulated persistence suggests that increased adhesive asymmetry downstream of EGF receptor signaling is merely permissive for *P*, with the level of cell-substratum adhesion actually controlling the effective level of EGFR signaling. Moreover, expression level-dependent differences in the magnitude of adhesive asymmetry downstream of EGFR signaling might also explain why the 4×-CHO subpopulation shows higher *P* than the 1×-CHO subpopulation at all Fn concentrations (Fig. 3.5.4).

The rate of actin polymerization in membrane protrusions and ruffles has been shown to be independent of adhesion (Bailly et al., 1998b; Felder and Elson, 1990). Our

observations are consistent with this fact in that EGF-stimulated protrusion velocity (~2.2 μm/min) does not depend on Fn coating concentration. In contrast, that EGF-stimulated lamellipodial stability increases with Fn concentration (Fig. 3.5.7), and that *P* and lamellipodial stability are reduced concurrently by GRDGSP peptide (Fig. 3.5.8), both imply that cell-substratum adhesion mediates the connection between short-timescale lamellipodial protrusion and long-timescale directional persistence in our experiments. Our findings recall a previous report correlating lamellipodial protrusion rate with net cell translocation speed under weakly adhesive conditions (Maheshwari et al., 1999); both *S* and *P* regulate the amount of net cell motility. However, Maheshwari et al. measured lamellipodial extension using the same long-timescale temporal rate of image capture as their experiments studying net cell translocation. As a result, their reported lamellipodial extension rates would intrinsically be related to *S*. On the basis of our results, we suggest that the lamellipodial extension rates of Maheshwari et al. might conceal an analogous relationship between short-timescale protrusion stability and long-timescale cell speed. Others have reported such a relationship, though not in the context of cell-substratum adhesion (Bear et al., 2002).

Our observations of Fn- and GRGDSP-dependent variations in protrusion stability likely derive from mass action kinetics, in that greater amounts of Fn surface coating lead to more efficient short-timescale binding of CHO $\alpha_5\beta_1$ integrins and the formation of more protrusion-stabilizing focal complexes near the leading edge. In turn, the directional persistence of migration could be considered a long-timescale temporal integration of the net amount of adhesion formation on the much shorter timescale of individual lamellipodial protrusion waves. Cells forming new adhesions more slowly would be more likely to retract a lamellipod and attempt to migrate in a new direction. Consistent with this idea is the work of Bailly et al. demonstrating that EGF-stimulated actin polymerization and membrane extension do not require adhesion to occur, but that a lack of cell-substratum adhesion reduces the stability of protrusions (Bailly et al., 1998b).

Overall, our studies of Fn- and GRGDSP-dependent variations in protrusion stability point towards the regulated assembly of adhesion complexes as a locus of molecular control of directionality in motility. What proteins might play a key role as molecular switches linking adhesion formation to directional persistence? Recent studies suggest that vinculin is a necessary focal complex protein for transmitting cytoskeletal traction force and linking membrane protrusion to matrix adhesion (DeMali et al., 2002; Galbraith et al., 2002). The spatially or temporally regulated addition of vinculin or other specific proteins to lamellipodial adhesions could serve as a link coordinating short-timescale actin polymerization dynamics with directed cell translocation that occurs over longer timescales. Another recent report indicates that myosin light-chain kinase (MLCK) plays a role in stabilizing lamellipodial protrusions (Totsukawa et al., 2004). Totsukawa and colleagues found that in MLCK-inhibited fibroblasts, nascent adhesions at the tips of lamellipodia did not mature into larger adhesive structures; moreover, the protrusions of these MLCK-inhibited cells were less stable and retracted more frequently. Interestingly, they report wind-rose plots indicating that MLCK inhibition substantially reduces cell motility by increasing the directional tortuosity of cell paths. Given the well-established role of MLCK-promoted contractility in focal adhesion assembly and the modulation of both cell adhesion and cell motility (Brahmbhatt and Klemke, 2003; Burridge and Chrzanowski-Wodnicka, 1996; Klemke et al., 1997), it is plausible that lamellipodial MLCK activity, like vinculin recruitment, could act as a molecular switch modulating adhesion-mediated directional persistence.

It is interesting to speculate that underlying the results of this study there exists a monotonic relationship between directional persistence, protrusion stability, and the quantitative lamellipodial recruitment and activation of specific adhesion-related proteins such as vinculin or MLCK. To our knowledge, this hypothesis has not been tested rigorously. We note that the quantity of recruitment need not depend solely on the amount of extracellular adhesion substrate. Presumably such recruitment would also occur

downstream of both integrin- and growth factor-mediated signaling pathways known to potentiate cell polarization and directional cell migration such as PLCγ, PI3K, Cdc42, and Rac (Kiosses et al., 2001; Ridley, 2001; Weiner, 2002; Wells et al., 1999).

3.5 Figures

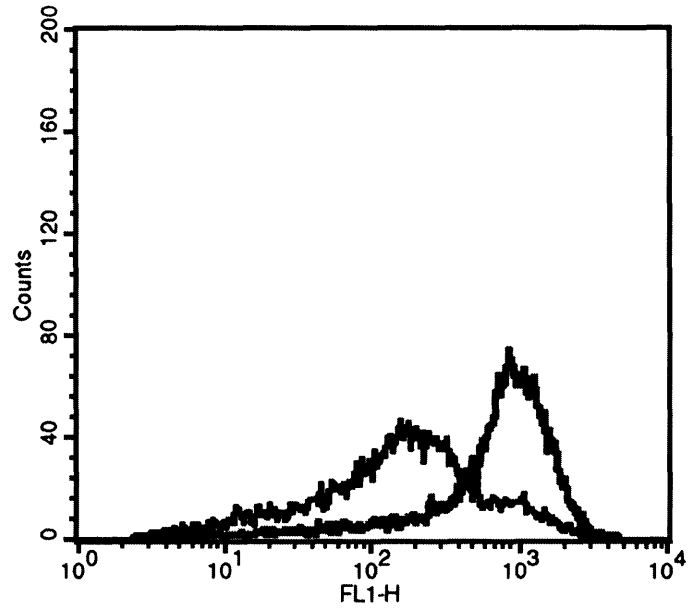

Figure 3.5.1 Creation of EGFR-transfected CHO cell lines.
CHO cells were transfected with an EGFR-GFP construct and stable transfectants selected with G418. Fluorescence-activated cell sorting was used to create two subpopulations of 1×- and 4×- relative expression level. Plot shows number of 1×-CHO (black) and 4×-CHO (gray) cells versus GFP fluorescence intensity (arbitrary units).

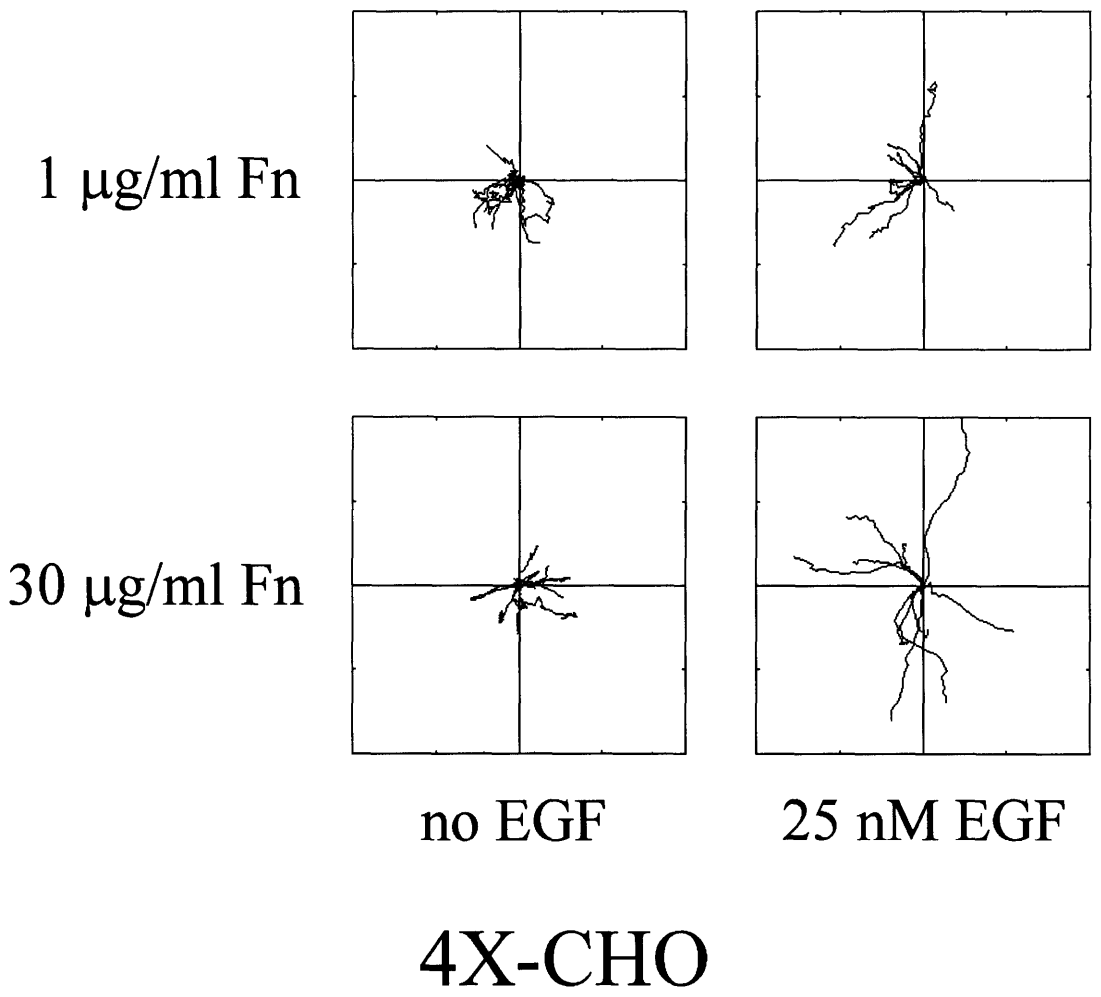

Figure 3.5.2 Migration behavior of EGFR-transfected CHO cells is affected by Fn and EGF. Time-lapse videomicroscopy was used to capture the motility responses of individual 4×-CHO (this page) and 1×-CHO (next page) cells. Digital images were taken every 15 minutes for a total of 6 hours per experiment. Each wind-rose plot shows centroid tracks from ten representative cells in a typical experiment, with the initial position of each track superimposed at 0,0 for clarity. Distance between hatch marks on both axes is 50 μm.

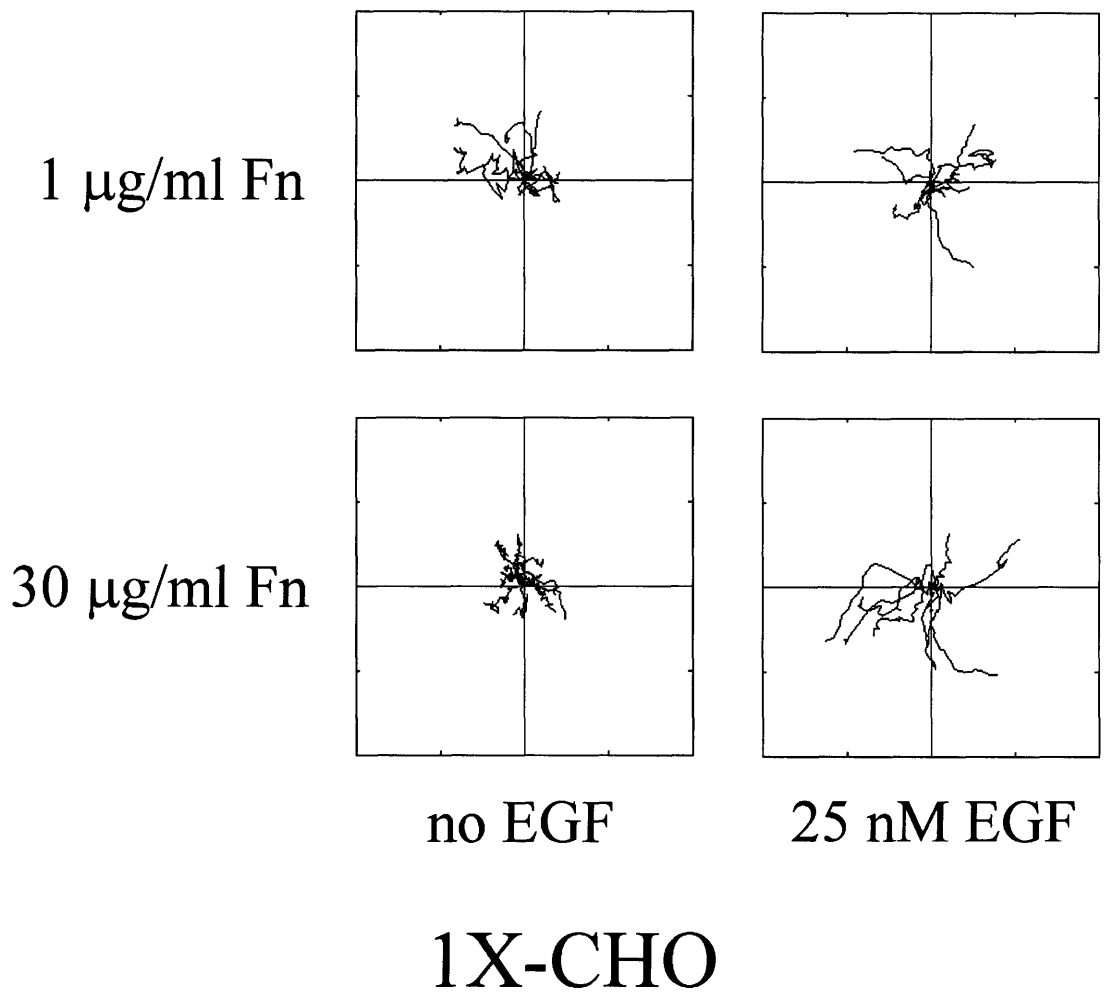

Figure 3.5.2 (continued from previous page)

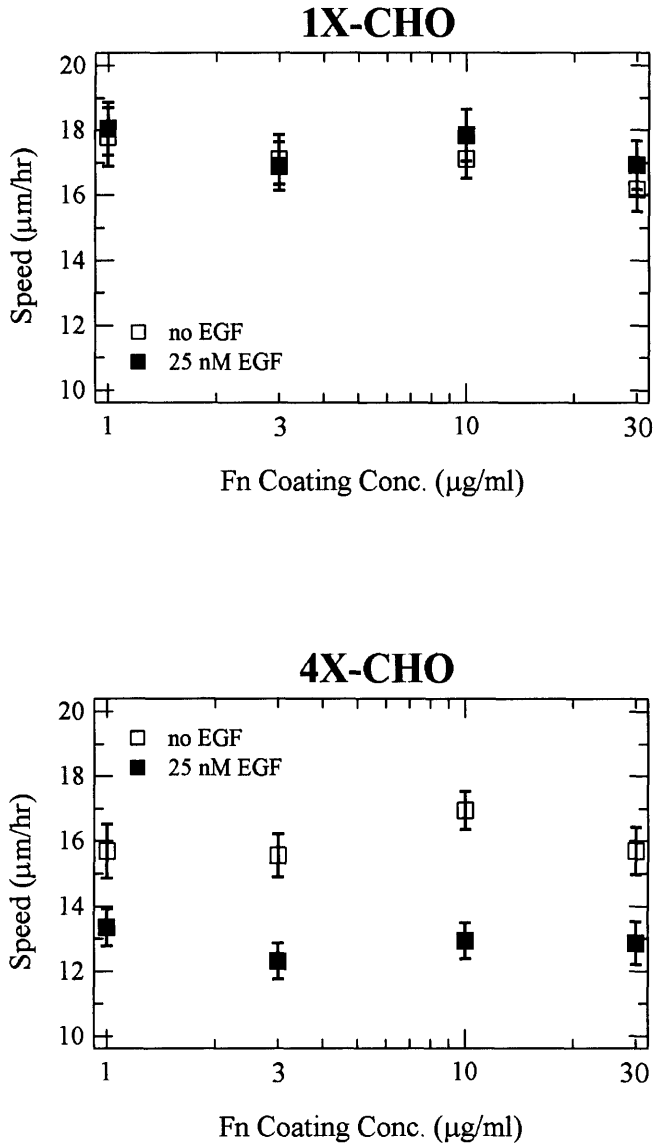

Figure 3.5.3 Effects of EGF and Fn on speed of migrating CHO-EGFR cells.
EGF stimulation, but not Fn coating concentration, modulates 4×-CHO cell speed. In contrast, neither EGF nor Fn modulates 1×-CHO speed. To derive the speed of a single cell, total cell path length was divided by the total time of observation. The mean speed of each experiment resulted from averaging the speed of 80-100 total cells. Reported speeds represent the average ± 2 SEM for 3 experiments per condition. Single-factor ANOVA for Fn, 1×-CHO: $p = 0.89$ (-EGF), $p = 0.94$ (+EGF); 4×-CHO: $p = 0.54$ (-EGF), $p = 0.90$ (+EGF). Single-factor ANOVA for ±EGF, all Fn levels pooled, 1×-CHO: $p = 0.69$; 4×-CHO: $p < 0.0001$.

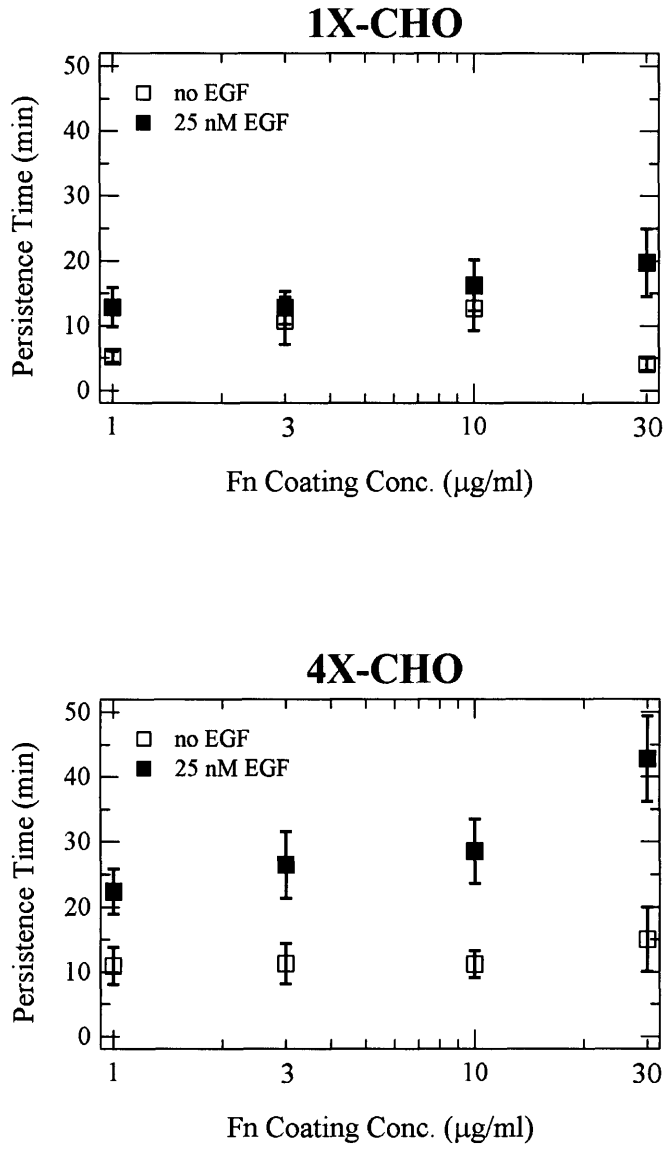

Figure 3.5.4 Effects of EGF and Fn on persistence of migrating CHO-EGFR cells.
Persistence time increases with Fn coating concentration in the presence of EGF for both cell subpopulations. However, this Fn-dependence is only statistically significant for the 4×-CHO cells. Single cell persistence times were derived from non-linear least-squares regression using individual cell speed and mean-square displacement data as inputs. Reported persistence times are calculated using the same methodology as cell speed. Single-factor ANOVA for Fn, 1×-CHO: $p = 0.46$ (-EGF), $p = 0.69$ (+EGF); 4×-CHO: $p = 0.88$ (-EGF), $p = 0.03$ (+EGF). Single-factor ANOVA for ±EGF, all Fn levels pooled, 1×-CHO: $p = 0.04$; 4×-CHO: $p < 0.00001$.

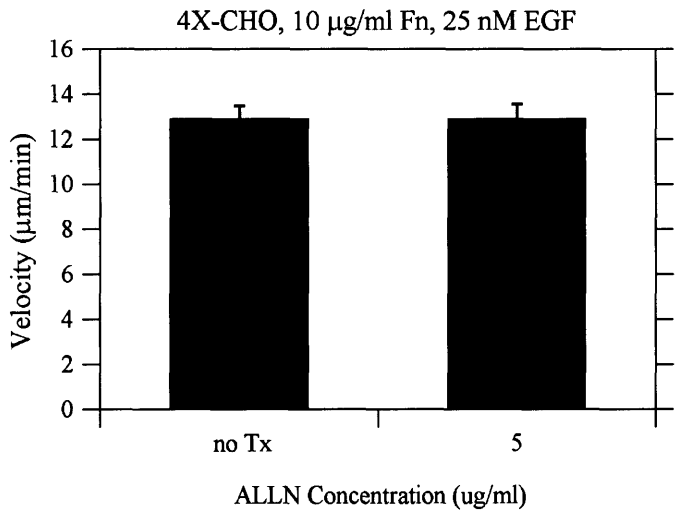

Figure 3.5.5 Calpain inhibition does not reduce CHO-EGFR cell speed.
Time-lapse videomicroscopy was performed on 4×-CHO cells stimulated with EGF in the presence of ALLN, an M-calpain inhibitor. Data analysis was performed as in Fig 3.5.3.

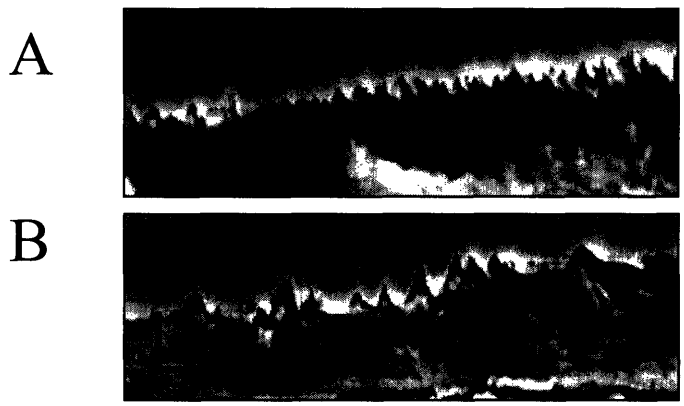

Figure 3.5.6 Lamellipodial membrane dynamics of CHO-EGFR cells.
Representative short-timescale kymographs are shown from time-lapse movies of 4×-CHO cells stimulated with EGF and migrating on 1 μg/ml (*A*) and 30 μg/ml (*B*) Fn. Kymographs depict variations in lamellipodial activity along a one-pixel wide line drawn perpendicularly to the cell membrane in sequential phase contrast images. Ascending contours show lamellipodial protrusion, while descending contours show lamellipodial retraction. Dark regions indicate membrane ruffling.

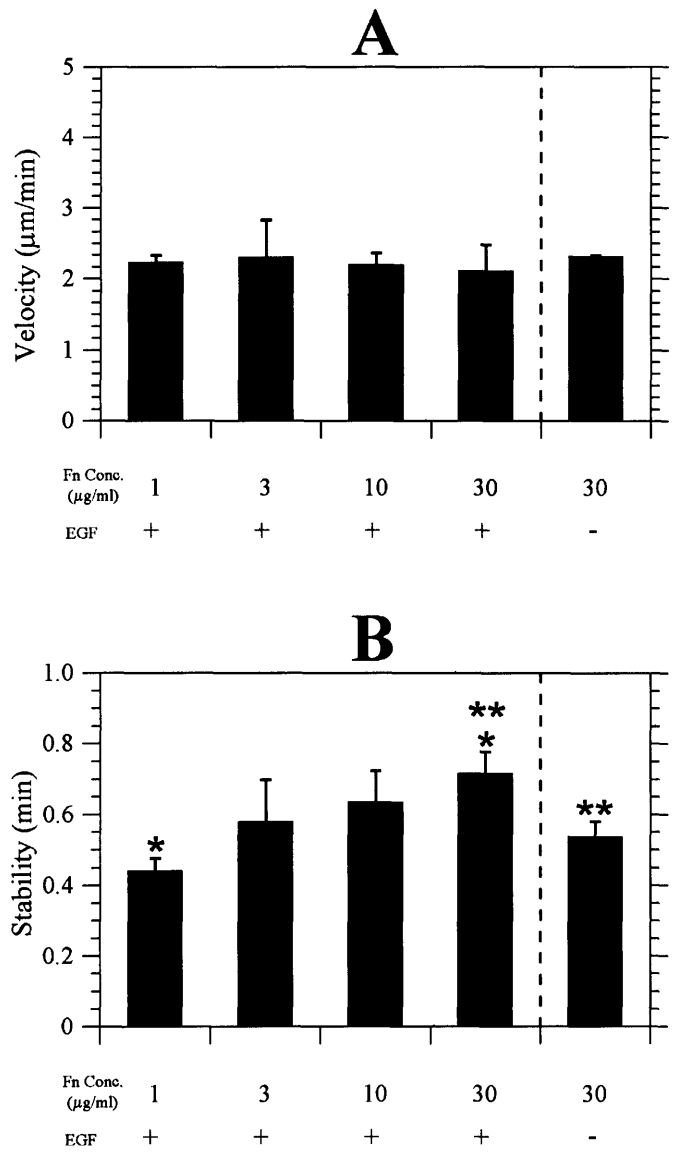

Figure 3.5.7 Lamellipodial stability correlates with directional persistence in CHO-EGFR migration.
(*A*) Fn coating concentration does not affect the average velocity of 4×-CHO membrane protrusion. The average slope of ascending kymograph membrane waves defines protrusion velocity. ANOVA: $p = 0.86$
(*B*) 4×-CHO protrusion stability increases with Fn concentration in the presence of EGF. Stability represents the time elapsed between the beginning of a single protrusion wave and its spatial peak. Nonoverlapping 95% confidence intervals are indicated by asterisks. ANOVA: $p = 0.03$.

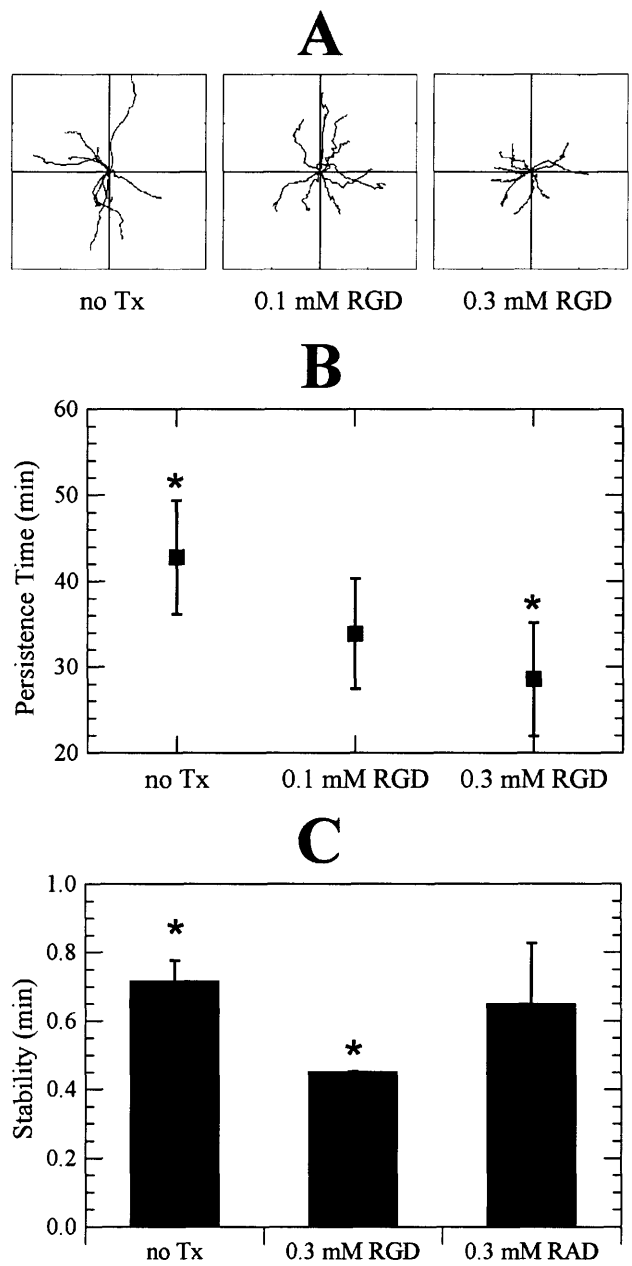

Figure 3.5.8 Soluble RGD peptide reduces both long-timescale directional persistence and short-timescale protrusion stability.
(*A*) Wind-rose plots of migrating 4×-CHO cells plated on 30 μg/ml Fn in the presence of EGF and varying amounts of GRGDSP. Distance between hatch marks is 50 μm.
(*B*) Persistence times for the RGD migration experiments. Persistence times were derived as in Fig. 3.5.4. Non-overlapping 95% confidence intervals are indicated by asterisks. ANOVA: $p = 0.002$ for RGD concentration.
(*C*) Kymography was performed on 4×-CHO cells plated on 30 μg/ml Fn in the presence of EGF and either GRGDSP or control GRADSP peptide. Non-overlapping 95% confidence intervals are indicated by asterisks ($p = 0.01$).

3.6 References

Bailly, M., J.S. Condeelis, and J.E. Segall. 1998a. Chemoattractant-induced lamellipod extension. *Microsc. Res. Techniq.* 43:433-443.

Bailly, M., L. Yan, G.M. Whitesides, J.S. Condeelis, and J.E. Segall. 1998b. Regulation of protrusion shape and adhesion to the substratum during chemotactic responses of mammalian carcinoma cells. *Exp. Cell Res.* 241:285-299.

Bear, J.E., T.M. Svitkina, M. Krause, D.A. Schafer, J.J. Loureiro, G.A. Strasser, I.V. Maly, O.Y. Chaga, J.A. Cooper, G.G. Borisy, and F.B. Gertler. 2002. Antagonism between Ena/VASP proteins and actin filament capping regulates fibroblast motility. *Cell.* 109:509-521.

Brahmbhatt, A.A., and R.L. Klemke. 2003. ERK and RhoA Differentially Regulate Pseudopodia Growth and Retraction during Chemotaxis. *J. Biol. Chem.* 278:13016-13025.

Burridge, K., and M. Chrzanowski-Wodnicka. 1996. Focal adhesions, contractility, and signaling. *Annu. Rev. Cell Dev. Biol.* 12:463-519.

Cuevas, B.D., A.N. Abell, J.A. Witowsky, T. Yujiri, K. Kesavan, M. Ware, P.L. Jones, S.A. Weed, R.L. DeBiasi, Y. Oka, K.L. Tyler, and G.L. Johnson. 2003. MEKK1 regulates calpain-independent proteolysis of focal adhesion proteins for rear-end detachment of migrating fibroblasts. *EMBO. J.* 22:3346-3355.

DeMali, K.A., C.A. Barlow, and K. Burridge. 2002. Recruitment of the Arp2/3 complex to vinculin: coupling membrane protrusion to matrix adhesion. *J. Cell Biol.* 159:881-891.

Dickinson, R.B., and R.T. Tranquillo. 1993a. Optimal estimation of cell movement indices from the statistical analysis of cell tracking data. *AIChE J.* 39:1995-2010.

Dickinson, R.B., and R.T. Tranquillo. 1993b. A stochastic model for adhesion-mediated cell random motility and haptotaxis. *J. Math. Biol.* 31:563-600.

DiMilla, P.A., K. Barbee, and D.A. Lauffenburger. 1991. Mathematical model for the effects of adhesion and mechanics on cell migration speed. *Biophys. J.* 60:15-37.

DiMilla, P.A., J.A. Stone, J.A. Quinn, S.M. Albelda, and D.A. Lauffenburger. 1993. Maximal migration of human smooth muscle cells on fibronectin and Type IV collagen occurs at an intermediate attachment strength. *J. Cell Biol.* 122:729-737.

Dunn, G.A. 1983. Characterizing a kinesis response; time averaged measures of cell speed and directional persistance. *Agents Actions [Suppl.].* 12:14-33.

Felder, S., and E.L. Elson. 1990. Mechanics of fibroblast locomotion: quantitative analysis of forces and motions at the leading lamellas of fibroblasts. *J. Cell Biol.* 111:2513-2526.

Fontanini, G., S. Vignati, D. Bigini, A. Mussi, H. Lucchi, C.A. Angeletti, R. Pingitore, S. Pepe, F. Basolo, and G. Bevilacqua. 1995. Epidermal growth factor receptor (EGFr) expression in non-small cell lung carcinomas correlates with metastatic involvement of hilar and mediastinal lymph nodes in the squamous subtype. *Eur. J. Cancer.* 31A:178-183.

Fujii, H., N. Nishikawa, H. Komazawa, M. Suzuki, M. Kojima, I. Itoh, A. Obata, K. Ayukawa, I. Azuma, and I. Saiki. 1998. A new pseudo-peptide of Arg-Gly-Asp (RGD) with inhibitory effect on tumor metastasis and enzymatic degradation of extracellular matrix. *Clin. Exp. Metastas.* 16:94-104.

Gail, M.H., and C.W. Boone. 1970. The locomotion of mouse fibroblasts in tissue culture. *Biophys. J.* 10:980-993.

Galbraith, C.G., K.M. Yamada, and M.P. Sheetz. 2002. The relationship between force and focal contact development. *J. Cell Biol.* 159:695-705.

Glading, A., P. Chang, D.A. Lauffenburger, and A. Wells. 2000. Epidermal growth factor receptor activation of calpain is required for fibroblast motility and occurs via an ERK/MAP kinase signaling pathway. *J. Biol. Chem.* 275:2390-2398.

Glading, A., D.A. Lauffenburger, and A. Wells. 2002. Cutting to the chase: calpain proteases in cell motility. *Trends Cell. Biol.* 12:46-54.

Goodman, S.L., G. Risse, and K.v.d. Mark. 1989. The E8 subfragment of laminin promotes locomotion of myoblasts over extracellular matrix. *J. Cell Biol.* 109:799-809.

Hart, J. 2002. Inflammation. 1: Its role in the healing of acute wounds. *J. Wound Care.* 11:205-209.

Hinz, B., W. Alt, C. Johnen, V. Herzog, and H.W. Kaiser. 1999. Quantifying lamella dynamics of cultured cells by SACED, a new computer-assisted motion analysis. *Exp. Cell Res.* 251:234-43.

Huttenlocher, A., S.P. Palecek, Q. Lu, W. Zhang, R.L. Mellgren, D.A. Lauffenburger, M.H. Ginsberg, and A.F. Horwitz. 1997. Regulation of cell migration by the calcium-dependent protease calpain. *J. Biol. Chem.* 272:32719-32722.

Jorissen, R.N., F.W. Walker, N. Pouliot, T.P.J. Garrett, C.W. Ward, and A.W. Burgess. 2003. Epidermal growth factor receptor: mechanisms of activation and signaling. *Exp. Cell Res.* 284:31-53.

Kassis, J., D.A. Lauffenburger, T. Turner, and A. Wells. 2001. Tumor invasion as dysregulated cell motility. *Semin. Cancer Biol.* 11:105-117.

Keller, R. 2002. Shaping the vertebrate body plan by polarized embryonic cell movements. *Science.* 298:1950-1954.

Kiosses, W.B., S.J. Shattil, N. Pampori, and M.A. Schwartz. 2001. Rac recruits high-affinity integrin $\alpha_v\beta_3$ to lamellipodia in endothelial cell migration. *Nat. Cell Biol.* 3:316-320.

Klemke, R.S., S. Kai, A. Giannini, P. Gallagher, P.d. Lanerolle, and D. Cheresh. 1997. Regulation of cell motility by mitogen-activated protein kinase. *J. Cell Biol.* 137:481-492.

Kraemer, R. 2000. Regulation of cell migration in atherosclerosis. *Curr. Atheroscler. Rep.* 2:445-452.

Kurokawa, K., R.E. Itoh, H. Yoshizaki, Y. Ohba, T. Nakamura, and M. Matsuda. 2004. Coactivation of Rac1 and Cdc42 at lamellipodia and membrane ruffles induced by epidermal growth factor. *Mol. Biol. Cell.* 15:1003-1010.

Lauffenburger, D.A. 1989. A simple model for the effects of receptor-mediated cell-substratum adhesion on cell migration. *Chem. Eng. Sci.* 44:1903-1914.

Lauffenburger, D.A., and A.F. Horwitz. 1996. Cell migration: a physically integrated molecular process. *Cell.* 84:359-369.

Libotte, T., H.-W. Kaiser, W. Alt, and T. Bretschneider. 2001. Polarity, protrusion-retraction dynamics and their interplay during keratinocyte cell migration. *Exp. Cell Res.* 270:129-137.

Maheshwari, G., and D.A. Lauffenburger. 1998. Deconstructing (and reconstructing) cell migration. *Microsc. Res. Techniq.* 43:358-368.

Maheshwari, G., A. Wells, L.G. Griffith, and D.A. Lauffenburger. 1999. Biophysical integration of effects of epidermal growth factor and fibronectin on fibroblast migration. *Biophys. J.* 76:2814-2823.

Martin, P. 1997. Wound healing: aiming for perfect regeneration. *Science.* 275:75-81.

McCrawley, I.J., P. O'Brian, and L.G. Hudson. 1997. Overexpression of the epidermal growth factor receptor contributes to enhanced ligand-mediated motility in keratinocyte cell lines. *Endocrinology.* 138:121-127.

Mitchison, T.J., and L.P. Cramer. 1996. Actin-based cell motility and cell locomotion. *Cell.* 84:371-379.

Nogami, M., M. Yamazaki, H. Watanabe, Y. Okabayashi, Y. Kido, M. Kasuga, T. Sasaki, T. Maehama, and Y. Kanaho. 2003. Requirement of autophosphorylated tyrosine 992 of EGF receptor and its docking protein phospholipase Cγ1 for membrane ruffle formation. *FEBS Lett.* 536:71-76.

Othmer, H.G., S.R. Dunbar, and W. Alt. 1988. Models of dispersal in biological systems. *J. Math. Biol.* 26:263-298.

Palecek, S.E., J.C. Loftus, M.H. Ginsburg, D.A. Lauffenburger, and A.F. Horwitz. 1997. Integrin-ligand binding properties govern cell migration speed through cell-substratum adhesiveness. *Nature.* 385:537-540.

Palecek, S.P., A. Huttenlocher, A.F. Horwitz, and D.A. Lauffenburger. 1998. Physical and biochemical regulation of integrin release during rear detachment of migrating cells. *J. Cell Sci.* 111:929-940.

Ridley, A.J. 2001. Rho GTPases and cell migration. *J. Cell Sci.* 114:2713-2722.

Schlessinger, J. 2000. Cell signaling by receptor tyrosine kinases. *Cell.* 103:211-225.

Segall, J.E., S. Tyerech, L. Boselli, S. Masseling, J. Helft, A. Chan, J. Jones, and J. Condeelis. 1996. EGF stimulates lamellipod extension in metastatic mammary adenocarcinoma cells by an actin-dependent mechanism. *J. Cell Sci.* 14:61-72.

Shimizu, M., K. Minakuchi, S. Kaji, and J. Koga. 1997. Chondrocyte migration to fibronectin, type I collagen, and type II collagen. *Cell Struct. Funct.* 22:309-315.

Szekanecz, Z., and A.E. Koch. 2000. Endothelial cells and immune cell migration. *Arthritis Res.* 2:368-373.

Totsukawa, G., Y. Wu, Y. Sasaki, D.J. Hartshorne, Y. Yamakita, S. Yamashiro, and F. Matsumura. 2004. Distinct roles of MLCK and ROCK in the regulation of membrane protrusions and focal adhesion dynamics during cell migration of fibroblasts. *J. Cell Biol.* 164:427-439.

Turner, T., P. Chen, L.J. Goodly, and A. Wells. 1996. EGF receptor signaling enhances in vivo invasiveness of DU-145 human prostate carcinoma cells. *Clin. Exp. Metastas.* 14:409-418.

Verbeek, B.S., S.S. Adriaansen-Slot, T.M. Vroom, T. Beckers, and G. Rijksen. 1998. Overexpression of EGFR and c-erbB2 causes enhanced cell migration in human breast cancer cells and NIH3T3 fibroblasts. *FEBS Lett.* 425:145-150.

Ware, M.F., A. Wells, and D.A. Lauffenburger. 1998. Epidermal growth factor alters fibroblast migration speed and directional persistence reciprocally and in a matrix-dependent manner. *J. Cell Sci.* 111:2423-2432.

Weiner, O.D. 2002. Regulation of cell polarity during eukaryotic chemotaxis: the chemotactic compass. *Curr. Opin. Cell Biol.* 14:196-202.

Wells, A., K. Gupta, P. Chang, S. Swindle, A. Glading, and H. Shiraha. 1998. Epidermal growth factor receptor-mediated motility in fibroblasts. *Microsc. Res. Techniq.* 43:395-411.

Wells, A., M.F. Ware, F.D. Allen, and D.A. Lauffenburger. 1999. Shaping up for shipping out: PLCγ signaling of morphology changes in EGF-stimulated fibroblast migration. *Cell Motil. Cytoskel.* 44:227-233.

Xie, H., M.A. Pallero, D. Gupta, P. Chang, M.F. Ware, W. Witke, D.J. Kwiatkowski, D.A. Lauffenburger, J.E. Murphy-Ullrich, and A. Wells. 1998. EGF receptor regulation of cell motility: EGF induces dissassembly of focal adhesions independently of the motility-associated PLCγ signaling pathway. *J. Cell Sci.* 111:615-624.

CHAPTER 4

EFFECTS OF ERK AND PI3K SIGNALING ON LAMELLIPODIAL DYNAMICS AND DIRECTIONAL PERSISTENCE IN EGF-INDUCED MOTILITY

Cells migrate via receptor-mediated activation of intracellular signaling networks. While myriad pro-migration signaling targets are known, detailed understanding is still lacking regarding how their activation relates to biophysical processes that underlie motility. Here we report the effects of epidermal growth factor (EGF)-stimulated extracellular signal-related kinase (ERK) and phosphotidylinositol 3-kinase (PI3K) signaling on the speed, persistence, and lamellipodial dynamics of EGF receptor-transfected Chinese Hamster Ovary cells. Graded addition of pharmacological inhibitors revealed that persistence varied biphasically with both ERK and PI3K signaling. To attempt to explain these results, we used kymography to correlate lamellipodial dynamics to ERK and PI3K signaling. Responses distinct to each signaling target were found: lamellipodial protrusion velocity correlated biphasically with PI3K signaling, while protrusion stability increased and then plateaued with decreasing levels of ERK signaling. While the connection of PI3K signaling to protrusion velocity is novel, our previous work defining the role of adhesion-mediated lamellipodial stability in modulating persistence suggested that the biphasic ERK-persistence relationship resulted from ERK-mediated adhesive effects. We confirmed this hypothesis by showing that a competitive soluble RGD peptide decreased persistence at a high level of ERK signaling but increased persistence at a lower level.

Overall, our results show that the control of directional persistence is an important component of how biochemical signaling affects chemokinesis. For ERK, motility does not correlate uniformly with signal, but depends on the magnitude of its biophysical effects. For PI3K, usually connected to the regulation of chemotaxis, these results are the first report that its activity affects directional migration in isotropic environments.

4.1 Introduction

Cell migration is a key aspect of a wide variety of biological processes including embryonic development, angiogenesis, and the immune response. The movement of cells requires highly coordinated biophysical processes including actin polymerization and lamellipodial protrusion, adhesion formation and turnover, and contractile force generation (Lauffenburger and Horwitz, 1996). These biophysical events occur downstream of intracellular signaling cascades activated by the binding of soluble and extracellular matrix ligands to transmembrane receptors (Ridley et al., 2003). Myriad important signaling targets have been identified in the regulation of motility, including small GTPases (Ridley, 2001), phosphatidylinositol kinases (Huang et al., 2003; Weiner, 2002), phospholipase Cγ□ (Piccolo et al., 2002; Wells et al., 1998), calpains (Glading et al., 2002), and extracellular signal-regulated kinases (Stupack et al., 2000). In most cases, however, detailed understanding is still lacking as to the mechanisms by which activation of intracellular signaling targets control cell motility.

Cell paths can be described by two parameters: rate of motion (speed) and the time period over which a cell maintains a roughly constant direction of motion (persistence time) (Dunn, 1983; Othmer et al., 1988). Previously, this quantitative parameterization of the migratory behavior of cells has been valuable for deconstructing how biophysical processes control motility (DiMilla et al., 1991; Maheshwari et al., 1999; Palecek et al., 1997; Ware et al., 1998). Currently, however, little data exists relating the activation of key intracellular signaling targets to their effects on cell speed and directional persistence. As such, the use

of S and P as quantitative dependent variables in signaling studies of motility may give mechanistic insights into how intracellular signaling integrates to control cell migration and the biophysical processes governing it.

The signaling network downstream of the epidermal growth factor receptor (EGFR) is an excellent model system for studying the biochemical regulation of speed and persistence. Both the epidermal growth factor (EGF) and its cognate EGF receptor (EGFR) are widely studied pro-motility cues (Wells et al., 1998), and elevated levels of EGFR correlate with increased invasion potential of tumor cells and increased migration of cultured cell lines (Fontanini et al., 1995; Jorissen et al., 2003; Kaufmann et al., 1994; McCrawley et al., 1997; Turner et al., 1996; Verbeek et al., 1998). Two key molecules activated in EGFR signaling are extracellular signal-regulated kinase (ERK) and phosphotidylinositol 3-kinase (PI3K) (Jorissen et al., 2003; Moghal and Sternberg, 1999). Experiments relating ERK activation to the promotion of cell motility and invasive growth are myriad (see, for example, Klemke et al., 1997; Krueger et al., 2001; Vial et al., 2003; Xie et al., 1998), with ERK affecting migration via its calpain-dependent role in EGF-induced deadhesion (Glading et al., 2000; Glading et al., 2001; Maheshwari et al., 1999) as well as its myosin light chain kinase-dependent role in haptokinetic contractile force generation (Cheresh et al., 1999; Klemke et al., 1997). PI3K appears to be critical for the generation of polarity and directional orientation of cells (Haugh et al., 2000; Huang et al., 2003; Wang et al., 2002; Weiner, 2002). The precise mechanisms behind this requirement are unclear, but seem to involve regulation of lamellipodial actin polymerization. Both PI3K and PI3K lipid products localize to the lamellipodia of chemotaxing cells (Chen et al., 2003; Funamoto et al., 2002; Weiner, 2002), and PI3K has been reported as a requirement for leading edge extension (Cox et al., 1999; Funamoto et al., 2002). EGF-induced migration in breast cancer cells has been reported to be entirely dependent on PI3K activation (Sturge et al., 2002), with PI3K activity essential for EGF-stimulated lamellipodial extension and actin assembly (Hill et al., 2000).

The focus of the work presented in this chapter was to determine the functional forms by which ERK and PI3K signaling regulate speed and persistence in epidermal growth factor-induced motility, and to examine how these forms might be explained by control effects of ERK and PI3K over biophysical processes. Our experiments, conducted in Chinese Hamster Ovary cells transfected with the EGF receptor (see Chapter 3), utilized graded pharmacological inhibition of the ERK and PI3K signals. This methodology allowed the examination of how the effects of EGF-induced ERK and PI3K signaling on migration might change differentially with low, intermediate, and high levels of signal. This is important because it is not clear that in cell motility, where movement result from the integrated effects of signaling on multiple biophysical processes, that the effects of signaling pathway interventions are monotonic, as is usually assumed.

We find that neither ERK nor PI3K has a role in modulating CHO cell speed, but that both ERK and PI3K affect persistence time in a biphasic manner, with maximal persistence occurring at intermediate, non-maximal levels of signaling. In an initial examination of biophysical processes, we studied the role of ERK and PI3K signaling in controlling lamellipodial dynamics and cell adhesion. For PI3K, lamellipodial velocity varies biphasically in response to signal magnitude, but lamellipodial stability is unchanged. For ERK, lamellipodial stability increases and then plateaus as ERK signaling is increasingly inhibited, while lamellipodial protrusion velocity is unchanged. Finally, the entire biphasic ERK-*P* curve can be related to variations in the magnitude of ERK-mediated deadhesion, as addition of a competitive soluble adhesion peptide decreases P at high levels of ERK signaling and increases P at low levels of ERK signaling. Our findings suggest that the quantitative effects of signaling on biophysical processes can be an effective classification scheme for understanding how signaling controls cell migration behavior under specific experimental and environmental conditions.

4.2 Experimental methods

4.2.1 Reagents and cell culture

Antibodies against ERK and Akt were purchased from Upstate Biotechnology (Charlottesville, VA). Dulbecco's Modified Eagle's Medium (DMEM), OptiMEM, fetal bovine serum (FBS), L-glutamine, sodium pyruvate, non-essential amino acids, penicillin, streptomycin, geneticin/G418 sulfate, HEPES, trypsin, Versene (EDTA) and phosphate-buffered saline (PBS) were purchased from Life Technologies (Carlsbad, CA). Bovine serum albumin (BSA), human fibronectin (Fn) and recombinant human epidermal growth factor (EGF) were purchased from Sigma Chemical (St. Louis, MO). PD98059 and LY294002 were purchased from Calbiochem (San Diego, CA). Unless noted, all other reagents were purchased from Sigma Chemical.

The generation of the CHO-EGFR cell line, consisting of CHO K1 cells stably transfected with an EGFR-GFP fusion protein, was described in Chapter 3. Cells were grown in high-glucose DMEM containing 10% FBS (v/v), 2 mM glutamine, 1 mM sodium pyruvate, 1 mM non-essential amino acids, 100 U/ml penicillin and 100 μg/ml streptomycin, and 500 μg/ml G418.

4.2.2 Cell pre-treatment for experiments

CHO-EGFR cells were serum-starved for 18 hours in medium substituting 2 mg/ml BSA for the FBS in growth medium. Cells were then lifted from culture plates using protease-devoid Versene, pelleted, and resuspended for 1 hour in serum-free medium buffered with 15 mM HEPES rather than sodium bicarbonate. After suspension, cells were pelleted and resuspended for plating in assay medium consisting of OptiMEM supplemented with penicillin (100 U/ml) and streptomycin (100 μg/ml), as well as 25 nM EGF as appropriate. For experiments using the MEK inhibitor PD98059 or the PI3K

inhibitor LY294002, both the HEPES-based serum-free medium and the assay medium contained inhibitor (stocks prepared by dissolving in DMSO at 50 mM).

4.2.3 Preparation of surfaces for experiments

For migration experiments, glass-bottomed dishes (Bioptechs, Butler, PA) were incubated overnight at 4°C with 10 μg/ml Fn dissolved in 0.5 ml PBS. The Fn solution was aspirated and the dishes rinsed twice with 1 ml PBS. Dishes were then incubated for 1 hour at 37°C with 0.5 ml 1% BSA in PBS. The BSA solution was aspirated and the dishes rinsed twice with 1 ml PBS. All prepared dishes were stored under PBS at 37 °C until ready for use (<30 minutes in all cases). This coating protocol was also used for the signaling experiments while maintaining an identical surface-to-volume ratio. For ERK studies, 60-mm round glass coverslips were adhered to tissue culture dishes using epoxy before coating with Fn. For Akt studies, 100-mm TC dishes were coated directly with Fn.

4.2.4 Migration assay and kymography

Cell speed and persistence was measured using single-cell time-lapse videomicroscopy performed on a Zeiss Axiovert 35 microscope with 10×-magnification differential interference contrast objective (Carl Zeiss Microimaging, Thornwood, NY). Cells suspended in assay medium (17500 total per experiment) were plated onto Fn-coated assay dishes and allowed to adhere for 3 hours in order for steady-state behavior to develop (data not shown). The dish was placed into a heated stage insert (Bioptechs) for a motorized stage (Ludl Electronic Products, Hawthorne, NY). Twenty separate fields containing 80-100 total cells were then digitally imaged every 15 minutes for 6 hours. Cell outlines and *xy*-centroids were determined using DIAS (Solltech, Inc., Oakdale, IA). Analysis of average experimental cell speed (S) and persistence time (P) followed the persistent random walk fitting method described in Chapter 3. Each experiment was repeated 3 times; associated

error bars represent ±2 SE. All computational routines were implemented in MATLAB 5.3 (The MathWorks, Inc., Natick, MA).

Generation and analysis of kymographs proceeded as described in Chapter 3. Briefly, to generate kymographs, cells were treated and plated as in the migration experiments. Time-lapse movies with length 25 minutes and image capture interval 5 seconds were obtained using a 40×-magnification phase-contrast objective. Kymographs were produced using Metamorph software (Universal Imaging Corp., Downington, PA). Kymographs were analyzed using the parameters of protrusion stability and velocity (Bear et al., 2002; also see Chapter 3). Reported averages ±2 SE represent the mean of two independent experiments per condition with 15-20 cells per experiment.

4.2.5 Cell stimulation and lysis

After cell suspension in assay medium, 1.5×10^6 (ERK) or 5×10^6 (Akt) cells per dish were plated in parallel onto Fn-coated plates. For lysis, cells were placed on ice, washed with cold PBS, and scraped into cold buffer containing 1% Triton X-100, 50 mM Tris-HCl (pH 7.5), 150 mM sodium chloride (NaCl), 50 mM β-glycerophosphate (pH 7.3), 10 mM sodium pyrophosphate, 30 mM sodium fluoride, 1 mM benzamidine, 2 mM EGTA, 100 μM sodium orthovanadate ($NaVO_4$), 1 mM dithiothreitol (DTT), 10 μg/ml aprotinin, 10 μg/ml leupeptin, 1 μg/ml pepstatin, 1 mM phenylmethylsulfonyl chloride (PMSF), and 1 μg/ml microcystin-LR. Lysates were clarified by centrifugation at 16000*g* for 15 minutes at 4°C. Supernatant protein concentrations were determined with a bicinchoninic acid assay (MicroBCA, Pierce Biotechnology, Rockford, IL) and ranged from 0.6-1 mg/ml for ERK and 3-4 mg/ml for Akt.

4.2.6 ERK and Akt kinase assay

Kinase activity was measured using an *in vitro* kinase assay performed in a 96-well microtiter plate format essentially as described previously (Asthagiri et al., 1999; Janes et al.,

2003). Protein A (ERK) or Protein G (Akt) coated microtiter wells (Reacti-Bind, Pierce) were incubated overnight at 4°C with 10 μg/ml anti-ERK or anti-Akt antibody in 50 μl blocking buffer (1% BSA in 50 mM Tris-HCl, 150 mM NaCl, and 0.05% Triton X-100). After washing thrice with 200 μl blocking buffer, wells were incubated with 50 μl (ERK) or 100 μl (Akt) cell lysate for 3 hours at 4°C. Wells were then washed twice with 200 μl wash buffer (50 mM Tris-HCl, 150 mM NaCl) and twice with 200 μl kinase wash buffer (20 mM Tris-HCl, 15 mM magnesium chloride, 5 mM β-glycerophosphate, 1 mM EGTA, 0.2 mM $NaVO_4$, and 0.2 mM DTT). After washing, each well was filled with 20 μl kinase wash buffer and 20 μl kinase assay buffer consisting of kinase wash buffer plus 0.4 μM protein kinase A inhibitor (Upstate), 4 μM protein kinase C inhibitor (Upstate), 4 μM calmidizolium, and 25 μM cold ATP mixed with 1 μCi [γ-^{32}P]ATP (PerkinElmer Life Sciences, Boston, MA) for ERK or 5 μM cold ATP mixed with 5 μCi [γ-^{32}P]ATP for Akt. The reaction was initiated by addition of 20 μl substrate solution (40 μg myelin basic protein for ERK or 10 μM Aktide (Janes et al., 2003) for Akt). Kinase reactions were run for 60 (ERK) or 30 (Akt) minutes at 37 °C on a Jitterbug plate shaker (Boekel Scientific, Feasterville, PA) and quenched via addition of 60 μl of 75 mM phosphoric acid. Forty μl of the quenched reaction mixture was transferred to a phosphocellulose filter plate (Millipore, Billerica, MA) and vacuum-filtered to bind kinase reaction products. Unreacted [γ-^{32}P]ATP was removed through washing five times with 200 μl H_3PO_4 followed by three times with 200 μl 70% ethanol. The filters were punched into scintillation vials and sample radioactivity quantified using a scintillation counter. Background radioactivity was subtracted from all samples; control wells were incubated with just lysis buffer during the immunoprecipitation step and carried though the assay with the other samples.

4.3 Results

4.3.1 Partial inhibition of ERK or PI3K increases CHO-EGFR motility but higher inhibition limits it

The important role of intracellular signaling through the ERK and PI3K pathways in controlling both haptokinetic and chemokinetic cell migration is well-established (Glading et al., 2000; Haugh et al., 2000; Hill et al., 2000; Huang et al., 2003; Klemke et al., 1997). However, it is unknown if there is an optimal level of activity that drives motility, while excess activity might contribute to competing cell responses. To address this question, we examined the motogenic effects of both ERK and PI3K signaling over a broad range of inhibitor concentrations. We note first that no significant variation in migration occurred, as visually inspected by wind-rose plots, when adding increasing levels of the MEK inhibitor PD98059 and the PI3K inhibitor LY294002 in the absence of EGF (data not shown). In contrast, Fig. 4.5.1 shows the difference in cell tracks resulting from increasing levels of these inhibitors in the presence of EGF. Relative to baseline EGF-stimulated migration (Fig. 4.5.1*A*), the dispersion response of CHO-EGFR cells increases with addition of 0.5 μM PD98059, and then increases again as the amount of PD98059 added rises to 5 μM. However, a PD98059 level of 50 μM resulted in a decrease in overall dispersion to a level below that of baseline (Fig. 4.5.1*B*). A similar biphasic response occurs for increasing levels of LY294002, with increased migration at 0.5 μM inhibitor, maximal migration at 5 μM, and decreased migration at 50 μM (Fig. 4.5.1*C*). Taken together, the wind-rose plots reveal an unexpected non-monotonic regulation of cell motility by ERK and PI3K.

4.3.2 Pharmacological inhibition of EGF-induced ERK and PI3K activation

As shown above, differential increasing inhibition of both ERK and PI3K signaling affects EGF-induced CHO-EGFR cell motility in a non-linear, non-monotonic fashion. To establish the levels of intracellular ERK and PI3K signaling underlying these biphasic

effects, a microtiter plate-based combined immunoprecipitation and kinase assay was utilized to examine signaling timecourses during migration experiments. We first examined the role of Fn in affecting signaling in our system. EGF-stimulated cells were plated on dished coated with four different levels of Fn and lysed at timepoints ranging from 10 minutes to 9 hours post-plating (3-9 hours post-plating corresponds to the 6-hour observation window for migration experiments). Fig. 4.5.2*A* shows the resultant ERK timecourses. Because no dependence of ERK signal on Fn was noted, we chose one coating concentration only (10 μg/ml) for further studies. Next, we examined the timecourse of ERK signaling resulting from the range of inhibitors used in the wind-rose plots of Fig. 4.5.1*B*. Our primary purpose in generating these timecourses was to assess whether quantitative changes in signal strength affected the qualitative shape of the EGF-induced signaling response. As is shown by Fig. 4.5.2*B*, ERK activation at all inhibition levels peaked at 10 minutes and then declined in magnitude until 1 hour, after which the level of activity remained roughly constant. Thus increasing levels of inhibitor quantitatively reduced the magnitude of signal without affecting its activation dynamics.

We next ascertained the timecourse of Akt activation during migration experiments. Akt is an important downstream effector of PI3K signaling in motility (Firtel and Chung, 2000; Qian et al., 2004). Fig. 4.5.2*C* shows representative timecourses for ERK and Akt in the absence of pharmacological inhibition. In contrast to the decaying initial spike in initial ERK activation, Akt signaling rose over a 20-minute period after plating and then remained constant through the remainder of the experiment.

As migration experiments began at 3 hours after cell plating and both ERK and Akt signaling are essentially steady-state at that point, we chose the 3-hour timepoint to assess the overall level of ERK and Akt signaling in the presence of pharmacological inhibitors. Both ERK and Akt show dose-dependent reduction in signaling across a wide range of activation levels (Table 1). Thus in both cases we were able to assay broad ranges of signal strength for a thorough exploration of the role of ERK and Akt in cell motility.

4.3.3 Biphasic regulation of persistence time by both ERK and PI3K signaling

The wind-rose plots of Fig. 4.5.1 indicate that the dispersion response of EGF-stimulated CHO-EGFR cells is maximal at intermediate levels of both ERK and PI3K signal abrogation. To quantify the cell motility parameters underlying these effects, we calculated speed (*S*) and persistence time (*P*) for each individual cell and obtained experimental averages for both parameters (Fig. 4.5.3 and 4.5.4). CHO-EGFR speed remained constant across all levels of intracellular ERK signaling tested, at about ~13 μm/hr (Fig. 4.5.3*A*). Similarly, increasing abrogation of the level of PI3K signaling did not significantly affect cell speed (Fig. 4.5.3*B*).

In contrast, the directional persistence of EGF-induced CHO-EGFR migration shows a marked biphasic response to the levels of both ERK and PI3K signaling (Fig. 4.5.4). Reduction of ERK signaling via addition of 0.5 and 5 μM PD98059 increased persistence time approximately 14% and 50%, respectively, while higher ERK inhibition using 10, 25, and 50 μM PD98059 reduced persistence 28%, 28%, and 35% below baseline response, respectively (Fig. 4.5.4*A*). Similarly, addition of 0.5, 5, and 50 μM LY294002 changed CHO-EGFR directional persistence relative to baseline by 25%, 82%, and -57% (Fig. 4.5.4*B*). From these results, we conclude that the differences in CHO-EGFR migration shown by the wind-rose plots of Fig. 4.5.1 result from previously unobserved biphasic variations in directional persistence in response to changing ERK and PI3K signaling levels.

4.3.4 Distinct effects of ERK and PI3K signaling on CHO-EGFR lamellipodial dynamics

EGF is known to induce both acute (Segall et al., 1996) and long-term (Maheshwari et al., 1999; Ware et al., 1998) induction of membrane protrusive activity. Moreover, both ERK and PI3K are linked to chemokinetic lamellipodial extension and actin polymerization (Brahmbhatt and Klemke, 2003; Hill et al., 2000; Stähle et al., 2003). Finally, our work

described in Chapter 3 indicates that changes in lamellipodial dynamics can affect directional persistence in CHO-EGFR cells. Thus, in an initial attempt to understand the biophysical basis for how ERK and PI3K signaling modulate directional persistence, we next determined the lamellipodial dynamics of CHO-EGFR cells as a function of EGF-induced ERK and PI3K signaling. Fig. 4.5.5 shows the effects of ERK signaling on lamellipodial protrusion events. The average velocity of protrusion remained constant across all levels of PD98059 examined (Fig. 4.5.5*A*; ANOVA p = 0.35). In contrast, lamellipodial stability tended to increase and then plateau with decreasing levels of ERK signaling (Fig. 4.5.5*B*). This inverse ERK-stability correlation was modest (p = 0.11) and surprising in that lamellipodial stability did not decline at 50 μM PD98059 as was seen with persistence (Fig. 4.5.4*A*).

Unexpectedly, we observed distinctly different lamellipodial dynamics as a function of PI3K signaling (Fig. 4.5.6). The average temporal stability of individual protrusion events remained constant through the entire range of PI3K signaling (Fig. 4.5.6*B*; p = 0.67). In contrast, the average velocity of protrusion varied biphasically in concert with the overall magnitude of directional persistence, with maximal response in both cases occurring at 5 μM LY294002 (Fig. 4.5.6*A*; cf. Fig. 4.5.4*B*). These changes in protrusion velocity, while statistically significant (p = 0.001), were of smaller relative magnitude than the corresponding PI3K-dependent changes in persistence described above.

4.3.5 Monotonic effects of ERK signaling on cell adhesion account for the biphasic ERK-persistence response

Our work in Chapter 3 connected adhesion-mediated changes in lamellipodial stability to modulation of directional persistence in CHO-EGFR migration. Moreover, EGF stimulates cell deadhesion through an ERK-mediated signaling pathway that activates the cytoskeletal protease calpain (Glading et al., 2000; Maheshwari et al., 1999; Xie et al., 1998). We reasoned that the observed inverse correlation between ERK signaling and lamellipodial

protrusion stability reflected this deadhesive effect, and hypothesized that ERK effects on cell adhesion might account for the biphasic ERK-persistence response.

To test this hypothesis, we examined the effects of soluble GRGDSP peptide on directional persistence at various levels of ERK inhibition. Synthetic peptides containing the RGD sequence are competitive inhibitors of Fn binding to the $\alpha_5\beta_1$ integrins expressed by CHO cells, and have been shown previously to inhibit cell migration (Fujii et al., 1998; Libotte et al., 2001; Shimizu et al., 1997). Addition of RGD peptide at 5 μM PD98059, corresponding to the level of ERK signaling giving maximal *P*, reduced *P* substantially (Fig. 4.5.7). In marked contrast, we found that at higher levels of ERK inhibition (10 and 25 μM PD98059), the addition of RGD peptide increased *P*. Control addition of GRADSP peptide had no effect on *P* (data not shown). These results indicate that the complex biphasic ERK-*P* curve results from simple monotonic changes in cell adhesion strength downstream of ERK signaling. It is unlikely that any changes in ERK signaling itself come from addition of RGD peptide, as our experiments were unable to find any Fn-dependent variation in ERK signaling (Fig. 4.5.2).

4.4 Discussion

Cellular processes such as proliferation, differentiation, apoptosis, and migration are controlled by the coordinated activation of intracellular signaling networks. Proliferation, differentiation, and apoptosis present binary decisions to a cell. In such a context, greater activation of a key signaling protein might well be expected to correlate directly with a downstream cell process via a switch-like mechanism. However, a binary "on-off" view of cell signaling clearly does not fit in modeling migration, where effective motility is the result of a coordinated balance of biochemically-controlled biophysical processes like adhesion formation and turnover, contractile force generation, and lamellipodial protrusion that themselves are not binary responses. Nevertheless, the operating assumption in most experimental approaches to studying signaling in motility is that signaling proteins exert

their effects on cells in a linear fashion, and that increased signal activation correlates with motility (see for instance, Krueger et al., 2001).

We have tested the validity of this assumption by examining the role of ERK and PI3K signaling in the EGF-induced motility of EGF receptor-transfected CHO cells, focusing on the differential changes in cell speed (S), directional persistence (P), and lamellipodial dynamics that result from increasing levels of pharmacological signal inhibition. We found the following: *(a)* neither ERK nor PI3K plays a role in modulating S; *(b)* the level of activation of both ERK and PI3K affects P in a biphasic manner, with maximal persistence occurring at intermediate, non-maximal levels of signaling; *(c)* lamellipodial velocity varies biphasically in response to PI3K signal strength; *(d)* lamellipodial stability increases and then plateaus as ERK signaling is increasingly inhibited; and *(e)* the biphasic ERK-persistence curve can be related to monotonic variation in cell adhesion due to ERK signaling, as addition of a competitive soluble adhesion peptide decreases P at high levels of ERK signaling and increases P at low levels of ERK signaling. A schematic summarizing these results may be found in Fig. 4.5.8.

Our experimental protocols for studying the role of signaling in motility were critical for the results presented in this chapter. The use of S and P as descriptive parameters for motility allowed us to ascertain more clearly the role of ERK and PI3K activation in EGF-induced migration. Specifically, had we chosen to use other typical assays of cell motility such as Boyden chambers and in vitro 'wound healing' assays, we would likely have established biphasic relationships between signal activation and general migratory potential, but would not have ascertained that both ERK and PI3K signaling regulate migration by modulating directional persistence only. Changes in migratory potential are usually assumed to derive from variations in cell speed, but overall cell scattering is actually proportional to S^2P and thus has a persistence component as well (Maheshwari and Lauffenburger, 1998). We also note that our more extensive protocol involving multiple levels of signal strength was necessary in order to not miss the biphasic nature of the

persistence regulation; typical use of high levels of both PD98059 (50 μM) and LY294002 (50 μM) would have established a positive correlation between signaling and persistence (Fig. 4.5.4) while missing the strong negative correlation at lower levels of inhibition and higher levels of signaling.

Our work in Chapter 3 indicating that changes in persistence are a key part of the regulation of CHO-EGFR migration motivated our choice of PI3K as a signaling target of interest. PI3K plays a well-established role in potentiating cell polarity and chemotaxis in eukaryotic cells (Haugh et al., 2000; Huang et al., 2003; Wang et al., 2002; Weiner, 2002), but we believe our results are the first evidence of a role for PI3K in directional migration in a uniform chemokinetic environment. We currently lack mechanistic understanding of the biphasic relationship between PI3K activity and directional persistence, in particular whether that relationship is caused by or merely correlates with the similar relationship between PI3K signal and lamellipodial protrusion velocity. Clearly, however, the results correlating PI3K activity with control of lamellipodial protrusion velocity are consistent with previous studies reporting PI3K and its lipid products as requirements for leading edge extension and lamellipodial actin polymerization (Chen et al., 2003; Cox et al., 1999; Funamoto et al., 2002).

Further studies are needed, but this PI3K effect on protrusion suggests a possible intermediary role for Rho family GTPases, in particular Rac and Cdc42, in regulating CHO-EGFR directional persistence. Rac and Cdc42 are downstream of EGF-mediated PI3K activation and chemotaxis in breast cancer cells (Sturge et al., 2002), and Rac and Cdc42 are activated by EGF and combine to induce lamellipodia and membrane ruffles in both Cos1 and A431 cells (Kurokawa et al., 2004). Moreover, PIP_3 binding is necessary for activation of the Rac effector WAVE upstream of Arp2/3 complex activation and actin polymerization (Oikawa et al., 2004). A positive feedback loop between PI3K and Rac regulates leading edge actin polymerization in neutrophils, with Cdc42 activity guiding the location and stability of the leading edge (Srinivasan et al., 2003; Wang et al., 2002; Weiner et al., 2002).

Thus the interplay of Rac, Cdc42, and PI3K is likely to be important in the persistence behavior of our cells as well. Alternatively, the effects of PI3K signaling on directional persistence in chemokinesis may be due to an interaction with FAK. FAK activation has been shown to promote directionally persistent migration (Gu et al., 1999); moreover, PI3K is known to associate with FAK downstream of PDGF stimulation (Chen and Guan, 1994), and to be required for FAK-dependent migration of CHO cells (Reiske et al., 1999).

We showed in Chapter 3 that higher cell-substratum adhesion strength causes increased stability of CHO-EGFR lamellipodial protrusions leading to increased persistence time. The protrusive stabilization effect, in concert with the known deadhesive function of EGF-induced ERK activation of calpain (Glading et al., 2000; Glading et al., 2001; Maheshwari et al., 1999), accounts for our data showing a monotonic increase in lamellipodial stability with decreasing ERK signaling (Fig. 4.5.5*B*). Interestingly, lamellipodial stability plateaus at 5 μM PD98059, with further decreases in ERK signal strength having no stability effect. This result is consistent our observations of an increase in average cell area between 0-5 μM PD98059 but not between 5-50 μM (data not shown). Significantly, this plateau in lamellipodial stability indicates that ERK effects on adhesion-mediated protrusive stability are not the sole cause of ERK-mediated variations in CHO-EGFR persistence. If that were the case, the ERK-persistence plot would be monotonic and addition of soluble RGD peptide would reduce *P* at all levels of ERK signaling.

Instead, we see that at the lowest levels of ERK signal studied, *P* drops in a biphasic manner, and addition of RGD peptide increases *P* (Fig. 4.5.4*A* and 4.5.7). To account for these results, we propose an extension of the idea of adhesion-mediated persistence time to a framework where competing effects of ERK signaling on contractile force generation (Brahmbhatt and Klemke, 2003; Cheresh et al., 1999; Klemke et al., 1997; Totsukawa et al., 2004) and adhesion (Glading et al., 2000; Glading et al., 2001) controls ERK-mediated CHO-EGFR persistence (Fig. 4.5.9). Recently, pseudopodia growth in COS-7 and NIH3T3 cells was associated with strong chemotactic ERK activation leading to MLC phosphorylation

specifically localized to the leading edge (Brahmbhatt and Klemke, 2003). In contrast, inhibition of ERK via addition of PD98059 prevented both MLC activity and protrusive activity. Importantly, the level of PD98059 used by Brahmbhatt and Klemke was 50 μM, the same high level at which the CHO-EGFR cells show decreased *P*. Applying this information to our experiments, the biphasic ERK-persistence curve would thus result from two opposing effects: (1) adhesion-mediated increases in *P* at low levels of ERK inhibition, shown by increasing levels of lamellipodial stability (Fig. 4.5.8) and the ability of RGD peptide to reduce *P* (Fig. 4.5.7) (also see Chapter 3); and (2) contractility-dependent decreases in *P* at higher levels of ERK inhibition. In the second case, while individual waves of lamellipodial protrusion are relatively stable with low ERK signaling, the lack of MLC-mediated contractility at the leading edge prevents the cell from generating sufficient cytoskeletal and adhesion organization for persistent cell polarity and directional migration. In such a situation, addition of RGD peptide increases *P* (Fig. 4.5.7) by reducing adhesion and thereby lowering the level of force necessary for the cytoskeletal and adhesive organization necessary for persistent migration. We mention here that one paper has indeed reported increases in the directional persistence of migration that correlate with more extensive actin cytosketetal organization (Gu et al., 1999).

Implicit in the above explanation is the idea that specific signaling proteins like ERK can affect multiple biophysical aspects of cell motility simultaneously, in this case adhesion and force generation. Moreover, a signaling molecule's regulation of any one biophysical process can be either rate-limiting for motility or merely permissive depending on specific intracellular conditions. This implies that for full understanding of the function of ERK, PI3K, or any other critical signaling network component in cell migration, quantitative experiments sampling a large experimental parameter space are necessary. We believe that such an approach, when combined with other genomic and proteomic tools, should lead to a model of *in vitro* cell signaling that results in improved guidance in how to design motility-altering therapeutics for use *in vivo*.

4.5 Figures

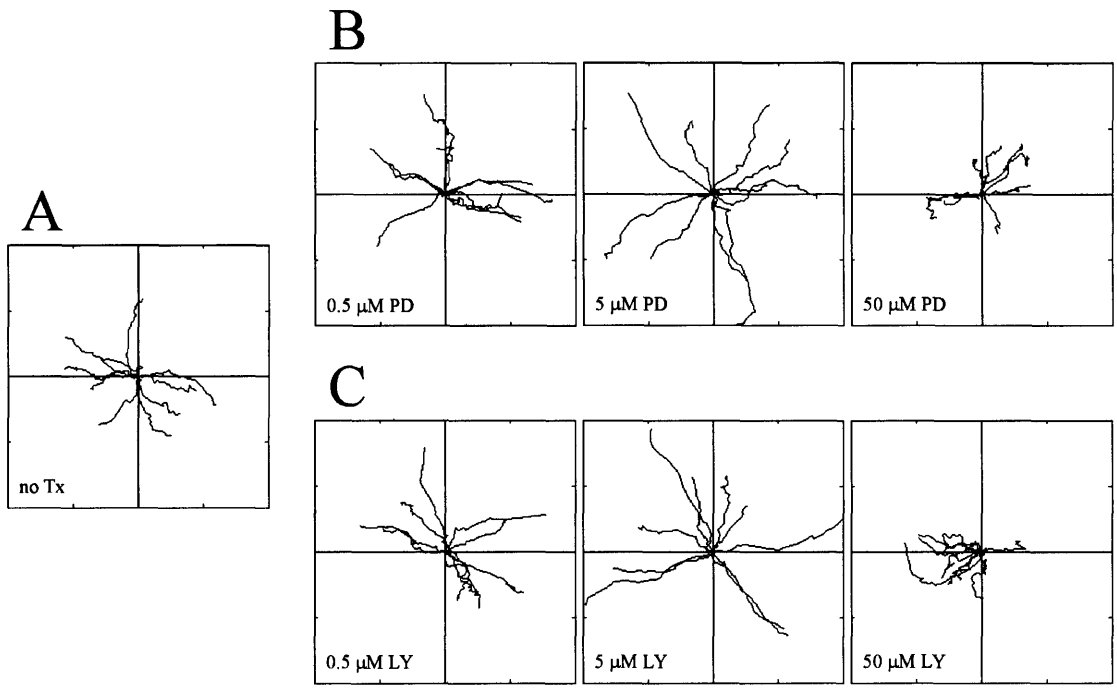

Figure 4.5.1 Effects of variations in ERK and PI3K signaling level on EGF-stimulated migration of CHO-EGFR cells.
Time-lapse videomicroscopy was used to capture the migration of individual cells on 10 μg/ml Fn over a 6 hour period. Each wind-rose plot shows centroid tracks from ten representative cells in a typical experiment, with the initial position of each track superimposed at (0,0] for clarity. Distance between hatch marks on both axes is 50 μm. PD = PD98059; LY = LY294002.

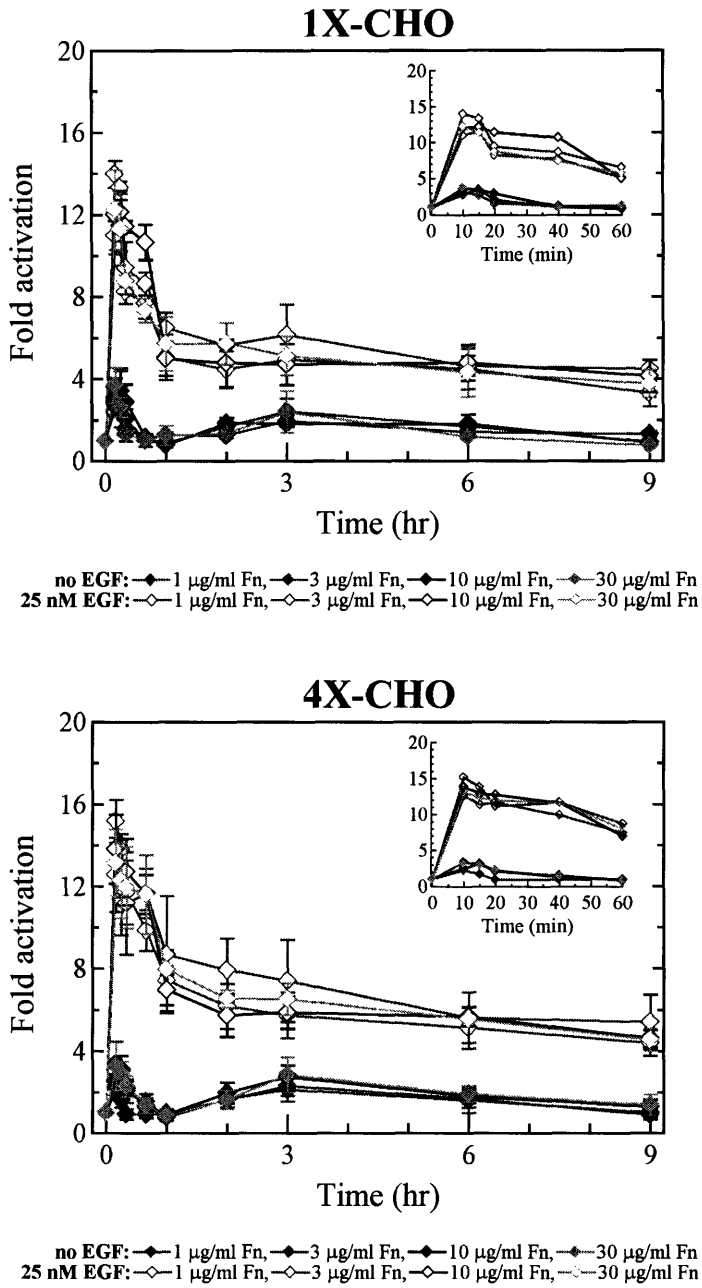

Figure 4.5.2*A* Effects of EGF and Fn on ERK activation of CHO-EGFR cells.
Cells were plated on dishes coated with varying amounts of Fn to ascertain the combined role of EGF and Fn in CHO-EGFR signaling. ERK activity in lysates was ascertained using a microtiter plate-formated *in vitro* kinase assay. No dependence of signal on Fn coating concentration was found, and EGFR expression level had only a small positive effect on signal. Data in each experiment was normalized to lysates from cells suspended but not replated on dishes. Error bars represent ± SE of three independent experiments.

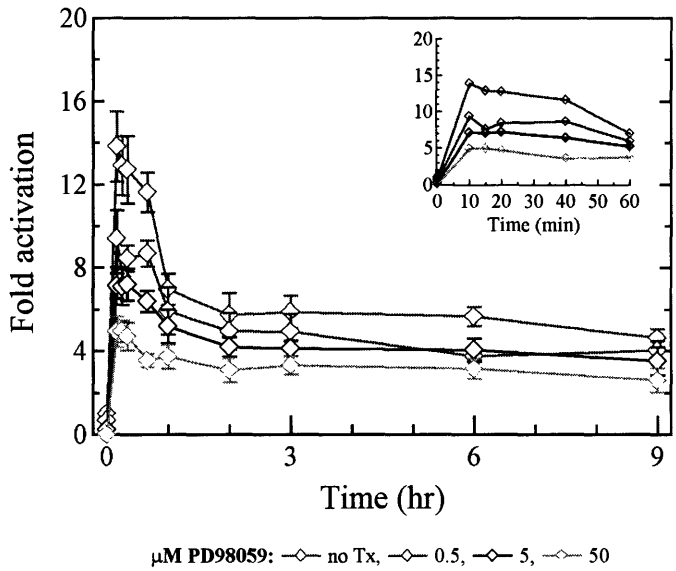

Figure 4.5.2*B* Modulation of 4×-CHO ERK activation using graded levels of soluble inhibitor.
Cells were plated on dishes coated with 10 μg/ml Fn in media containing EGF and listed concentrations of the MEK inhibitor PD98059. After lysis at the appropriate times, ERK activity in lysates was ascertained using a microtiter plate-formated *in vitro* kinase assay. Data in each experiment was normalized to lysates from cells suspended but not replated on dishes. Error bars represent ± SE of three independent experiments.

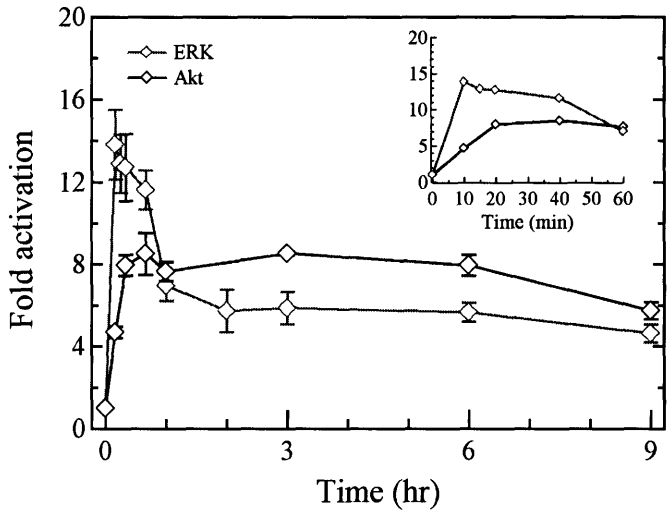

TABLE 1 Modulation of EGF-induced ERK and Akt signal using soluble inhibitors*

[PD98059] (μM)	ERK induction**	Relative ERK activity	[LY294002] (μM)	Akt induction**	Relative Akt activity
0	5.89 ± 0.79	1	**0**	8.06 ± 2.15	1
0.5	4.93 ± 0.86	0.84	**0.5**	6.86 ± 1.65	0.85
5	4.12 ± 0.36	0.70	**5**	3.95 ± 0.12	0.49
50	3.31 ± 0.43	0.56	**50**	1.04 ± 0.03	0.13

*At 3-hr timepoint
**Errors represent ±SE

Figure 4.5.2C Representative timecourses of EGF-induced ERK and Akt signaling in CHO-EGFR cells.
4×-CHO cells were plated on dishes coated with 10 μg/ml Fn and lysed at the appropriate times. ERK and Akt activities in lysates were ascertained using a microtiter plate-formated *in vitro* kinase assay. Data was normalized to lysates from cells suspended but not replated on dishes. Error bars represent ± SE.

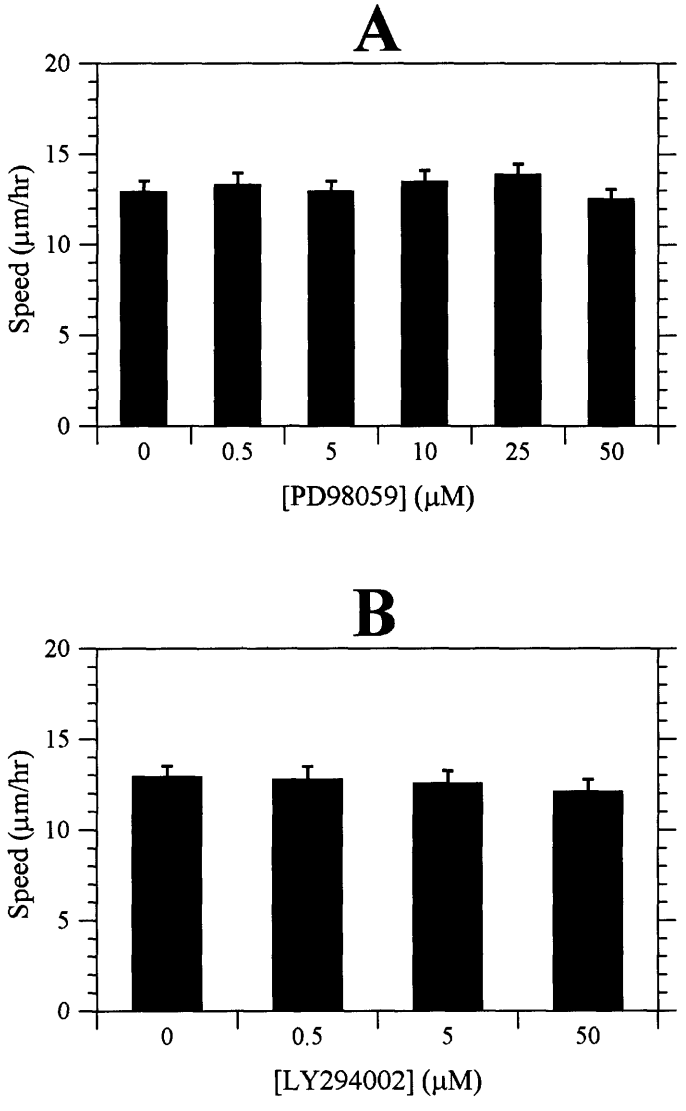

Figure 4.5.3 Neither ERK (*A*) nor PI3K (*B*) signal strength affects 4×-CHO speed.
Cell speed is derived by dividing cell path length by total tracking time. The mean speed of each experiment resulted from averaging the speed of 80-100 total cells; reported speeds represent the mean ± 2 SE of 3 experiments per condition. ANOVA: $p = 0.97$ (ERK), $p = 0.96$ (PI3K).

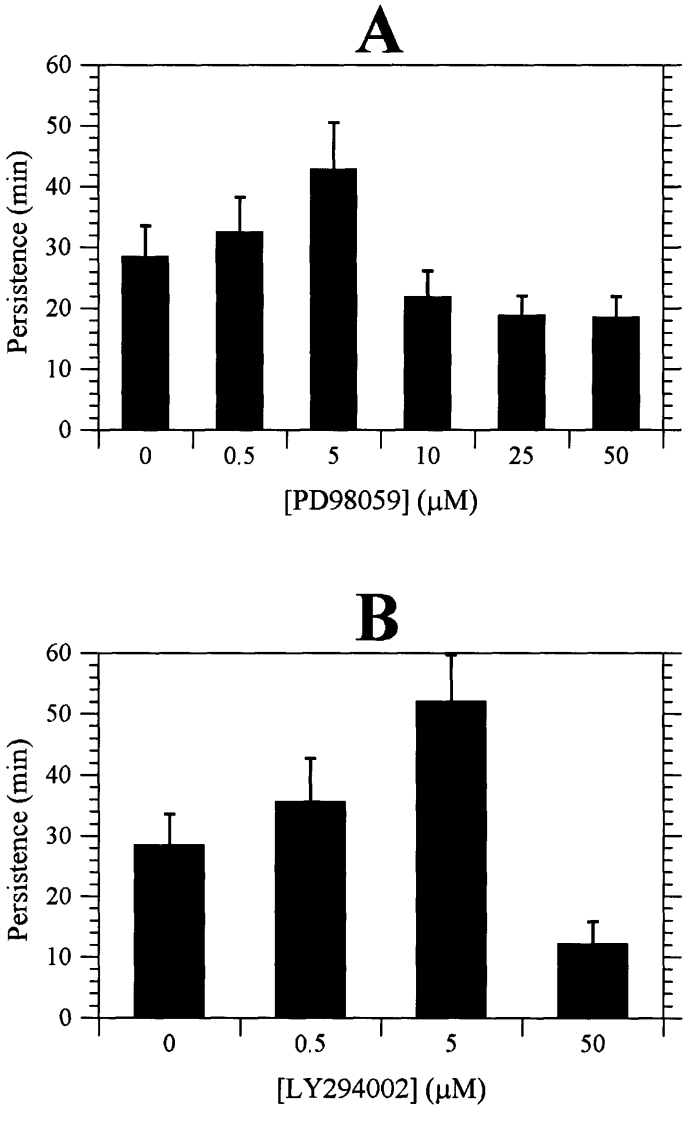

Figure 4.5.4 Biphasic relationships between EGF-induced ERK (*A*) and PI3K (*B*) signaling and 4×-CHO directional persistence.
Single cell persistence times were derived from non-linear least-squares regression using individual cell speed and root-mean-square displacement data as inputs. Reported persistence times are calculated using the same methodology as cell speed. ANOVA: $p = 0.02$ (ERK), $p = 0.01$ (PI3K).

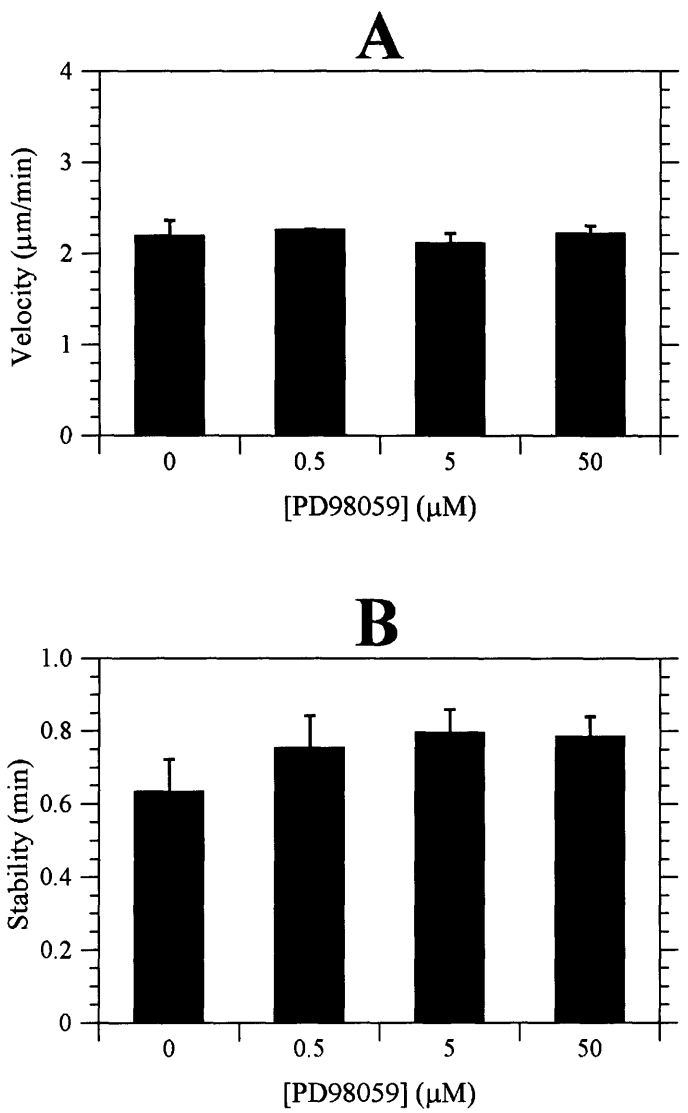

Figure 4.5.5 Quantification of CHO-EGFR lamellipodial dynamics as a function of ERK signaling level.
(*A*) ERK does not affect the average velocity of 4×-CHO membrane protrusion. The average slope of ascending kymograph membrane waves defines protrusion velocity. ANOVA: $p = 0.35$.
(*B*) 4×-CHO protrusion stability increases and then plateaus as ERK signal strength decreases. Stability represents the time elapsed between the beginning of a single protrusion wave and its spatial peak. ANOVA: $p = 0.11$. Reported data for (*A*) and (*B*) represent analysis of 30-36 total cells from two independent experiments per condition.

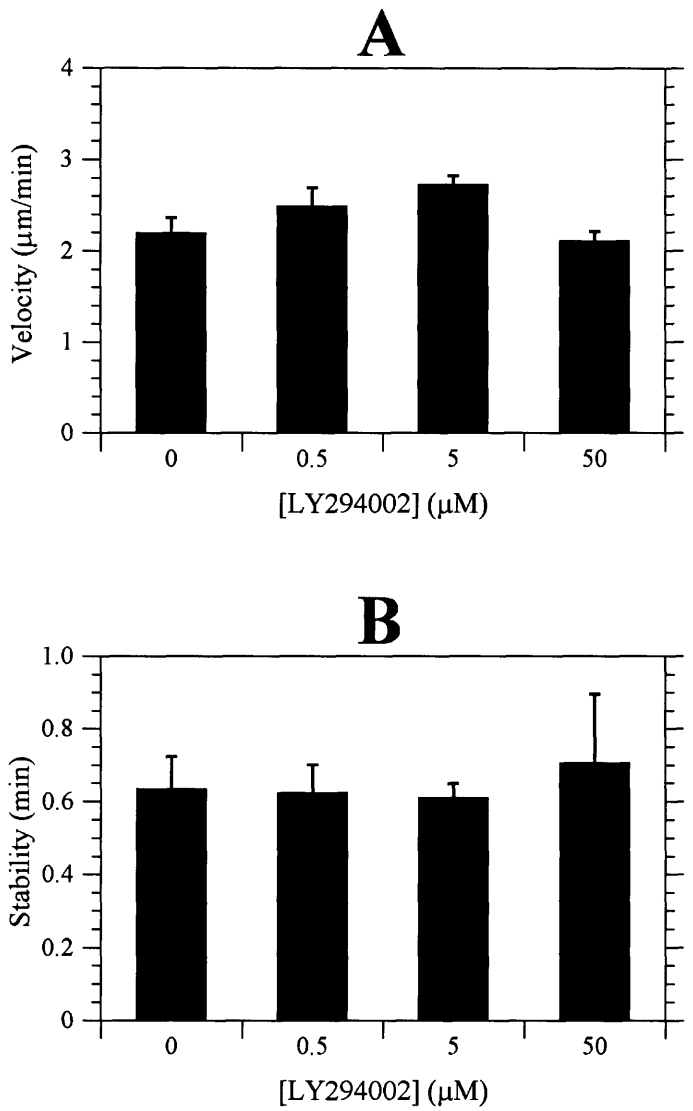

Figure 4.5.6 Quantification of CHO-EGFR lamellipodial dynamics as a function of PI3K signaling level.
(*A*) PI3K affects the velocity of 4×-CHO membrane protrusions in a biphasic manner. ANOVA: p = 0.001.
(*B*) 4×-CHO protrusion stability is not affected by the level of PI3K signaling. ANOVA: p = 0.67. Reported data for (*A*) and (*B*) represent analysis of 30-36 total cells from two independent experiments per condition.

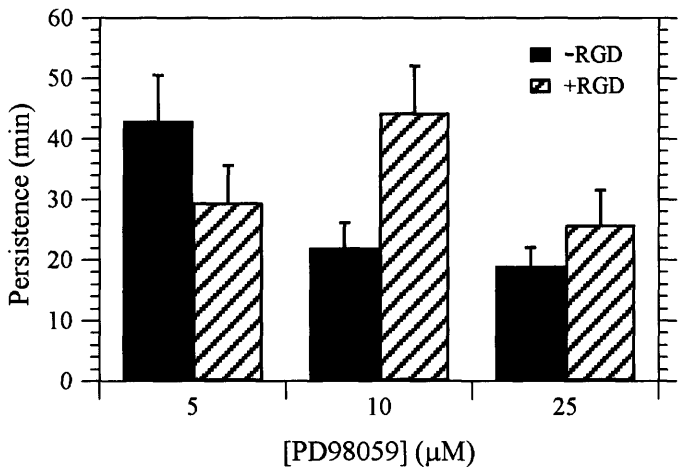

Figure 4.5.7 Effect of anti-adhesion peptides on biphasic ERK-persistence curve.
Thirty μM soluble GRGDSP peptide was added to 4×-CHO migration experiments also containing the MEK inhibitor PD98059. RGD peptide reduces persistence at high levels of ERK signaling but increases persistence at low levels.

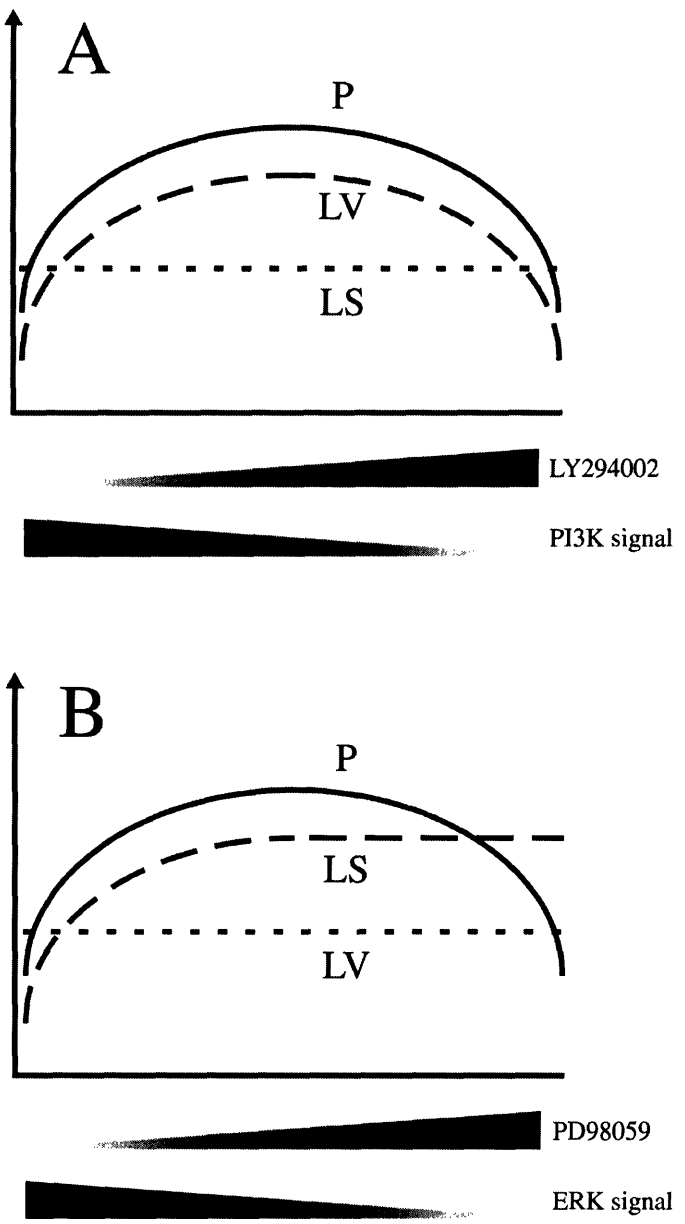

Figure 4.5.8
Schematics depicting the dependence of persistence (*P*), lamellipodial velocity (*LV*), and lamellipodial stability (*LS*) on the level of EGF-induced PI3K (*A*) and ERK (*B*) signaling.

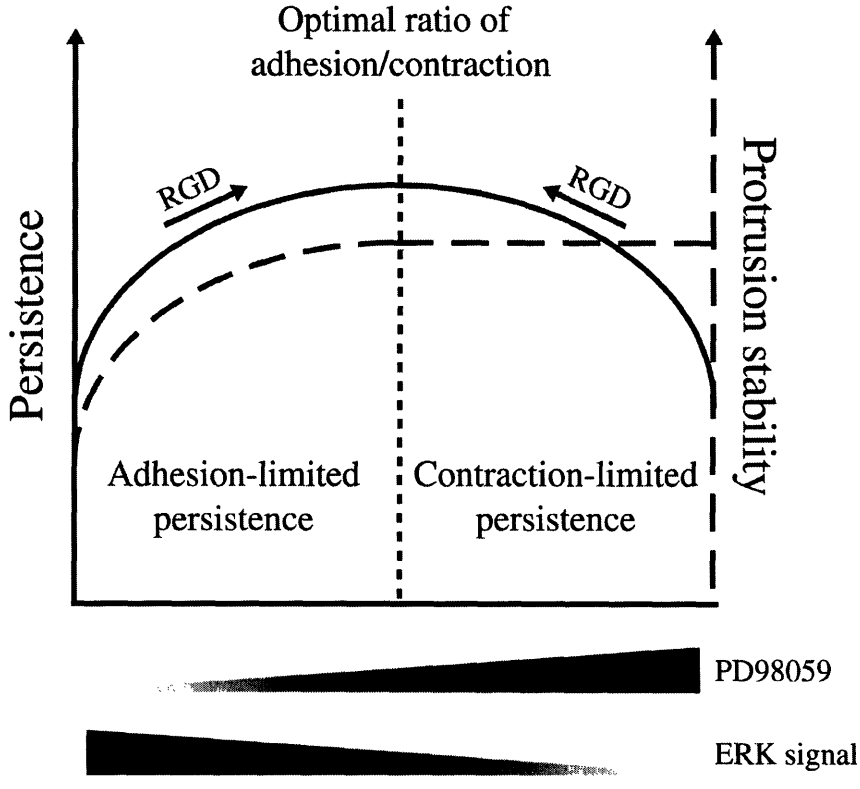

Figure 4.5.9 Hypothetical qualitative model depicting control of persistence through a balance of ERK effects on adhesion and contractility.
High levels of ERK signaling limit *P* through control of adhesion-mediated protrusion stability. Low levels of ERK signaling reduce the amount of MLC phosphorylation and contractility, thus limiting *P* through a lack of cellular ability to organize cytoskeleton. The predicted effects in this model of adding soluble RGD peptide are shown with arrows.

4.6 References

Asthagiri, A.R., A.F. Horwitz, and D.A. Lauffenburger. 1999. A rapid and sensitive quantitative kinase activity assay using a convenient 96-well format. *Anal. Biochem.* 269:342-347.

Bear, J.E., T.M. Svitkina, M. Krause, D.A. Schafer, J.J. Loureiro, G.A. Strasser, I.V. Maly, O.Y. Chaga, J.A. Cooper, G.G. Borisy, and F.B. Gertler. 2002. Antagonism between Ena/VASP proteins and actin filament capping regulates fibroblast motility. *Cell.* 109:509-521.

Brahmbhatt, A.A., and R.L. Klemke. 2003. ERK and RhoA Differentially Regulate Pseudopodia Growth and Retraction during Chemotaxis. *J. Biol. Chem.* 278:13016-13025.

Chen, H.-C., and J.-L. Guan. 1994. Stimulation of phosphatidylinositol 3'-kinase association with focal adhesion kinase by platelet-derived growth factor. *J. Biol. Chem.* 269:31229-31233.

Chen, L., C. Janetopoulos, Y.E. Huang, M. Iijima, J. Borleis, and P.N. Devreotes. 2003. Two phases of actin polymerization display different dependencies on PI(3,4,5)P3 accumulation and have unique roles during chemotaxis. *Mol. Biol. Cell.* 14:5028-5037.

Cheresh, D.A., J. Leng, and R.L. Klemke. 1999. Regulation of cell contraction and membrane ruffling by distinct signals in migratory cells. *J. Cell Biol.* 146:1107-1116.

Cox, D., C.-C. Tseng, G. Bjekic, and S. Greenberg. 1999. A requirement for phosphatidylinositol 3-kinase in pseudopod extension. *J. Biol. Chem.* 274:1240-1247.

DiMilla, P.A., K. Barbee, and D.A. Lauffenburger. 1991. Mathematical model for the effects of adhesion and mechanics on cell migration speed. *Biophys. J.* 60:15-37.

Dunn, G.A. 1983. Characterizing a kinesis response; time averaged measures of cell speed and directional persistance. *Agents Actions [Suppl.].* 12:14-33.

Firtel, R.A., and C.Y. Chung. 2000. The molecular genetics of chemotaxis: sensing and responding to chemoattractant gradients. *BioEssays.* 22:603-615.

Fontanini, G., S. Vignati, D. Bigini, A. Mussi, H. Lucchi, C.A. Angeletti, R. Pingitore, S. Pepe, F. Basolo, and G. Bevilacqua. 1995. Epidermal growth factor receptor (EGFr) expression in non-small cell lung carcinomas correlates with metastatic involvement of hilar and mediastinal lymph nodes in the squamous subtype. *Eur. J. Cancer.* 31A:178-183.

Fujii, H., N. Nishikawa, H. Komazawa, M. Suzuki, M. Kojima, I. Itoh, A. Obata, K. Ayukawa, I. Azuma, and I. Saiki. 1998. A new pseudo-peptide of Arg-Gly-Asp (RGD) with inhibitory effect on tumor metastasis and enzymatic degradation of extracellular matrix. *Clin. Exp. Metastas.* 16:94-104.

Funamoto, S., R. Meili, S. Lee, L. Parry, and R.A. Firtel. 2002. Spatial and temporal regulation of 3-phosphoinositides by PI 3-kinase and PTEN mediates chemotaxis. *Cell.* 109:611-623.

Glading, A., P. Chang, D.A. Lauffenburger, and A. Wells. 2000. Epidermal growth factor receptor activation of calpain is required for fibroblast motility and occurs via an ERK/MAP kinase signaling pathway. *J. Biol. Chem.* 275:2390-2398.

Glading, A., D.A. Lauffenburger, and A. Wells. 2002. Cutting to the chase: calpain proteases in cell motility. *Trends Cell. Biol.* 12:46-54.

Glading, A., F. Überall, S.M. Keyse, D.A. Lauffenburger, and A. Wells. 2001. Membrane proximal ERK signaling is required for M-calpain activation downstream of epidermal growth factor receptor signaling. *J. Biol. Chem.* 276:23341-23348.

Gu, J., M. Tamura, R. Pankov, E.H.J. Danen, T. Takino, K. Matsumoto, and K.M. Yamada. 1999. Shc and FAK differentially regulate cell motility and directionality modulated by PTEN. *J. Cell Biol.* 146:389-403.

Haugh, J.M., F. Codazzi, M. Teruel, and T. Meyer. 2000. Spatial sensing in fibroblasts mediated by 3' phosphoinositides. *J. Cell Biol.* 151:1269-1279.

Hill, K., S. Welti, J. Yu, J.T. Murray, S.-C. Yip, J.S. Condeelis, J.E. Segall, and J.M. Backer. 2000. Specific requirement for the p85-p110α phosphatidylinositol 3-kinase during epidermal growth factor-stimulated actin nucleation in breast cancer cells. *J. Biol. Chem.* 275:3741-3744.

Huang, Y.E., M. Iijima, C.A. Parent, S. Funamoto, R.A. Firtel, and P. Devreotes. 2003. Receptor-mediated regulation of PI3ks confines $PI(3,4,5)P_3$ to the leading edge of chemotaxing cells. *Mol. Biol. Cell.* 14:1913-1922.

Janes, K.A., J.G. Albeck, L.X. Peng, P.K. Sorger, D.A. Lauffenburger, and M.B. Yaffe. 2003. A high-throughput quantitative multiplex kinase assay for monitoring information flow in signaling networks. *Mol. Cell. Proteomics.* 2:463-473.

Jorissen, R.N., F.W. Walker, N. Pouliot, T.P.J. Garrett, C.W. Ward, and A.W. Burgess. 2003. Epidermal growth factor receptor: mechanisms of activation and signaling. *Exp. Cell Res.* 284:31-53.

Kaufmann, A.M., K. Khazaie, M. Wiedemuth, B. Rohde-Schulz, A. Ullrich, V. Schirrmacher, and R.B. Lichtner. 1994. Expression of epidermal growth factor receptor correlates with metastatic potential of 13762NF rat mammary adenocarcinoma cells. *Int. J. Oncol.* 4:1149-1155.

Klemke, R.S., S. Kai, A. Giannini, P. Gallagher, P.d. Lanerolle, and D. Cheresh. 1997. Regulation of cell motility by mitogen-activated protein kinase. *J. Cell Biol.* 137:481-492.

Krueger, J.S., V.G. Keshamouni, N. Atanaskova, and K.B. Reddy. 2001. Temporal and quantitative regulation of mitogen-activated protein kinase (MAPK) regulates cell motility and invasion. *Oncogene.* 20:4209-4218.

Kurokawa, K., R.E. Itoh, H. Yoshizaki, Y. Ohba, T. Nakamura, and M. Matsuda. 2004. Coactivation of Rac1 and Cdc42 at lamellipodia and membrane ruffles induced by epidermal growth factor. *Mol. Biol. Cell.* 15:1003-1010.

Lauffenburger, D.A., and A.F. Horwitz. 1996. Cell migration: a physically integrated molecular process. *Cell.* 84:359-369.

Libotte, T., H.-W. Kaiser, W. Alt, and T. Bretschneider. 2001. Polarity, protrusion-retraction dynamics and their interplay during keratinocyte cell migration. *Exp. Cell Res.* 270:129-137.

Maheshwari, G., and D.A. Lauffenburger. 1998. Deconstructing (and reconstructing) cell migration. *Microsc. Res. Techniq.* 43:358-368.

Maheshwari, G., A. Wells, L.G. Griffith, and D.A. Lauffenburger. 1999. Biophysical integration of effects of epidermal growth factor and fibronectin on fibroblast migration. *Biophys. J.* 76:2814-2823.

McCrawley, I.J., P. O'Brian, and L.G. Hudson. 1997. Overexpression of the epidermal growth factor receptor contributes to enhanced ligand-mediated motility in keratinocyte cell lines. *Endocrinology.* 138:121-127.

Moghal, N., and P.W. Sternberg. 1999. Multiple positive and negative regulators of signaling by the EGF-receptor. *Curr. Opin. Cell Biol.* 11:190-6.

Oikawa, T., H. Yamaguchi, T. Itoh, M. Kato, T. Ijuin, D. Yamazaki, S. Suetsugu, and T. Takenawa. 2004. PtdIns(3,4,5)P_3 binding is necessart for WAVE2-induced formation of lamellipodia. *Nat. Cell Biol.* 6:420-426.

Othmer, H.G., S.R. Dunbar, and W. Alt. 1988. Models of dispersal in biological systems. *J. Math. Biol.* 26:263-298.

Palecek, S.E., J.C. Loftus, M.H. Ginsburg, D.A. Lauffenburger, and A.F. Horwitz. 1997. Integrin-ligand binding properties govern cell migration speed through cell-substratum adhesiveness. *Nature.* 385:537-540.

Piccolo, E., P.F. Innominato, M.A. Mariggio, T. Maffucci, S. Iacobelli, and M. Falasca. 2002. The mechanism involved in the regulation of phospholipase Cgamma1 activity in cell migration. *Oncogene.* 21:6520-9.

Qian, Y., L. Corum, Q. Meng, J. Blenis, J.Z. Zheng, X. Shi, D.C. Flynn, and B.-H. Jiang. 2004. PI3K induced actin filament remodeling through Akt and p70S6K1: implication of essential role in cell migration. *Am. J. Physiol. Cell. Physiol.* 286:C153-C163.

Reiske, H.R., S.C. Kao, L.A. Cary, J.L. Guan, J.F. Lai, and H.C. Chen. 1999. Requirement of phosphatidylinositol 3-kinase in focal adhesion kinase-promoted cell migration. *J. Biol. Chem.* 274:12361-12366.

Ridley, A.J. 2001. Rho GTPases and cell migration. *J. Cell Sci.* 114:2713-2722.

Ridley, A.J., M.A. Schwartz, K. Burridge, R.A. Firtel, M.H. Ginsberg, G. Borisy, J.T. Parsons, and A.R. Horwitz. 2003. Cell migration: integrating signals from front to back. *Science.* 302:1704-1709.

Segall, J.E., S. Tyerech, L. Boselli, S. Masseling, J. Helft, A. Chan, J. Jones, and J. Condeelis. 1996. EGF stimulates lamellipod extension in metastatic mammary adenocarcinoma cells by an actin-dependent mechanism. *J. Cell Sci.* 14:61-72.

Shimizu, M., K. Minakuchi, S. Kaji, and J. Koga. 1997. Chondrocyte migration to fibronectin, type I collagen, and type II collagen. *Cell Struct. Funct.* 22:309-315.

Srinivasan, S., F. Wang, S. Glavas, A. Ott, F. Hofmann, K. Aktories, D. Kalman, and H.R. Bourne. 2003. Rac and Cdc42 play distinct roles in regulating PI(3,4,5)P3 and polarity during neutrophil chemotaxis. *J. Cell Biol.* 160:375-385.

Stähle, M., C. Veit, U. Bachfischer, K. Schierling, B. Skripczynski, A. Hall, P. Gierschik, and K. Giehl. 2003. Mechanisms in LPA-induced tumor cell migration: critical role of phosphorylated ERK. *J. Cell. Sci.* 116:3835-3846.

Stupack, D.G., S.Y. Cho, and R.L. Klemke. 2000. Molecular signaling mechanisms of cell migration and invasion. *Immunol. Res.* 21:83-88.

Sturge, J., J. Hamelin, and G.E. Jones. 2002. N-WASP activation by a β1-integrin-dependent mechanism supports PI3K-independent chemotaxis stimulated by urokinase-type plasminogen activator. *J. Cell Sci.* 115:699-711.

Totsukawa, G., Y. Wu, Y. Sasaki, D.J. Hartshorne, Y. Yamakita, S. Yamashiro, and F. Matsumura. 2004. Distinct roles of MLCK and ROCK in the regulation of membrane protrusions and focal adhesion dynamics during cell migration of fibroblasts. *J. Cell Biol.* 164:427-439.

Turner, T., P. Chen, L.J. Goodly, and A. Wells. 1996. EGF receptor signaling enhances in vivo invasiveness of DU-145 human prostate carcinoma cells. *Clin. Exp. Metastasis.* 14:409-418.

Verbeek, B.S., S.S. Adriaansen-Slot, T.M. Vroom, T. Beckers, and G. Rijksen. 1998. Overexpression of EGFR and c-erbB2 causes enhanced cell migration in human breast cancer cells and NIH3T3 fibroblasts. *FEBS Lett.* 425:145-150.

Vial, E., E. Sahal, and C.J. Marshall. 2003. ERK-MAPK signaling coordinately regulates activity of Rac1 and RhoA for tumor cell motility. *Cancer Cell.* 4:67-79.

Wang, F., P. Herzmark, O.D. Weiner, S. Srinivasan, G. Servant, and H.R. Bourne. 2002. Lipid products of PI(3)Ks maintain persistent cell polarity and directed motility in neutrophils. *Nat. Cell Biol.* 4:513-518.

Ware, M.F., A. Wells, and D.A. Lauffenburger. 1998. Epidermal growth factor alters fibroblast migration speed and directional persistence reciprocally and in a matrix-dependent manner. *J. Cell Sci.* 111:2423-2432.

Weiner, O.D. 2002. Regulation of cell polarity during eukaryotic chemotaxis: the chemotactic compass. *Curr. Opin. Cell Biol.* 14:196-202.

Weiner, O.D., P.O. Neilsen, G.D. Prestwich, M.W. Kirschner, L.C. Cantley, and H.R. Bourne. 2002. A PtdInsP3- and Rho GTPase-mediated positive feedback loop regulates neutrophil polarity. *Nat. Cell Biol.* 4:509-512.

Wells, A., K. Gupta, P. Chang, S. Swindle, A. Glading, and H. Shiraha. 1998. Epidermal growth factor receptor-mediated motility in fibroblasts. *Microsc. Res. Techniq.* 43:395-411.

Xie, H., M.A. Pallero, D. Gupta, P. Chang, M.F. Ware, W. Witke, D.J. Kwiatkowski, D.A. Lauffenburger, J.E. Murphy-Ullrich, and A. Wells. 1998. EGF receptor regulation of cell motility: EGF induces dissassembly of focal adhesions independently of the motility-associated PLCγ signaling pathway. *J. Cell Sci.* 111:615-624.

CHAPTER 5

CORRELATION AND TIME SERIES ANALYSIS OF CHO-EGFR CELL PATHS

Quantitative analysis of cell paths typically proceeds by fitting experimental plots of mean-squared displacement versus time to a persistent random walk model describing cell speed and persistence time. These parameters are averages of cell motility behavior over an entire experiment and thus may mask the local dynamics of cell movement over shorter periods of time. To obtain more detailed information about the structure of CHO-EGFR cell paths, we investigated the presence of auto- and cross-correlations amidst the speed and direction of motion characterized by cell displacement vectors determined at uniform short time intervals. Plots of turn angle distributions revealed that increased instantaneous cell speed correlated with smaller rates of turning. Time-based cross-correlation analysis determined that this speed-turn angle relationship is "local," in that turn angles depend only on the current speed of the cell and not previous speeds. Further time-series analysis using autocorrelation functions for speed and displacement vectors revealed that CHO-EGFR cells have virtually no "memory" of previous cell speed, but a small memory of previous directionality that deviates from the Markov assumption usually ascribed to cell paths. Overall, our methods demonstrate the usefulness of correlation analyses for determining fundamental characteristics of cell paths not accessible by traditional analysis using the persistent random walk equation.

5.1 Introduction

Observations in myriad cell types indicate that the paths of motile cells are locally persistent and globally random. Mathematical derivations of this persistent random walk behavior result in an equation relating mean-squared displacement to parameters of cell speed (S) and directional persistence (P) (Gail and Boone, 1970; Othmer et al., 1988; Stokes and Lauffenburger, 1991):

$$\left\langle (\Delta x)^2 \right\rangle = 2S^2 P \left[\Delta t - P(1 - exp\{-\Delta t/P\}) \right], \quad x \in \Re^n .$$

One potential pitfall in using this equation to quantify motility is that speed and persistence are defined as single, average measures of cell path behavior taken over a long period of observation time. As such, they may conceal information about local cell path structure that might better deconstruct the mechanisms governing migration. An attractive technique of cell path analysis is thus the study of the speed and directional characteristics of cell tracks as defined by the minimum length of time available experimentally—the image frame rate used for videotracking. At this timescale, appropriate parameterization and quantification of "local" cell speed and directionality takes full advantage of all the information inherent in digitized cell tracks.

This thesis chapter addresses two particular questions in the study of CHO-EGFR paths. First, does local path speed correlate with the local directional behavior of migrating cells? Second, are there time-dependent correlations in speed or directionality that underlie the behavior of cell tracks? Identification of such statistical dependencies would reveal information about the underlying the dynamics of the biophysical and biochemical processes by which CHO-EGFR cells move.

Our first tool for studying the local behavior of CHO-EGFR cell paths is a simple graphical method we have termed a turn angle distribution (TAD) plot. These plots display the frequency of occurrence of a given angular turning rate within discretized cell paths.

What results is a two-dimensional representation of the directional information summarized by the one-dimensional parameter of persistence time. Decomposing these two-dimensional plots into a 3rd dimension of local cell speed allows us to see whether the instantaneous speed of a cell affects its directional behavior at that point in its path.

To examine CHO-EGFR cell tracks for time-dependent correlations, we utilize a second tool known as time series analysis (TSA). A widely used technique, TSA is found in fields as diverse as economics and meteorology (Dunn and Brown, 1987). TSA studies the 2nd statistical moments about the data of interest through the use of auto- and cross-correlation functions that describe the average dependencies between data offset by certain time lags. While TSA tools exist in both the time domain and the frequency domain (Box and Jenkins, 1976; Mills, 1990), we will concern ourselves only with time domain methods. For a time-delineated series of cell path measurements $x = [x_0, x_1, x_2, \ldots, x_{N-1}]$ with mean μ, the autocorrelation function (ACF) at lag interval k is defined as:

$$ACF_k = \frac{E[(x_t - \mu)(x_{t-k} - \mu)]}{\left(E[(x_t - \mu)^2] \cdot E[(x_{t-k} - \mu)^2]\right)^{1/2}} = \frac{Cov(x_t, x_{t-k})}{(Var(x_t) \cdot Var(x_{t-k}))^{1/2}}.$$

Note that this definition results in a normalized function ($ACF_0 \equiv 1$ and $0 \leq ACF_k \leq 1$). A further tool used in autocorrelation analysis is the partial autocorrelation function (PACF), which measures the correlation at a given time lag after allowing for the effects of correlation at smaller time lags (Dunn and Brown, 1987). Thus, the PACF acts as a filter for removing previous correlations, identifying the true timescale of system memory for the quantity of interest (Dunn and Brown, 1987).

Autocorrelation functions describe the time-dependent behavior of cell speed and directionality separately; however, time-based cross-dependencies between speed and directionality may also occur in cell tracks. To study these we utilize the cross-correlation function (CCF). For two time series x and y, it is defined in a manner analogous to the ACF for one series:

$$CCF_k = \frac{E[(x_t - \mu)(y_{t-k} - \mu)]}{\left(E\left[(x_t - \mu)^2\right] \cdot E\left[(y_{t-k} - \mu)^2\right]\right)^{1/2}} = \frac{Cov(x_t, y_{t-k})}{(Var(x_t) \cdot Var(y_{t-k}))^{1/2}}.$$

In contrast to the autocorrelation function, in general CCF_0 is less than unity. Moreover, by definition $ACF_m = ACF_{-m}$, but $CCF_m \neq CCF_{-m}$ and thus the cross-correlation function is defined for both positive and negative time lags.

We find that while CHO-EGFR cell speed shows essentially no time autocorrelation, directionality shows significant autocorrelation, the magnitude of which corresponds to fitted persistence times. Partial correlation functions for directionality reveal that CHO-EGFR cells appear to have a small time "memory" that deviates from the Markov assumption usually ascribed to cell paths. Cross-correlation and TAD plot analysis indicates that while CHO-EGFR cells exhibit a correlation between local cell path speed and local persistence, no cellular memory exists between current local cell speed and future local path angles. That is, while the speed and directionality of migrating CHO-EGFR cells are linked at a local level, they are uncoupled over entire cell tracks, a result that extends to overall fits for average speed and persistence. Overall, our methods demonstrate the usefulness of correlation analyses for determining fundamental characteristics of cell paths not accessible via use of the persistent random walk equation.

5.2 Experimental Methods

5.2.1 Migration assays

CHO-EGFR cell migration assays were performed as described in Chapters 3 and 4, with cell positions recorded every 15 minutes. Migration path data for human mammary epithelial cells was provided by Dr. Bart Hendriks; the observation interval for HMEC migration data was 10 minutes. Path data for Rat2 fibroblasts was provided by Dr. James Bear; the Rat2 observation interval was 5 minutes.

5.2.2 Turn angle distribution plots

Lines drawn between three successive cell centroid positions in a cell path define an angle $\alpha \in [0, 2\pi]$. The turn angle for the time t_n associated with the vertex of the angle is defined as $\theta_n = (\pi - \alpha_n) \in [-\pi, \pi]$ (Fig. 5.5.1). TAD datasets consisted of pooled cell centroid path data from all long-timescale migration experiments performed under listed conditions (e.g. 4×-CHO cells, all Fn concentrations, no EGF). Turn angles from the pooled cell paths were calculated and binned within the abscissa range of $[-\pi, \pi]$. Bins were then normalized by the total number of calculated angles to obtain a turn angle distribution plot. Zero radians represents straight-ahead motion, while an instantaneous turn angle of π = $-\pi$ radians represent a complete directional reversal of centroid translocation by the cell. For some plots, angle bins were separated into a third dimension by sorting by increasing cell speed at time t_n, with bins in the new speed dimension containing equal numbers of observations. Speed at time t_n was defined as the geometric mean of the magnitude of the two displacement vectors forming the angle with vertex time t_n.

5.2.3 Auto- and cross-correlation analysis

Scalar time series analysis was performed on both cell speed and the absolute value of turn angles. For a time-delineated group of scalar cell path measurements $[x_0, x_1, \ldots, x_{N-1}]$, the sample ACF is defined as:

$$ACF_k = \frac{\sum_{t=0}^{N-|k|-1} (x_{t+k} - \bar{x})(x_t - \bar{x})}{\sum_{t=0}^{N-1} (x_t - \bar{x})^2}, \quad k = 0,1,2,\ldots,N-1$$

$$\bar{x} = N^{-1} \sum_{t=0}^{N-1} x_t$$

The sample CCF is defined similarly:

$$CCF_k = \frac{\sum_{t=0}^{N-|k|-1}\left(x_{t+k}-\bar{x}\right)\left(y_t-\bar{x}\right)}{\sqrt{\sum_{t=0}^{N-1}\left(x_t-\bar{x}\right)^2}\sqrt{\sum_{t=0}^{N-1}\left(y_t-\bar{y}\right)^2}}, \quad k = 0, \pm 1, \pm 2, \ldots, \pm N-1$$

$$\bar{x} = N^{-1}\sum_{t=0}^{N-1} x_t, \qquad \bar{y} = N^{-1}\sum_{t=0}^{N-1} y_t$$

Vector autocorrelation analysis of cell displacements [$\boldsymbol{d}_0$, $\boldsymbol{d}_1$, ..., $\boldsymbol{d}_{N-1}$] followed the dot-product formalism of Dunn and Brown (Dunn and Brown, 1987):

$$ACF_k = \left(\frac{N}{N-k}\right)\frac{\sum_{t=0}^{N-k-1}\left(\boldsymbol{d}_{t+k}\cdot\boldsymbol{d}_t\right)}{\sum_{t=0}^{N-1}\left(\boldsymbol{d}_t\cdot\boldsymbol{d}_t\right)}, \quad k = 0,1,2,\ldots,N-1$$

Partial autocorrelation analysis utilized the Durbin-Levinson recursion algorithm (Durbin, 1960; Box and Jenkins, 1976; Mills, 1990). All computational routines were implemented in MATLAB 5.3 (The MathWorks, Inc., Natick, MA).

5.3 Results

5.3.1 Turn angle distributions correlate to overall persistence times

Speed and persistence are time-averaged measures of cell motility, and do not take full advantage of the path information available in cell tracks. We reasoned that analysis of the distributions of cell speed and directionality over shorter time intervals could provide useful additional information about the structure of CHO-EGFR cell paths. Our first approach to this analysis utilized the "turn angle" concept of directionality in cell paths. In any discretized cell path, lines drawn between three successive centroid positions define an angle $\alpha \in [0, 2\pi]$. The turn angle for the time t_n associated with the vertex of the angle is defined as $\theta_n = (\pi - \alpha_n) \in [-\pi, \pi]$. This turn angle approximates the cell's instantaneous

turning rate over the period centered on the time t_n (Fig. 5.5.1). Pooling turn angle data from multiple cells results in turn angle distribution (TAD) plots characterizing cell persistence in direction at a "local" or "instantaneous" level.

Fig 5.5.2*A* shows the Fn-dependent variation of angular distribution for 4×-CHO cells migrating in the presence of EGF. In all cases, turn angle distribution biases towards maintenance of directionality, with the most probable behavior being continued motion in the same direction ($\theta = 0$ radians). Cells also have a smaller bias towards a complete change in direction of translocation ($\theta = \pm\pi$); they are least likely to extend lamellipods laterally ($\theta = \pm\pi/2$). Furthermore, comparison of Fig. 5.5.2*A* with the data of Table 5.1 indicates that turn angle distributions correlate with average persistence times fitted from the random walk motility model. Higher persistence results in a greater bias towards maintaining a constant direction of migration. This result is general; Fig. 5.5.2*B* shows a similar correlation when modulating EGF-stimulated 4×-CHO cell migration via addition of PD98059.

5.3.2 Local correlations between speed and persistence in multiple cell types

To ascertain whether the local directional behavior of migrating CHO-EGFR cells was speed-dependent, TAD data was decomposed into a third dimension representing average speed through the tracking period comprising each angle. Speeds were grouped into ten deciles of increasing speed containing equal numbers of angles. Fig. 5.5.3, *A* and *B* depict 4×-CHO TAD data from experiments conducted in the absence and presence of EGF, respectively. In both cases, at low local speeds cells exhibit an unbiased, uniform turning distribution. However, as local cell speed increases, turn angle orientation biases towards a primary peak corresponding to straight-ahead motion ($\theta = 0$) and a secondary peak corresponding to complete reversal of direction ($\theta = \pm\pi$). Fig. 5.5.3, *A* and *B* also show that this local speed-turn angle correlation is general for CHO-EGFR cells and can be separated

from other biochemical determinants of overall experimental persistence time (e.g. addition of EGF).

Interestingly, this local relationship between speed and turn angle distribution also holds for other cell types. Fig. 5.5.4 depicts results for human mammary epithelial cells (*A* and *B*) and Rat2 fibroblasts (*C* and *D*). Thus, despite the disparate characteristics and developmental origins of the three cell types tested, their similar TAD structure suggests that the local speed-persistence connection is a general phenomenon of migrating cells.

5.3.3 TAD plots of highly persistent CHO-EGFR cells

The highest probability peak within CHO-EGFR TAD plots occurs at zero radians, corresponding to a maximum likelihood of straight-ahead motion over short periods of time. This is expected for cells exhibiting persistent random walk behavior. However, the presence of a smaller, secondary probability peak at π radians (corresponding to a complete directional reversal of cell translocation) contradicts the monotonic and symmetric decay of turn angle probability about $\theta = 0$ expected in a persistent random walk (Othmer et al., 1988).

Interestingly, both Fig. 5.5.2 and 5.5.3 indicate that CHO-EGFR experiments with higher average persistence times have smaller secondary TAD probability peaks. Moreover, CHO-EGFR cells are relatively unpolarized when migrating, and data resulting from the more polarized HMEC and Rat2 cells exhibit virtually no secondary peaks (Fig. 5.5.4). As such, we hypothesized that the TAD "tail" at π radians reflects the weak polarity of CHO-EGFR cells and their tendency not to form clearly dominant lamellipodia. To address this possibility indirectly, we used persistence time as a proxy for the polarity of migrating CHO-EGFR cells and generated a subpopulation of highly persistent cells taken from the data of Fig. 5.5.2*A*. As predicted, TAD plots of these cells do not exhibit a secondary probability peak, and thus appear to more closely obey the persistent random walk model (Fig. 5.5.5).

5.3.4 Autocorrelation analysis of CHO-EGFR cell paths

In addition to using TAD plots to study the relationship between local speed and directionality, we also used the tools of time series analysis (TSA) to examine the time-dependence of local migratory behavior in CHO-EGFR cell paths.

Fig. 5.5.6 shows speed autocorrelation functions (ACF) for 4×-CHO cells migrating on 10 μg/ml Fn without EGF (*A*), with EGF (*B*), and with EGF and 5 μM LY294002 (*C*). Here, speed is defined as proportional to the distance traveled by a cell over one tracking observation interval. Despite substantial variations in overall cell speed and persistence between these experimental conditions (cf. Fig. 3.5.3, 3.5.4, 4.5.3, and 4.5.4), CHO-EGFR cell speed consistently appears not to have any time "memory" beyond a weak correlation over a 15-minute interval. In other words, CHO-EGFR speed is a largely to completely random process. We further confirmed this fact using the highly persistent cells of the TAD plot in Fig. 5.5.5 (Fig. 5.5.6*D*).

Fig. 5.5.7 shows analogous autocorrelation functions for 4×-CHO angular behavior as defined by the dot product of vectorial displacements over single tracking intervals. In contrast to the lack of speed autocorrelation, path directionality exhibits a substantial memory component. Moreover, the magnitude of this directional autocorrelation varies in concert with fitted persistence time, as defined by both the autocorrelation coefficient at lag interval one and the maximum lag time for which correlations are evident. Thus, cells migrating in the absence of EGF ($P \sim 10$ min) do not show any directional correlation over the tracking interval of 15 minutes (Fig. 5.5.7*A*), while cells migrating in the presence of EGF and LY294002 ($P \sim 45$ min) show correlations out to a lag time of 90-100 minutes (Fig. 5.5.7*C*). The highly persistent subset of cells exhibited correlations visible at 180 minutes (Fig. 5.5.7*D*).

5.3.5 Partial autocorrelation analysis of CHO-EGFR directionality

The partial autocorrelation function corrects the autocorrelation function at a given lag time for the effects of correlations at smaller lag times. In doing so, the PACF reveals the true correlation "memory" of a time series. Pooled average PACF for the directional ACF of Fig. 5.5.7 are shown in Fig. 5.5.8. Because cells migrating in the absence of EGF exhibit low persistence times and no time-dependent directional autocorrelation, it is unsurprising that Fig. 5.5.8*A* lacks any non-zero partial autocorrelation values. In contrast, cells migrating in the presence of EGF both without (*B*) and with LY294002 (*C*), and the highly persistent subset of cells (*D*) exhibit non-zero spikes at lag intervals one and two, suggestive of CHO-EGFR directional memory that manifests over a period of approximately 30 minutes. Interestingly, variations in overall fitted persistence time do correlate with the magnitude of the PACF at lags one and two suggesting that persistence results not from increasing time memory per se of the cellular directional system but from increased input magnitude of the cellular processes responsible for persistence.

5.3.6 Cross-correlations between CHO-EGFR speed and turn angles

Because the mathematical forms of autocorrelation analysis are easily extended to the cross-correlation analysis of two parallel series of data, we also examined the time-lag cross-correlations between local CHO-EGFR speed and turn angles. For this analysis, turn angles were defined as discussed previously, while local speed was defined as proportional to the magnitude of the first displacement vector comprising the turn angle. Fig. 5.5.9 shows representative results from cross-correlation analysis of several CHO-EGFR experimental conditions. Negative correlation exists between speed and the absolute magnitude of the turn angle, agreeing with the visual inspection of TAD plots described earlier (Fig. 5.5.3). Significantly, however, cross-correlation between local speed and turn angles only exists for lag intervals zero and one; that is, only the speeds given by the two displacement vectors that make up a turn angle are correlated with the absolute magnitude

of that angle. In other words, local cell speed has no memory effect on the directional characteristics of CHO-EGFR migration at later times in cell tracks.

5.4 Discussion

The results of Chapters 3 and 4 highlight the ability of quantitative parameterization of the paths of migrating cells to provide information useful for discerning the biochemical and biophysical mechanisms governing cell motility. However, the generation of speed and persistence from mean-squared displacement versus time plots is a "1st order" statistical analysis that does not fully utilize the cell path information available from videotracking studies. Here, we present two "2nd order" analysis tools, turn angle distribution plots and time series analysis, that generate additional quantitative information based on the local speeds and angular behavior of cells that are time-averaged in speed and persistence fitting. Applied to CHO-EGFR cell paths, we have determined the following: (1) as expected, increased persistence time manifests as a greater likelihood that a cell's local direction of motion remains constant; (2) both CHO-EGFR and other cell types exhibit a correlation between local cell path speed and local persistence, but no cellular memory exists between current local cell speed and future local path angles; (3) CHO-EGFR cell speed is very weakly autocorrelated and thus has essentially no time-dependent memory; (4) the magnitude of directional autocorrelation of CHO-EGFR cells varies in concert with fitted persistence time; and (5) partial autocorrelation analysis suggests that the process governing CHO-EGFR persistence has a constant characteristic "memory" time of about 30 minutes, and that variations in the absolute magnitude of this memory process account for variations in overall persistence of motion.

Our turn angle distribution analysis revealed that the most probable local directional behavior is maintenance of the direction of motion. This result held not only for CHO-EGFR cells, but two other cell lines examined (HMEC and Rat2). We believe that this result is general for two reasons. First, previous experimental studies in amoeba and mouse

fibroblasts have shown similar effects (Gail and Boone, 1970; Hall, 1977; Miyoshi et al., 2003). Second, for a differential cell centroid sampling interval of any cell type, a TAD plot would become a delta function centered at zero radians due to the persistent nature of migration. The converse situation, that turn angle distributions are uniform when measured over timescales much longer than the persistence time of the cells, was not tested, but it is supported by observations by Gail and Boone (Gail and Boone, 1970).

As discussed in Chapter 3, available evidence suggests that CHO-EGFR cells are only weakly adhesive, and that this limits the persistence of cell motility through limiting the stability of lamellpodial protrusions. Because weak adhesion can also limit cell speed (Maheshwari et al., 1999), the positive local correlation between CHO-EGFR cell speed and turning behavior (Fig. 5.5.3) was unsurprising. In the literature, this phenomenon has been reported previously in amoeba and neutrophils (Mandeville et al., 1995; Shenderov and Sheetz, 1997), other relatively weakly adherent cell types. However, the existence of similar local speed-persistence TAD results for fibroblasts and epithelial cells (Fig. 5.5.4) suggest that it is a general phenomenon not limited to weakly adherent cells.

Interestingly, however, the connection between local path speed and persistence does not extend to correlations between local speed and future path angles (Fig. 5.5.9), or to correlations between overall S and P either on a per-cell basis or in experimental averages (data not shown). The first situation can be explained by the fact no autocorrelation of cell speeds exists (Fig. 5.5.6). The second, a discrepancy on its face, can be explained by the fact that higher local speed does not uniformly result in greater local persistence, only a greater likelihood of local persistence. As such, a fast moving cell may indeed have a tortuous, low P path, while a slow moving cell can have a high P path. Alternatively, the random arrangement of high- and low- speed segments within a given cell path may prevent correlations between overall S and P in individual cells.

Stochastic models of motility, such as the well-known Ornstein-Uhlenbeck process (Doob, 1942; Stokes and Lauffenburger, 1991), usually have the Markov property, which

says that the future behavior of a system depends only on its present state. In motility, the Markov property asserts that migrating cells have no memory of their earlier path behavior or state. In time series analysis, a Markov process only has a non-zero partial autocorrelation coefficient at lag interval one (Dunn and Brown, 1987). In contrast, we observed that CHO-EGFR displacement vectors have non-zero PACF coefficients at lag interval two (Fig. 5.5.8). This suggests a small non-Markov memory component to their migration. Other non-Markov behavior has been documented in the literature in the form of periodic correlations in amoeba and neutrophils (Hartman et al., 1994; Shenderov and Sheetz, 1997). In contrast, an extensive time series analysis of fibroblast migration showed no evidence for non-Markov behavior (Dunn and Brown, 1987). In our CHO-EGFR cells, we have often seen mean-squared displacement deviations from the persistent random walk formulation (data not shown). Given that the Markov property is often used as a starting point for deriving the random walk behavior of cells (Stokes and Lauffenburger, 1991), it is thus not surprising that CHO-EGFR cells show non-Markov correlations.

In light of this memory in cell directionality (Fig 5.5.7 and 5.5.8), it is surprising that virtually no CHO-EGFR speed autocorrelation exists (Fig. 5.5.6), especially given that local speed cross-correlates with local persistence (Fig. 5.5.9). Taken together, these results suggest that while the biophysical or biochemical mechanisms that control S and P have some overlap, the time constants for the processes controlling P are much larger. At this point, a precise identification of the molecular basis for these time constants in P and S is speculative. One possibility is that cell speed is governed by relatively rapid stochastic fluctuations in the number of lamellipodial adhesions available to "tow" the cell along. In contrast, persistence might be governed by the overall polarity of the cell, for which stochastic fluctuations would be less dramatic on short timescales, and for which variations in the number and cellular location of adhesions is only one governing component.

We also note that the lag interval two (non-Markov) partial autocorrelation coefficients are substantially smaller than the lag one (Markov) coefficients. Because these

coefficients represent the strength of time lag correlations, the non-Markov memory effects in CHO-EGFR directionality are thus relatively weak, and in our results actually limited to cells migrating in the presence of EGF (Fig. 5.5.7, *B-D*). The memory is, however, not likely to be a fundamental biochemical effect of EGF on the structure of CHO-EGFR paths, but rather a consequence of the fact that the low persistence of cells in the absence of EGF prevents our seeing any time correlations at all at a sampling interval of 15 minutes (Fig. 5.5.7*A*).

This leads to a final comment, that a requirement for effective TSA is use of a sampling interval sufficiently small to detect potential correlations in the variables of interest. Given our sampling interval of 15 minutes for CHO-EGFR experiments, it is unsurprising that we identified no displacement autocorrelations for cells migrating in the absence of EGF, as the average fitted persistence time for such experiments is only 10-15 min (Fig. 5.5.7*A*; cf. Fig. 3.5.4). Presumably correlations do exist at smaller time intervals. In contrast, we saw displacement autocorrelations in 4×-CHO experiments containing EGF, since those experiments had persistence times of 30 minutes or more (Fig. 5.5.7, *B* and *C*; cf. Fig. 3.5.4 and 4.5.4). Even in this case, however, the weak nature of the correlation, as shown by the small partial autocorrelation coefficients (Fig. 5.5.8), required a relatively large number of cells to discern it. Unfortunately, for the CHO-EGFR cells, their slow migration speed of 10-15 μm/hr necessitated a relatively long sampling interval so that cell centroid movements were discernible. In general, then, the amount of information able to be gained from time series analysis of cell positions is limited by the speed of the cells of interest, and in fact, most other cell types that have been used for time series and correlation analyses are faster-moving cells (e.g. neutrophils, which move at ~10 μm/min) for which position data is able to be taken every 1 min or less (Dunn and Brown, 1987; Hartman et al., 1994; Mandeville et al., 1995).

5.5 Figures

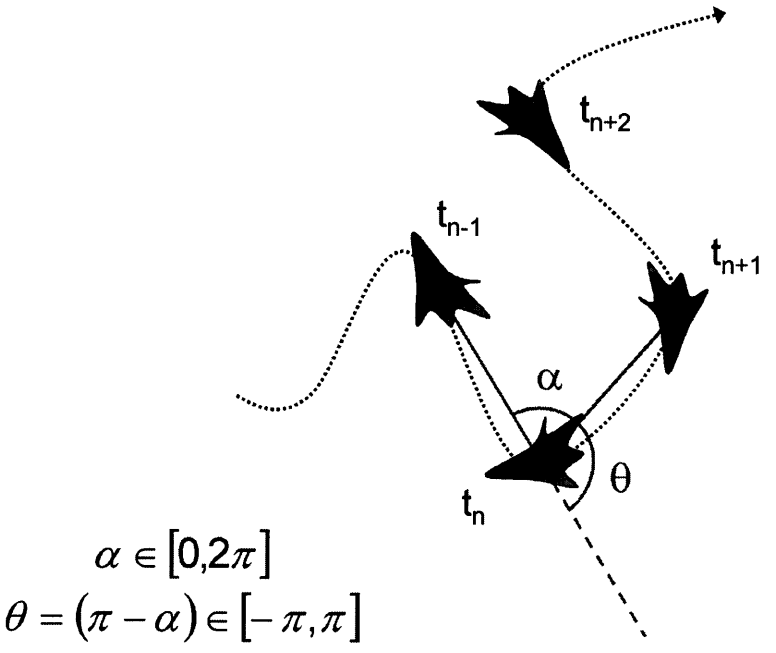

Figure 5.5.1 Definition of turn angles.
Lines drawn between three successive cell centroid positions define an angle $\alpha \in [0, 2\pi]$. The turn angle for time t_n is defined as $\theta = (\pi - \alpha) \in [-\pi, \pi]$. Note that the turn angle only approximates the turning behavior of the continuous cell path (dotted line) at time t_n.

A

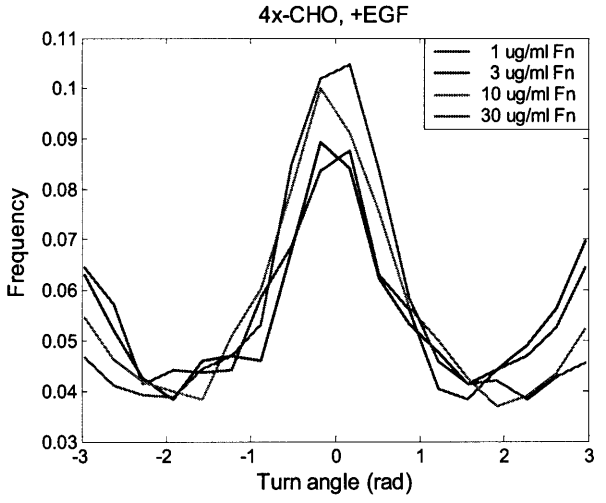

B

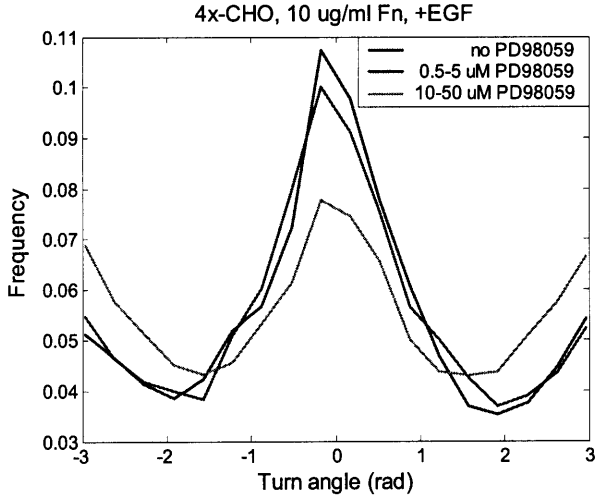

TABLE 1 EGF-induced persistence in 4x-CHO cells

[Fn] (μg/ml)	P (minutes)	[PD98059] (μM)
1	22.4 ± 3.5	0
3	26.5 ± 5.1	0
10	28.6 ± 5.0	0
30	42.8 ± 6.6	0
10	32.6 ± 5.8	0.5
10	43.0 ± 7.5	5
10	22.0 ± 4.2	10
10	18.9 ± 3.1	25
10	18.6 ± 3.4	50

Results taken from Fig. 3.5.4 and 4.5.4.
Errors represent ± 2 SE.

Figure 5.5.2 Turn-angle distributions correlate to directional persistence time.
EGF-stimulated 4x-CHO cell centroid data was used to create TAD plots studying the role of Fn (*A*) and PD98059 (*B*) in modulating angular distributions. For each indicated condition, turn angles from all cell paths were grouped into 18 bins within an abscissa range of $[-\pi,\pi]$. Bins were normalized by the total number of calculated angles. Zero radians represents straight-ahead motion, while an instantaneous turn angle of $\pi = -\pi$ radians represent a complete reversal of centroid translocation by the cell.

A

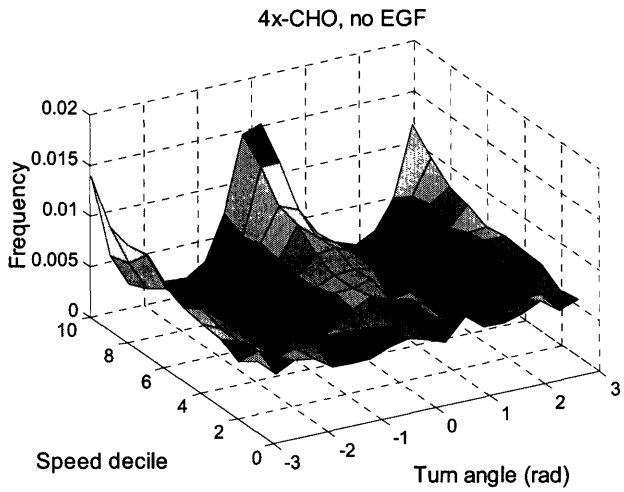

B

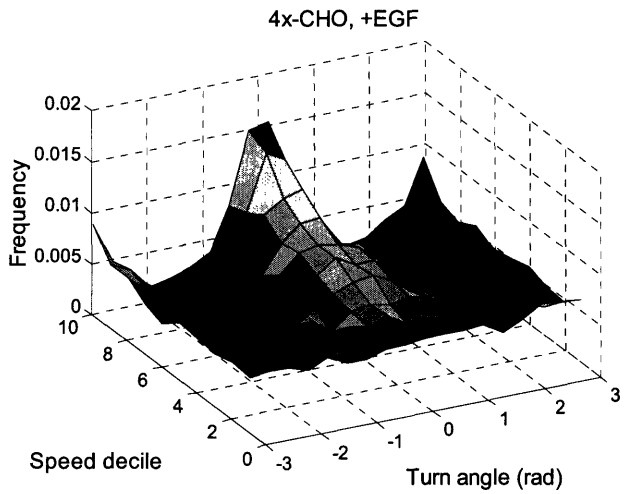

Figure 5.5.3 Instantaneous cell speed correlates with local turn angle distribution independent of overall persistence time.
TAD plot angle bins were separated into deciles of increasing cell speed, with each decile containing equal numbers of angles. Plots result from pooling all 4x-CHO data from experiments conducted on 1, 3, 10, and 30 μg/ml in either the absence (*A*) and presence (*B*) of EGF.

A

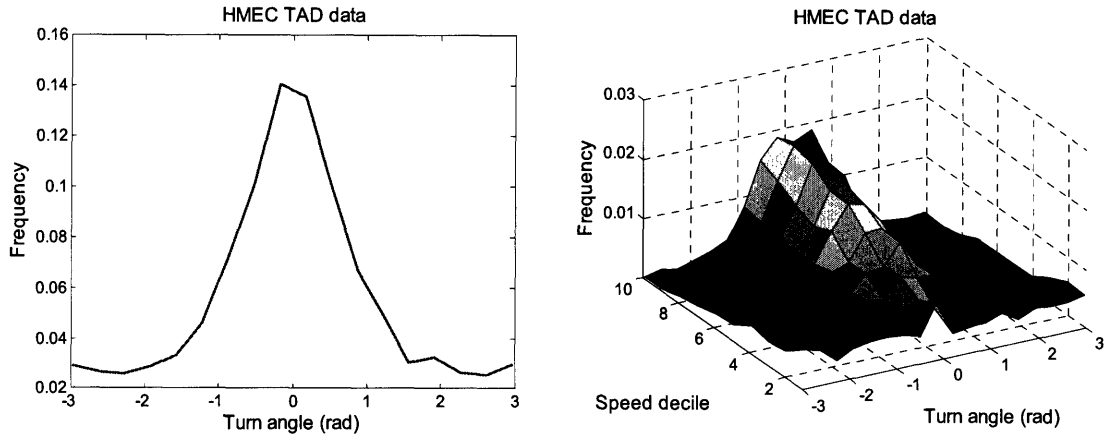

B

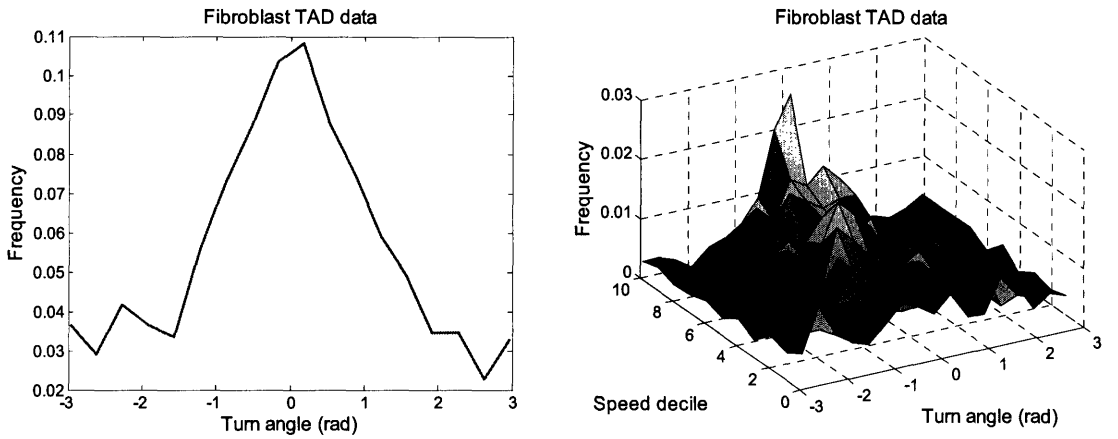

Figure 5.5.4 Both human mammary epithelial cells and fibroblasts also exhibit a local correlation between speed and persistence.
Unpublished HMEC migration data provided courtesy of Dr. Bart Hendriks. Rat2 fibroblast data provided courtesy of Dr. James Bear. In contrast to the CHO cells, note the lack of turning frequency at $\pi = -\pi$ radians for both cell types.

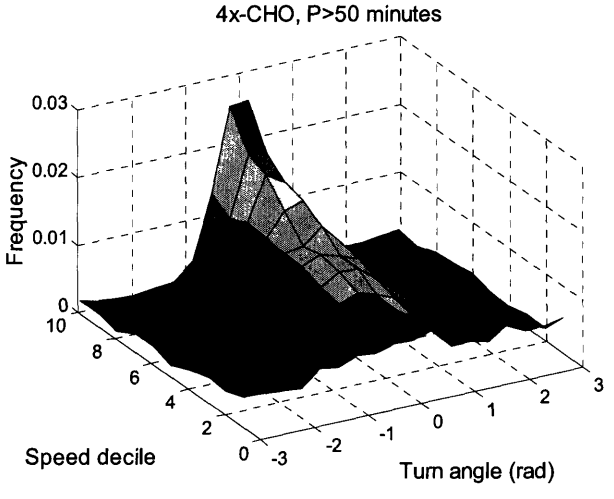

Figure 5.5.5 TAD plot of highly persistent 4×-CHO cells.
Using experimental data from Fig. 5.5.2, turn angles were compiled from all cells with fitted persistence times greater than 50 minutes. Highly persistent cells are less likely to completely reverse their direction of motion.

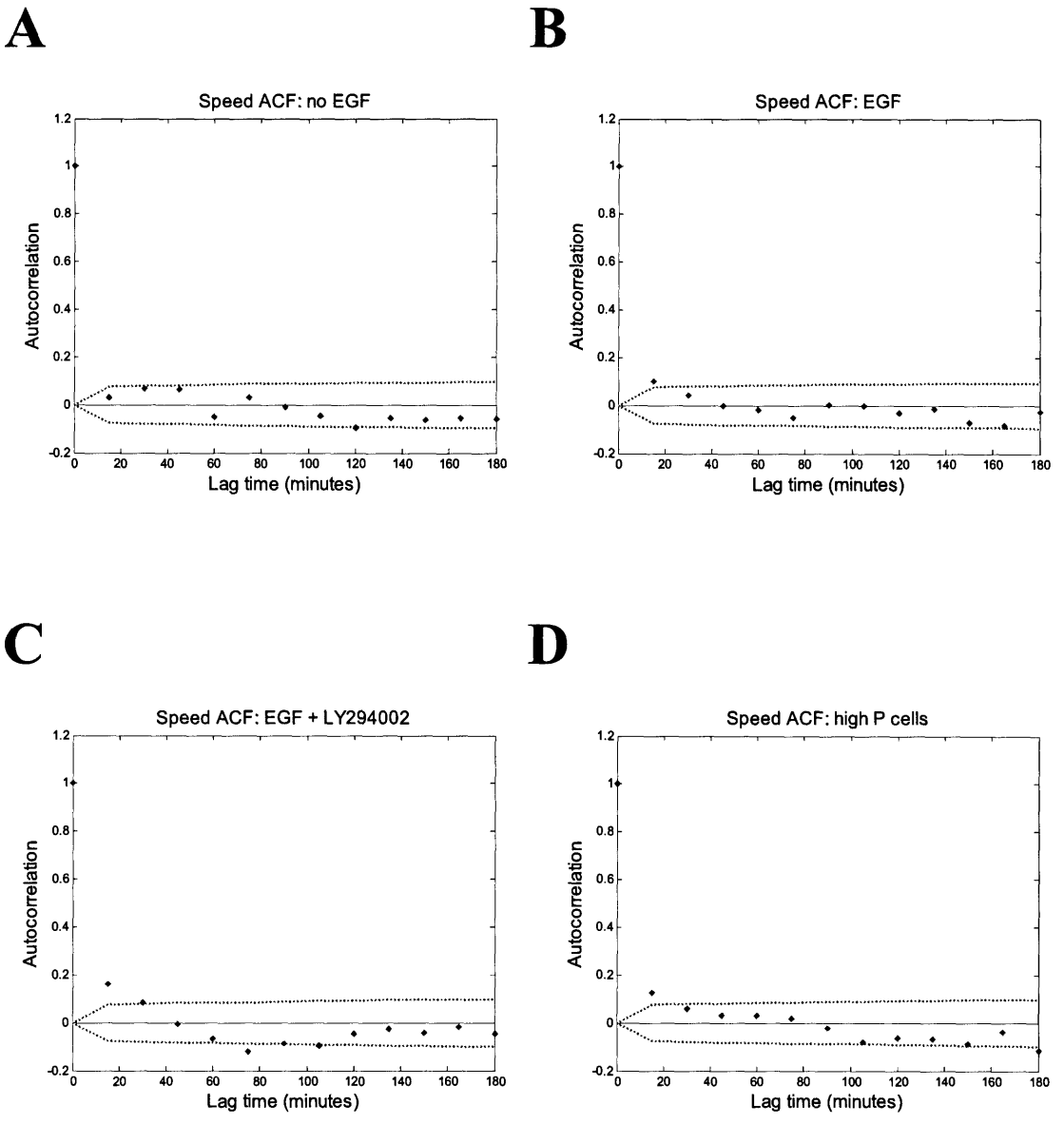

Figure 5.5.6 CHO-EGFR speed has virtually no "memory" over the tracking interval of 15 minutes. Each plot shows the mean speed autocorrelation function for 30 representative 4×-CHO cells migrating on 10 μg/ml Fn with *(A)* no EGF, *(B)* 25 nM EGF, and *(C)* EGF + 5 μM LY294002 in the media. For comparison, *(D)* represents highly persistent 4×-CHO cells taken from Fig. 5.5.5. Note that the average persistence time increases as one moves from plot *A* to *D*. Dotted lines represent 95% confidence intervals for zero autocorrelation according to Bartlett's approximation.

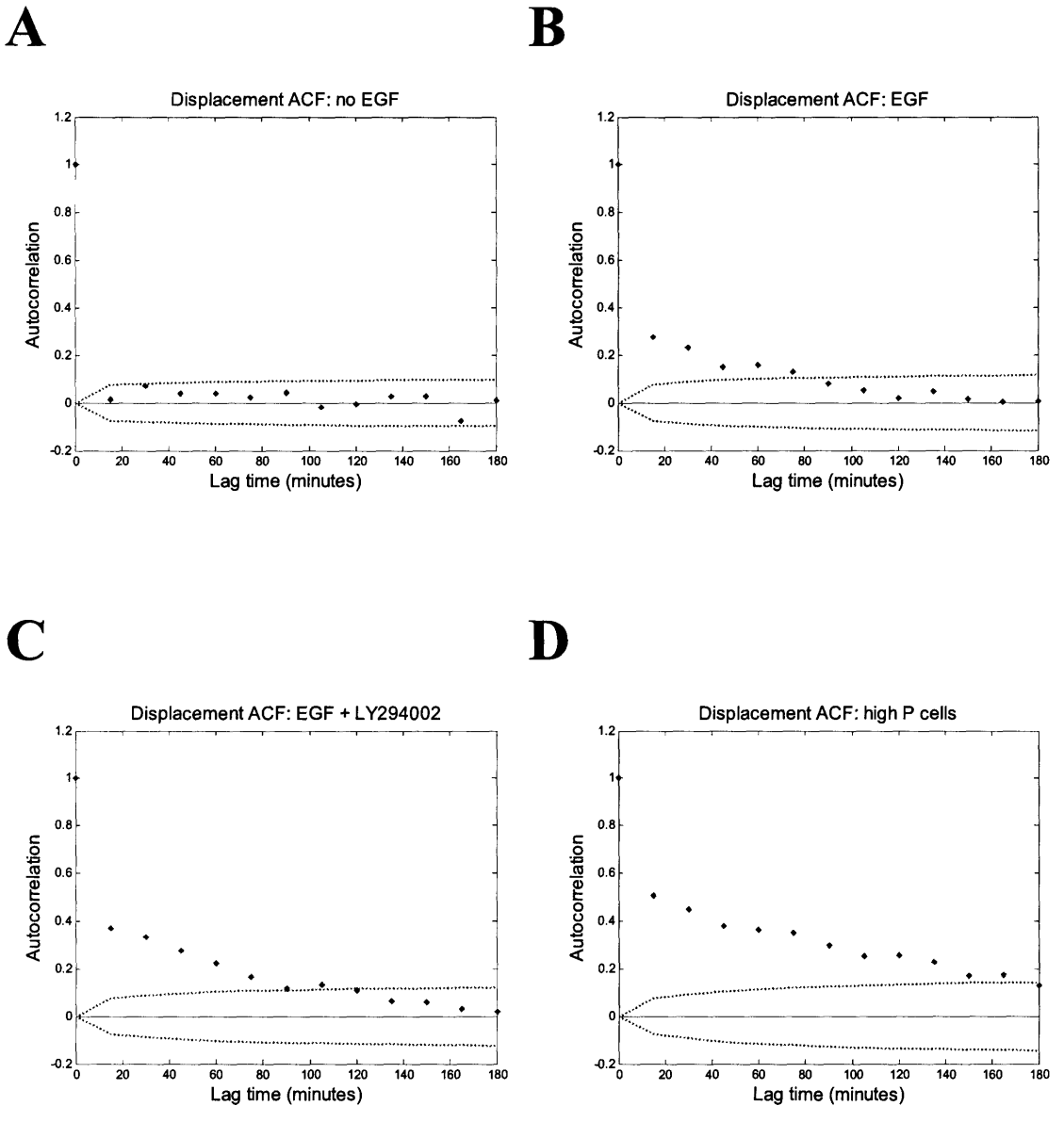

Figure 5.5.7 CHO-EGFR angular autocorrelation tracks overall persistence time.
Each plot shows the mean instantaneous displacement vector autocorrelation function for 30 representative 4×-CHO cells migrating on 10 μg/ml Fn with *(A)* no EGF, *(B)* 25 nM EGF, and *(C)* EGF + 5 μM LY294002 in the media. For comparison, *(D)* represents highly persistent 4×-CHO cells taken from Fig. 5.5.5. Note that the average persistence time increases as one moves from plot *A* to *D*. Dotted lines represent 95% confidence intervals for zero autocorrelation according to Bartlett's approximation.

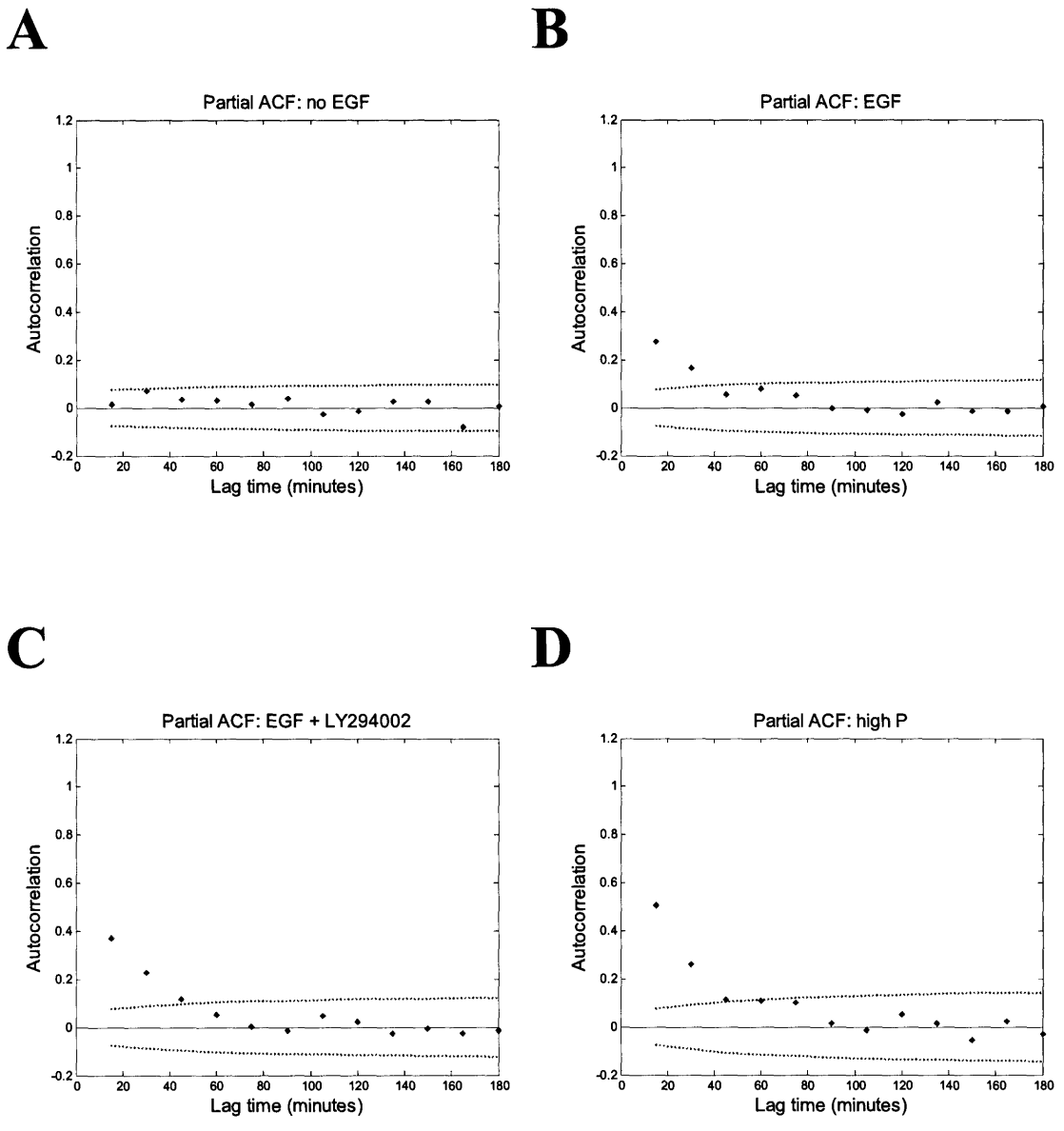

Figure 5.5.8 Angular partial autocorrelation functions for 4x-CHO cells.
Each plot shows PACF decompositions of the vector autocorrelation functions of Fig. 5.5.7. *(A)* The paths of cells migrating in the absence of EGF do not exhibit any memory behavior. *(B-D)* In the presence of EGF, CHO-EGFR cells migrate with a 30-minute memory. Increases in persistence time manifest only as increased partial correlation coefficients and not changes in the fundamental memory character of the cell paths. Dotted lines represent 95% confidence intervals for zero autocorrelation according to Bartlett's approximation.

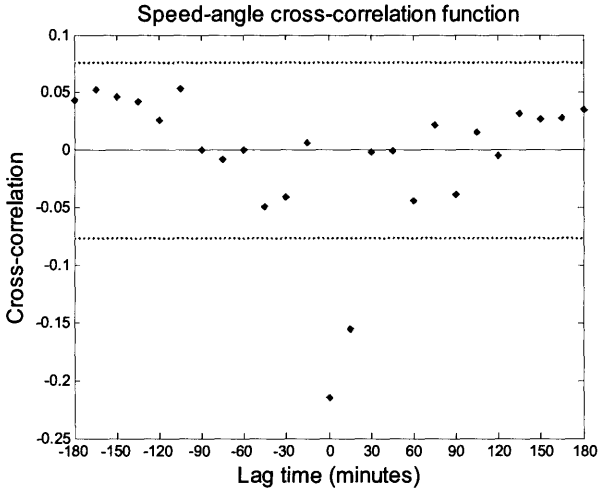

Figure 5.5.9 No cellular memory exists governing local speed and local path angle.
Three-dimensional TAD plots show that as local cell speed increases, the absolute value of the average local path angle decreases. Cross-correlation analysis indicates that this effect only extends to the two local speeds given by the adjacent displacement vectors that compose any given path angle. The first vector is represented by lag time 0, and the second by lag time 15 min. Shown is a representative cross-correlation plot for thirty 4×-CHO cells. Dotted lines represent 95% confidence intervals for zero cross-correlation according to Bartlett's approximation.

5.6 References

Box, G.E.P., and G.M. Jenkins. 1976. Time Series Analysis: Forecasting and Control. Holden-Day, San Francisco.

Doob, J.L. 1942. The Brownian motion and stochastic equations. *Ann. Math.* 43:351-369.

Dunn, G.A., and A.F. Brown. 1987. A unified approach to analysing cell motility. *J. Cell Sci. Suppl.* 8:81-102.

Durbin, J. 1960. The fitting of time series models. *Rev. Int. Stat. Inst.* 28:233-244.

Gail, M.H., and C.W. Boone. 1970. The locomotion of mouse fibroblasts in tissue culture. *Biophys. J.* 10:980-993.

Hall, R.L. 1977. Amoeboid movement as a correlated walk. *J. Math. Biol.* 4:327-335.

Hartman, R.S., K. Lau, W. Chou, and T.D. Coates. 1994. The fundamental motor of the human neutrophil is not random: evidence for the local non-Markov movement in neutrophils. *Biophys. J.* 67:2535-2545.

Maheshwari, G., A. Wells, L.G. Griffith, and D.A. Lauffenburger. 1999. Biophysical integration of effects of epidermal growth factor and fibronectin on fibroblast migration. *Biophys. J.* 76:2814-2823.

Mandeville, J.T.H., R.N. Ghosh, and F.R. Maxfield. 1995. Intracellular calcium levels correlate with speed and persistent forward motion in migrating neutrophils. *Biophys. J.* 68:1207-1217.

Mills, T.C. 1990. Time Series Techniques for Economists. Cambridge University Press, Cambridge.

Miyoshi, H., N. Masaki, and Y. Tsuchiya. 2003. Characteristics of trajectory in the migration of *Amoeba proteus*. *Protoplasma.* 222:175-181.

Othmer, H.G., S.R. Dunbar, and W. Alt. 1988. Models of dispersal in biological systems. *J. Math. Biol.* 26:263-298.

Shenderov, A.D., and M.P. Sheetz. 1997. Inversely correlated cycles in speed and turning in an ameba: an oscillatory model of cell locomotion. *Biophys. J.* 72:2382-2389.

Stokes, C.L., and D.A. Lauffenburger. 1991. Migration of individual microvessel endothelial cells: stochastic model and parameter measurement. *J. Cell Sci.* 99:419-430.

CHAPTER 6

CONCLUSIONS AND FUTURE DIRECTIONS

The guiding principles for the research conducted for this thesis were two-fold: that quantitative analysis of motility can result in novel insights not amenable to discovery by qualitative techniques, and that characterization of the biophysical effects of extracellular cues and intracellular signaling pathways is an effective method for the systematic deconstruction of how cells control cell motility.

In Chapter 3 we demonstrated that adhesion-dependent changes in the stability of lamellipodial protrusions accounted for the variation of persistence time in CHO-EGFR cells migrating on Fn in the presence of EGF. These studies implicate the kinetics of focal contact assembly as a possible means of controlling directional persistence, so future experiments quantifying the temporal recruitment of proteins to nascent focal complexes may give insight into the molecular mechanisms by which adhesion governs directionality. Furthermore, recent insights into the role of contractile force and substrate compliance in modulating adhesion complex generation and cell migration (Balaban et al., 2001; Galbraith et al., 2002; Lo et al., 2000) suggest that the examination of how force generation affects persistence would be a profitable avenue to pursue.

The studies of Chapter 4 analyzed the role of population-level ERK and PI3K signaling in modulating directional persistence in EGF-stimulated migration. Increasing amounts of pharmacological inhibition demonstrated the existence of optimal, intermediate levels of intracellular signaling for maximal persistence time. A question naturally following from these results is how intracellular signaling affects the ability of cells to

migrate up chemotactic gradients. Existing theoretical work indicates that connections exist between a cell's ability to persist in direction in isotropic chemical environments and its ability to orient properly in a chemotactic gradient (Tranquillo and Lauffenburger, 1987). To our knowledge this prediction has never been tested. Our CHO-EGFR cell system provides an excellent means to do so using experiments combining gradients of EGF with varying amounts of pharmacological inhibition. The functional relationship between PI3K-mediated persistence and PI3K-mediated chemotactic ability is of particular interest given the well-established central role of PI3K in directional orientation and sensing.

Our work in Chapter 4 utilized whole-cell lysates to determine ERK and PI3K signal strength. It is likely that our measurements are merely proxies for signaling mechanisms operating on a subcellular, localized level within a migrating cell. We expect that subcellular quantitative analysis of signaling protein localization and activity, perhaps via fluorescence resonance energy transfer (FRET) techniques, will be a vital approach in the future analysis of signaling in cell motility. We envision its importance in two areas. First, subcellular analysis would enable a better understanding of the roles of signaling targets in controlling specific biophysical aspects of motility. Second, the use of a real-time technique such as FRET for ascertaining signal strength in individual cells, in concert with single-cell time-lapse videomicroscopy, would allow the analysis of how population distributions of signaling correlate with population distributions of speed and persistence. This approach would be intriguing because while both experiment and theory amply demonstrate a wide cell-to-cell variability in migratory potential, the molecular basis for this variability is unclear.

We were unable to ascertain any variation in cell signaling due to changes in Fn concentration and cell adhesion, even though the migratory responses did vary. It is possible that adhesion-dependent variations in signal occurred but could not be detected within the experimental sensitivity of the microtiter plate assay due to the large amount of EGFR signaling. Future studies in cells expressing EGFR at a more physiological level

would aid in quantitative exploration of the regulation of motility downstream of joint, synergistic activation of key signaling network targets by both growth factor and adhesion receptors.

In Chapter 5, we used two statistical tools, turn angle distribution plots and time series analysis, to study the detailed structure of CHO-EGFR cell paths. The two key results from this work were: (1) a "local", short-timescale cell path connection between speed and persistence that does not extend to longer time intervals, and (2) time autocorrelations for cell directionality but not speed. We speculate that the molecular bases for these effects may lie in the kinetics of formation and dissolution of cell adhesion complexes. Attractive future experiments for parsing this possibility would be quantitative analyses of cell adhesion formation and turnover rates and testing whether molecular alteration of these rates changes the auto- and cross-correlative structure of cell paths. As discussed in Chapter 5, use of a more highly motile cell line than CHO-EGFR cells might be more appropriate for time series analysis studies such as these.

We note that the limiting experimental factor in this thesis was the generation of migration data using single-cell methods. Future combinatorial explorations of the simultaneous roles of multiple signaling molecules in controlling motility might thus require more qualitative migration experiments such as Boyden chambers or wound scrape assays. The value of faster motility data generation would have to be weighed carefully against the loss of speed and persistence distributions for the migrating cell populations. Extensive use of factorial experimental design could mitigate this issue of experimental throughput.

Cell motility is a tremendously complicated biological process, and much progress remains to be made in both deconstructing the precise molecular mechanisms by which cells control their movement and integrating those mechanisms into a model accounting for the biophysical processes that comprise cell translocation. We believe that research conducted with careful attention paid to quantitative, combinatorial experimentation combined with

mathematical and computational approaches to data deconvolution will ultimately lead to a predictive, systems-level understanding of cell migration at both the biochemical and biophysical level. Such understanding will offer excellent opportunities for engineering the improved design of motility-altering therapeutics via the use of antibody engineering, gene therapy, or synthetic medicinal chemistry.

6.1 References

Balaban, N.Q., U.S. Schwarz, D. Riveline, P. Goichberg, G. Tzur, I. Sabanay, D. Mahalu, S. Safran, A. Bershadsky, L. Addadi, and B. Geiger. 2001. Force and focal adhesion assembly: a close relationship studied using elastic micropatterned substrates. *Nat. Cell Biol.* 3:466-472.

Galbraith, C.G., K.M. Yamada, and M.P. Sheetz. 2002. The relationship between force and focal contact development. *J. Cell Biol.* 159:695-705.

Lo, C.-M., H.-B. Wang, M. Dembo, and Y.-L. Wang. 2000. Cell movement is guided by the rigidity of the substrate. *Biophys. J.* 79:144-152.

Tranquillo, R.T., and D.A. Lauffenburger. 1987. Stochastic model of leukocyte chemosensory movement. *J. Math. Biol.* 25:229-262.

APPENDIX A

This appendix consists of a collection of seven files written to generate cell speed and persistence time data and wind-rose path plots from input matrices of time-dependent individual cell centroid positions. Extensive annotation regarding proper matrix format, as well as code structure and function, can be found within the files themselves. This code was developed for use with MATLAB 5.3 (Mathworks, Inc., Natick, MA).

Brief descriptions of the programs are as follows:

LSMASTER - shell program calling data files, S and P fitting routines, and path plotting routines

NONOVERLAPMSD - derives mean-squared displacement data from centroid data files according to method of non-overlapping intervals (AIChE J., **39,** 1995-2010)

OVERLAPMSD - derives mean-squared displacement data from centroid data files according to method of overlapping intervals

PATHPLOT - plots the time-dependent paths of cells using a centroid data input file

INTERVALPLOT - plots the time-dependent speed of cells over the course of an experiment

LSFIT - provides S and P values for both individual cells and for cell populations

RANWALK - derives the displacement of a cell given hypothetical S and P values

A.1 LSmaster.m

```
%LSMASTER.M
%Brian Harms
%6.4.02
%
%This is the master code developed for persistent random walk cell
%migration data analysis.  It calls routines for fitting speed and
%persistence values to individual cell paths, as well plotting routines.
%%%%%%%

clear

%Call experiment data file
date = input('Input date of experiment in MMDDYY format:   ','s');
centfile = sprintf('%s%s',date,'cent.txt');
data = load(centfile);

%microns/pixel conversion factor for a 10X objective
conversion = 1/1.52;

%incoming DIAS centroid data is in pixels
data = data.*conversion;

%time between images, in hours
interval = 1/4;

%Call mean-square displacement calculation routine
nonoverlapmsd
%overlapmsd

%Call plotting routines
pathplot; pause
intervalplot; pause

%Call least squares parameter fit routine
LSfit
```

A.2 nonoverlapmsd.m

```
%NONOVERLAPMSD.M
%Brian Harms
%6.4.02
%
%This code was developed for cell migration data analysis.  It
%provides the mean-squared displacement data for both individual cells
%and the entire experiment of pooled cells.
%
%This code takes an input file of cell centroid positions with the
%following format: [x1 y1 x2 y2 x3 y3 ... xn yn].  Time increases in
%the data as the row number increases, and every two columns denote the
%track of a single cell.  This code will handle cell tracks of
%different lengths, but to do so, the input matrix of cell centroids
%must have placeholder zeros if some tracks are shorter than others.
%
%This code calculates and plots displacements using NONOVERLAPPING
%intervals according to the definition of Dickinson and Burgess,
%AIChE J, Vol. 39, 1993.
%%%%%%%

a = size(data);
%maximum number of centroid observations for any cell
nt = a(1);
%the number of cells tracked
ncells = a(2)/2;

%counter vector showing how many cells are tracked for a given number of
%centroid positions
tracking_distribution = zeros(1,nt);

%counter vector for the total number of displacement data points in
%the experiment (across all cells)
interval_counter = zeros(nt-1,1);

%loop separating the input data into individual cells
for b=1:ncells
   Cell{b} = data(:,2*b-1:2*b);
   I = find(Cell{b}(:,1));
   %truncates all zeros off the input data
   Cell{b} = Cell{b}(I,1:2);
   tracking_distribution(size(Cell{b},1)) =
   tracking_distribution(size(Cell{b},1))+1;

   x{b} = Cell{b}(:,1);
   y{b} = Cell{b}(:,2);

   %the time intervals possible in a cell track
   m = length(x{b})-1;
   n = (1:m)';
   %vector of number of nonoverlapping intervals in a cell track
   %for a given time interval
   q = floor(m./n);
```

```
   %loop over all possible time intervals for displacements
   %uses all possible starting points for a given time interval
   for i=1:m
      for j=1:q(i)
         %columns are different time intervals; rows are distances
         distance{b}(j,i) = (x{b}(1+i*j)-x{b}(1+i*(j-1)))^2 +
         (y{b}(1+i*j)-y{b}(1+i*(j-1)))^2;
      end

      %mean-square displacement data for Cell{b}
      msd(i,2*b-1) = sum(distance{b}(:,i))/q(i);
      %number of intervals of time interval I for Cell{b}
      msd(i,2*b) = q(i);
      %the total number of intervals for time period i
      %summed over all cells
      interval_counter(i) = interval_counter(i) + q(i);
   end

   %"fractional MSD": a cell's MSD weighted by its fraction of time
   %intervals in the expt total
    msd_fraction(:,b) = msd(:,2*b-1).*(msd(:,2*b)./interval_counter);
end

%the weighted average MSD data for the experiment
exp_msd = sum(msd_fraction,2);
%maximum experimental MSD
max_msd = max(exp_msd);
```

A.3 overlapmsd.m

```
%OVERLAPMSD.M
%Brian Harms
%6.4.02
%
%This code was developed for cell migration data analysis.  It provides
%the mean-squared displacement data for both individual cells and the
%entire experiment of pooled cells.
%
%This code takes an input file of cell centroid positions with the
%following format: [x1 y1 x2 y2 x3 y3 ... xn yn].  Time increases in the
%data as the row number increases, and every two columns denote the track
%of a single cell.  This code will handle cell tracks of different
%lengths, but to do so, the input matrix of cell centroids must have
%placeholder zeros if some tracks are shorter than others.
%
%This code calculates and plots displacements using OVERLAPPING intervals
%according to the definition of Dickinson and Burgess,
%AIChE J, Vol. 39, 1993.
%%%%%%%

a = size(data);
%maximum number of centroid observations for any cell
nt = a(1);
%the number of cells tracked
ncells = a(2)/2;

%counter vector showing how many cells are tracked for a given number
%of centroid positions
tracking_distribution = zeros(1,nt);

%counter vector for the total number of displacement data points in the
%experiment (across all cells)
interval_counter = zeros(nt-1,1);

%loop separating the input data into individual cells
for b=1:ncells
   Cell{b} = data(:,2*b-1:2*b);
   I = find(Cell{b}(:,1));
   %truncates all zeros off the input data
   Cell{b} = Cell{b}(I,1:2);
   tracking_distribution(size(Cell{b},1)) =
   tracking_distribution(size(Cell{b},1))+1;

   x{b} = Cell{b}(:,1);
   y{b} = Cell{b}(:,2);

   m = length(x{b})-1;
   %vector of number of overlapping intervals in a cell track
   %for a given time interval
   n = (m:-1:1)';
```

```
   %loop over all possible time intervals for displacements
   %uses all possible starting points for a given time interval
   for i=1:m
      for j=1:n(i)
         %columns are different time intervals; rows are distances
         distance{b}(j,i) = (x{b}(j+i)-x{b}(j))^2 + (y{b}(j+i)-
         y{b}(j))^2;
      end

      %mean-square displacement data for Cell{b}
      msd(i,2*b-1) = sum(distance{b}(:,i))/n(i);
      %number of intervals of time interval i for Cell{b}
      msd(i,2*b) = n(i);
      %the total number of intervals for time period i summed over
      %all cells
      interval_counter(i) = interval_counter(i) + n(i);
   end

   %"fractional MSD": a cell's MSD weighted by its fraction of time
   %intervals in the expt total
   msd_fraction(:,b) = msd(:,2*b-1).*(msd(:,2*b)./interval_counter);
end

%the weighted average MSD data for the experiment
exp_msd = sum(msd_fraction,2);
%maximum experimental MSD
max_msd = max(exp_msd);
```

A.4 pathplot.m

```
%PATHPLOT.M
%Brian Harms
%6.1.02
%
%This code plots the paths of the cells in the experiment.
%%%%%%%

for b=1:ncells
   x0 = x{b}(1)*ones(length(x{b}),1);
   y0 = y{b}(1)*ones(length(y{b}),1);

   plot(x{b}-x0,y{b}-y0);
   hold on;

   plot(x{b}-x0,y{b}-y0,'r*');
   hold off;

   xlabel('Distance traveled X (microns)');
   ylabel('Distance traveled Y (microns)');
   pause;
end
```

A.5 intervalplot.m

```
%INTERVALPLOT.M
%Brian Harms
%6.1.02
%
%This code plots the average shortest-interval displacement distance
%over the course of the experiment.  I use it to determine whether an
%experiment has constant speed throughout its entirety.
%%%%%%%

for b = 1:ncells
   %the next line accounts for cells tracked for less than
   %the whole experiment
   min_msd(:,b) = [distance{b}(:,1);zeros(nt-1-length(distance{b}),1)];

   sparse_msd = sparse(min_msd(:,b));
   sparse_ones = spones(sparse_msd);
   %placeholder matrix listing which min_msd entries are non-zero
   msd_ones(:,b) = full(sparse_ones);
end

M = sum(min_msd,2);
N = sum(msd_ones,2);
interval_msd = M./N;

%plot of displacements over the course of the experiment
X = interval*60;
plot([X:X:X*(nt-1)],interval_msd)
title('Minimum-interval MSDs plotted by time in the experiment')
xlabel('Time in the experiment (minutes)')
ylabel('Mean-square displacement (um^2)')
```

A.6 LSfit.m

```
%LSFIT.M
%Brian Harms
%6.4.02
%
%This code was developed for cell migration data analysis.  It provides
%speed and persistence values for individual cells, as well as
%experimental means.  Speed is found using the smallest-interval mean-
%square displacement for the cell.  Persistence is found using an
%ordinary least squares MATLAB algorithm.
%%%%%%%

SS = [];
PP = [];

for b = 1:ncells

   %time vector (hours)
   K = find(msd(:,2*b-1));
   timevector = interval*[1:length(K)]';

   %individual cell speed
   SS(b) = (1/interval)*sqrt(msd(1,2*b-1));
   S = SS(b);

   %initial guess for persistence time (hrs)
   Po = .25;
   save temp.mat S

   %least-squares fit for P
   P = lsqcurvefit('ranwalk',Po,timevector,msd(K,2*b-1));
   PP = [PP,P*60];
end

speed = mean(SS)
speed_sem = sqrt(cov(SS)/length(SS))
persistence = mean(PP)
persistence_sem = sqrt(cov(PP)/length(PP))

%histogram plot of persistence times
hist(PP)
xlabel('Persistence time (minutes)')
ylabel('Frequency')
```

A.7 ranwalk.m

```
%RANWALK.M
%Brian Harms
%6.4.02
%
%This code evaluates the displacement of a cell following the persistent
%random walk model with parameters S,P.
%%%%%%%

function f = ranwalk(P,timevector)

load temp.mat

f = 2*S^2*P*[timevector - P*(1-exp(-timevector/P))];
```

APPENDIX B

This appendix consists of files written to generate average area, membrane extension, and membrane retraction data from the appropriate input matrices of time-dependent individual cell data. Extensive annotation regarding proper matrix format, as well as code structure and function, can be found within the files themselves. This code was developed for use with MATLAB 5.3 (Mathworks, Inc., Natick, MA).

Brief descriptions of the programs are as follows:

AREAPROGRAM - determines cell areas for both individual cells and for cell populations

FLOWPROGRAM - code for membrane extension and retraction analysis of both individual cells and cell populations

B.1 areaprogram.m

```
%AREAPROGRAM.M
%Brian Harms
%4.6.02
%
%This code was developed for cell migration data analysis.  It determines
%cell areas for individual cells and the entire experiment of pooled
%cells.
%
%This code takes an input file of cell areas with the following format:
%[a1 a2 a3 ... an].  Time increases in the data as the row number
%increases, and each column denotes data from a single cell.  This code
%will handle cell tracks of different lengths, but to do so, the input
%matrix of cell areas must have placeholder zeros if some tracks are
%shorter than others.
%%%%%%%

clear

%number of minutes between images in the experiment
interval = 15;
%number of images you want to calculate a cell's area over
K = 8;

%Call experiment data file
date = input('Input date of experiment in MMDDYY format:   ','s');
areafile = sprintf('%s%s',date,'area.txt');
data = load(areafile);

a = size(data);
%the number of cells tracked
ncells = a(2);

%code to calculate the average area of all the cells at each timepoint
sparse_area = sparse(data);
sparse_ones = spones(sparse_area);

%placeholder matrix that lists which data matrix entries are non-zero
area_ones = full(sparse_ones);

M = sum(data,2);
N = sum(area_ones,2);
average_area = M./N;

percent_increase_area = average_area(a(1))/average_area(1);

plot([interval:interval:interval*a(1)],average_area)
title('Average pooled cell area plotted by time in the experiment')
xlabel('Time in the experiment (minutes)')
ylabel('Cell area (sq um)')
```

```
%code to calculate the average area of a given cell in the experiment
for b=1:ncells
   %separates the input data into individual cells
   Area{b} = data(1:K,b);
   I = find(Area{b});
   %truncates all zeros off the input data
   Area{b} = Area{b}(I);
   cell_area(b) = sum(Area{b})/length(Area{b});
end

%total experimental mean area
average_cell_area = mean(cell_area)
average_cell_area_sem = sqrt(cov(cell_area)/length(cell_area))
percent_increase_area
```

B.2 flowprogram.m

```
%FLOWPROGRAM.M
%Brian Harms
%4.6.02
%
%This code was developed for cell migration membrane extension and
%retraction analysis.  It analyzes individual cells and also gives
%experimental means.
%
%This code takes input files of cell flow measurements with the following
%format: [f1 f2 f3 ... fn].  Time increases in the data as the row number
%increases, and each column denotes data from a single cell. The code
%assumes that there are an equal number of membrane observations for each
%cell.
%%%%%%%

clear
%how many flow measurements you want to average from
NN = 8;

%Call experiment data file
date = input('Input date of experiment in MMDDYY format:   ','s');
pflowfile = sprintf('%s%s',date,'pflow.txt');
nflowfile = sprintf('%s%s',date,'nflow.txt');
pflowdata = load(pflowfile);
nflowdata = load(nflowfile);

%Membrane extension section

%average per-cell positive flow
average_pflow = sum(pflowdata(1:NN,:),1)./NN;
pflow = mean(average_pflow)
pflow_sem = sqrt(cov(average_pflow)/length(average_pflow))

%Membrane retraction section

%average per-cell negative flow
average_nflow = sum(nflowdata(1:NN,:),1)./NN;
nflow = mean(average_nflow)
nflow_sem = sqrt(cov(average_nflow)/length(average_nflow);
```

APPENDIX C

This appendix consists of files written to analyze the "instantaneous" speed and angular characteristics of migration cell paths, using input matrices of time-dependent individual cell centroid data. "Instantaneous" refers to data derived using the minimum observation interval in an experiment. Extensive annotation regarding proper matrix format, as well as code structure and function, can be found within the files themselves. This code was developed for use with MATLAB 5.3 (Mathworks, Inc., Natick, MA).

Brief descriptions of the programs are as follows:

TADPOL - generates turn-angle distribution plots in both two and three dimensions

TSA - time series analysis to determine autocorrelation functions for cell speed and discrete cell path angles

CCF - time series analysis to determine cross-correlation functions for cell speed and cell path angles

C.1 tadpol.m

```
%TADPOL.M
%Brian Harms
%8.18.03
%
%This code was developed for cell migration data analysis.  It calculates
%the dot product of successive cell movement vectors, giving both the
%angle and magnitude of successive movements of cells.  The angles can be
%plotted in a histogram.  Alternatively, you can sort the angles by dot
%product magnitudes (which is directly proportional to the square of the
%geometric mean of the cell speeds around any given turn), and then plot
%the binned angular distribution in a 3-dimensional histogram.  This code
%places the same number of angles in each bin; consequently the speed
%intervals within any two bins' edges are not equal.
%
%This code takes an input matrix of cell centroid positions with the
%following format: [x1 y1 x2 y2 x3 y3 ... xn yn].  Time increases in
%the data as the row number increases, and every two columns denote the
%track of a single cell.  This code will handle cell tracks of
%different lengths, but to do so, the input matrix of cell centroids
%must have placeholder zeros if some tracks are shorter than others.
%
%This code calculates and plots displacements using NONOVERLAPPING
%intervals according to the definition of Dickinson and Burgess,
%AIChE J, Vol. 39, 1993.
%%%%%%%

clear
%global variables must be cleared manually
global counter hist_data

%counter varible for how many iterations you've run
counter = [counter;1];

%reports the number of times you've run the program
iterations = length(counter)

%variable initialization
pooled_theta = [];
pooled_stepsize = [];

%calls cell data from data loading programs
%data_4x;

%microns/pixel conversion factor for 10X microscope objective
conversion_factor = 1/1.52;

%converts data from pixels to microns
data = data.*conversion_factor;

a = size(data);
%the number of cells tracked
ncells = a(2)/2;
```

```
for b=1:ncells
   %separates the input data into individual cells
   Cell{b} = data(:,2*b-1:2*b);
   I = find(Cell{b}(:,1));

   %truncates all zeros off the input data
   Cell{b} = Cell{b}(I,1:2);

   %x- and y-centroid data for each cell
   x{b} = Cell{b}(:,1);
   y{b} = Cell{b}(:,2);

   %setting the initial cell positions to (0,0)
   x_disp{b} = [x{b}(2:length(x{b}));0]-x{b};
   y_disp{b} = [y{b}(2:length(y{b}));0]-y{b};

   %n centroids give (n-1) displacements
   x_disp{b} = x_disp{b}(1:length(x_disp{b})-1);
   y_disp{b} = y_disp{b}(1:length(y_disp{b})-1);

   %converting the displacement vectors to complex numbers allows
   %simple multiplication to find the dot product of the vectors
   %(which is the real part of the complex multiple)
   comp{b} = complex(x_disp{b},y_disp{b});
   comp_conj{b} = conj(comp{b});
   dot_product{b} = comp{b}.*[comp_conj{b}(2:length(comp{b}));0];

   %n centroids give (n-2) angles
   dot_product{b} = dot_product{b}(1:length(comp{b})-1);

   %angle between cell steps
   theta{b} = angle(dot_product{b});

   %geometric mean of angle vector lengths
   stepsize{b} = abs(dot_product{b});

   pooled_theta = [pooled_theta; theta{b}];
   pooled_stepsize = [pooled_stepsize; stepsize{b}];
end

%sorting according to square of geometric mean of angle vector lengths
sorted_data = sortrows([pooled_stepsize, pooled_theta]);

%binning data into M speed-based datasets with N angle bins
%each speed bin has equal number of angles
M = 10;
N = 18;

%number of angles in a bin
width = floor((1/M)*size(sorted_data,1));
```

```
P = [];

%working with each binned dataset
for j=0:M-1
   P= 1 + width*j;

   %groups angle data based on stepsize
   bin{j+1} = sorted_data(P:P+width-1,:);

   %puts angle data into histogram bins of 2*pi/N width
   theta_bin(j+1,:)=hist(bin{j+1}(:,2),N);
end


%3-dimensional angle histogram plot

%X contains the centers of the N angle bins
X = [-(N-1)*pi/N:2*pi/N:(N-1)*pi/N];

Y = 1:M;

%normalizing data to frequencies
norm_bin = theta_bin./sum(sum(theta_bin));
figure(1)

%surface plot
surf(X,Y,norm_bin)
xlabel('Turn angle (rad)')
ylabel('Cell speed bin')
zlabel('Frequency')
shading faceted


%2-dimensional angle histogram plot (sums over speed bins)

figure(2)
plot(X,sum(norm_bin,1),'g')
xlabel('Turn angle (rad)')
ylabel('Frequency')

%bins histogram data by experiment for easy import into Excel
hist_data = [hist_data, (hist(pooled_theta,N))'];
```

C.2 TSA.m

```
%TSA.M
%Brian Harms
%6.13.04
%
%This code was developed for cell migration data analysis.  It performs
%time series analysis of cell paths, resulting in autocorrelation
%functions for both cell speed and vectorial cell displacements.
%Vectorial autocorrelations, because they are calculated using dot
products, essentially provide information regarding the time %correlation
of cell path angles.
%
%This code takes an input matrix of cell centroid positions with the
%following format: [x1 y1 x2 y2 x3 y3 ... xn yn].  Time increases in the
%data as the row number increases, and every two columns denote the track
%of a single cell.  This code will handle cell tracks of different
%lengths, but to do so, the input matrix of cell centroids must have
%placeholder zeros if some tracks are shorter than others.
%
%This code calculates and plots displacements using NONOVERLAPPING
%intervals according to the definition of Dickinson and Burgess,
%AiCHE J, Vol. 39, 1993.
%
%References:
%T.C. Mills. "Time series techniques for economists." Cambridge Univ.
%Press, 1990.
%G.A. Dunn and A.F. Brown. "A unified approach to analysing cell
%motility." J. Cell Sci. Suppl. 8: 81-102 (1987).
%%%%%%%

clear

%calls cell data
data_4x;

%images taken per hr in an experiment
J = 4;

%microns/pixel conversion factor for 10X objective
conversion_factor = 1/1.52;

%converts data from pixels to microns
data = data.*conversion_factor;

a = size(data);
%the number of cells tracked
ncells = a(2)/2;
```

```
for b=1:ncells
   %separates the input data into individual cells
   Cell{b} = data(:,2*b-1:2*b);
   I = find(Cell{b}(:,1));

   %truncates all zeros off the input data
   Cell{b} = Cell{b}(I,1:2);

   %x- and y-centroid data for each cell
   x{b} = Cell{b}(:,1);
   y{b} = Cell{b}(:,2);

   %setting the initial cell positions to (0,0)
   x_disp{b} = [x{b}(2:length(x{b}));0]-x{b};
   y_disp{b} = [y{b}(2:length(y{b}));0]-y{b};

   %n centroids give (n-1) displacements
   x_disp{b} = x_disp{b}(1:length(x_disp{b})-1);
   y_disp{b} = y_disp{b}(1:length(y_disp{b})-1);

   %converting displacements to complex numbers
   comp{b} = complex(x_disp{b},y_disp{b});
   comp_conj{b} = conj(comp{b});
   speed{b} = abs(comp{b});
   alpha{b} = angle(comp{b});

   N = length(alpha{b});

   for n=0:N-1
      %calculating the lag n sample autocovariance for alpha{b};
      %done by taking the dot product of the displacement vectors
      alpha_AC(b,n+1) = sum(real((comp{b}(1+n:N)).*(comp_conj{b}(1:N-
            n))));

      %normalizing to obtain the lag n sample autocorrelation function
      alpha_AC2(b,n+1) = alpha_AC(b,n+1)./alpha_AC(b,1);

      %calculating the lag n sample autocovariance for speed{b};
      %because average speed is expected to be non-zero,
      %this code subtracts sample means
      speed_AC(b,n+1) = sum((speed{b}(1+n:N)-
            mean(speed{b})).*(speed{b}(1:N-n)-mean(speed{b})));

      %normalizing to obtain the lag n sample autocorrelation function
      speed_AC2(b,n+1) = speed_AC(b,n+1)./speed_AC(b,1);
```

```
      %calculate autocorrelation sample variance (see Mills, p.65)
      if n == 0
         sample_varD(b,n+1) = 0;
         sample_varS(b,n+1) = 0;
      elseif n == 1
         sample_varD(b,n+1) = 1/N;
         sample_varS(b,n+1) = 1/N;
      else
         sample_varD(b,n+1) = sample_varD(b,n) +
            (1/N)*2*alpha_AC2(b,n)^2;
         sample_varS(b,n+1) = sample_varS(b,n) +
            (1/N)*2*speed_AC2(b,n)^2;
      end
   end
end

%mean across all cells for alpha
Z = mean(alpha_AC2,1);
%mean across all cells for speed
ZZ = mean(speed_AC2,1);
%error propagation for displacement variance
Z_varD = sum(sample_varD,1)./ncells^2;
% 95% confidence interval
Z_confD = 2*sqrt(Z_varD);
%error propagation for speed variance
Z_varS = sum(sample_varS,1)./ncells^2;
% 95% confidence interval
Z_confS = 2*sqrt(Z_varS);

%plotting routine

K = 60/J;       %time interval per image taken (minutes)
Y = 3*J + 1;    %number of data points to plot (3-hr lag here)

figure(1)
clf
hold on
plot(K*[0:Y-1],Z(1:Y),'d',K*[0:Y-1],Z_confD(1:Y),'r:',K*[0:Y-1],-
      Z_confD(1:Y),'r:')
v = axis;
plot([v(1):v(2)],0*[v(1):v(2)],'-k');
xlabel('Lag time (minutes)')
ylabel('Autocorrelation')
title('Displacement autocorrelation function')

figure(2)
clf
hold on
plot(K*[0:Y-1],ZZ(1:Y),'d',K*[0:Y-1],Z_confS(1:Y),'r:',K*[0:Y-1],-
      Z_confS(1:Y),'r:')
v = axis;
plot([v(1):v(2)],0*[v(1):v(2)],'-k');
xlabel('Lag time (minutes)')
ylabel('Autocorrelation')
title('Speed autocorrelation function')
```

C.3 CCF.m

```
%CCF.M
%Brian Harms
%6.13.04
%
%This code was developed for cell migration data analysis.  It performs
%cross-correlation analysis of speed and discrete path angles of
%migrating cells.
%
%This code takes an input matrix of cell centroid positions with the
%following format: [x1 y1 x2 y2 x3 y3 ... xn yn].  Time increases in the
%data as the row number increases, and every two columns denote the track
%of a single cell.
%
%This code calculates and plots displacements using NONOVERLAPPING
%intervals according to the definition of Dickinson and Burgess,
%AiCHE J, Vol. 39, 1993.
%
%References:
%T.C. Mills. "Time series techniques for economists." Cambridge Univ.
%Press, 1990.
%G.E.P. Box and G.M. Jenkins. "Time series analysis: forecasting and
%control." Holden-Day Press, 1976.
%%%%%%%

clear

%calls cell data
data_4x;

%images taken per hr in an experiment
J = 4;

%microns/pixel conversion factor for 10X objective
conversion_factor = 1/1.52;

%converts data from pixels to microns
data = data.*conversion_factor;

a = size(data);
%the number of cells tracked
ncells = a(2)/2;
```

```
for b=1:ncells
   %separates the input data into individual cells
   Cell{b} = data(:,2*b-1:2*b);
   I = find(Cell{b}(:,1));

   %truncates all zeros off the input data
   Cell{b} = Cell{b}(I,1:2);

   %x- and y-centroid data for each cell
   x{b} = Cell{b}(:,1);
   y{b} = Cell{b}(:,2);

   %setting the initial cell positions to (0,0)
   x_disp{b} = [x{b}(2:length(x{b}));0]-x{b};
   y_disp{b} = [y{b}(2:length(y{b}));0]-y{b};

   %n centroids give (n-1) displacements
   x_disp{b} = x_disp{b}(1:length(x_disp{b})-1);
   y_disp{b} = y_disp{b}(1:length(y_disp{b})-1);

   %converting the displacement vectors to complex numbers allows
   %simple multiplication to find the dot product of the vectors
   %(which is the real part of the complex multiple)
   comp{b} = complex(x_disp{b},y_disp{b});
   comp_conj{b} = conj(comp{b});
   dot_product{b} = comp{b}.*[comp_conj{b}(2:length(comp{b}));0];

   %n centroids give (n-2) angles
   dot_product{b} = dot_product{b}(1:length(comp{b})-1);

   %angle between cell steps
   theta{b} = angle(dot_product{b});

   %geometric mean of angle vector lengths
   stepsize{b} = abs(dot_product{b});

   %instantaneous speed of cell
   speed{b} = abs(comp{b}(1:length(comp{b})-1));

   %calcular normalized cross-correlation
   CC(:,b) = xcov(speed{b},abs(theta{b}),'coeff');
end

%cross-correlation mean across all cells
Z = mean(CC,2);

%calculate cross-correlation variance (see Mills, p.65; Box and
%Jenkins, ch.2)
%Bartlett's 95% approximation for variance
sample_var = (1/(a(1)-2))*ones(size(Z));
%error propagation for variance
Z_var = sample_var/ncells;
% 95% confidence interval
Z_conf = 2*sqrt(Z_var);
```

```
%plotting routine

K = 60/J;        %time interval per image taken
Y = 3*J + 1;     %number of data points to plot (3-hr lag here)

figure(1)
clf
hold on
index = (length(Z)-1)/2;
plot_index = [index-Y+2:index+Y];
plot(K*[1-Y:Y-1],Z(plot_index),'d',K*[1-Y:Y-1],Z_conf(1:2*Y-1),'r:',K*[1-
      Y:Y-1],-Z_conf(1:2*Y-1),'r:')
v = axis;
plot([v(1):v(2)],0*[v(1):v(2)],'-k');
xlabel('Lag time (minutes)')
ylabel('Cross-correlation')
title('Speed and angle cross-correlation function')
```

APPENDIX D EGFPN1-EGFR VECTOR INFORMATION

Listed below is the DNA sequence for the pEGFP-N1-EGFR expression construct. The DNA sequence for the fusion protein itself is highlighted in bold (base pairs 4412-5311). Details regarding vector construction may be found in Chapter 3. Also included below is pEGFP-N1 vector information provided by Clontech.

```
         10          20          30          40          50          60
TAGTTATTAATAGTAATCAATTACGGGGTCATTAGTTCATAGCCCATATATGGAGTTCCG
         70          80          90         100         110         120
CGTTACATAACTTACGGTAAATGGCCCGCCTGGCTGACCGCCCAACGACCCCCGCCCATT
        130         140         150         160         170         180
GACGTCAATAATGACGTATGTTCCCATAGTAACGCCAATAGGGACTTTCCATTGACGTCA
        190         200         210         220         230         240
ATGGGTGGAGTATTTACGGTAAACTGCCCACTTGGCAGTACATCAAGTGTATCATATGCC
        250         260         270         280         290         300
AAGTACGCCCCCTATTGACGTCAATGACGGTAAATGGCCCGCCTGGCATTATGCCCAGTA
        310         320         330         340         350         360
CATGACCTTATGGGACTTTCCTACTTGGCAGTACATCTACGTATTAGTCATCGCTATTAC
        370         380         390         400         410         420
CATGGTGATGCGGTTTTGGCAGTACATCAATGGGCGTGGATAGCGGTTTGACTCACGGGG
        430         440         450         460         470         480
ATTTCCAAGTCTCCACCCCATTGACGTCAATGGGAGTTTGTTTTGGCACCAAAATCAACG
        490         500         510         520         530         540
GGACTTTCCAAAATGTCGTAACAACTCCGCCCCATTGACGCAAATGGGCGGTAGGCGTGT
        550         560         570         580         590         600
ACGGTGGGAGGTCTATATAAGCAGAGCTGGTTTAGTGAACCGTCAGATCCGTCTAGAGAG
        610         620         630         640         650         660
CTTATCGATTCTAGCCGAGTCCCCGCCTCGCCGCCAACGCCACAACCACCGCGCACGGCC
        670         680         690         700         710         720
CCCTGACTCCGTCCAGTATTGATCGGGAGAGCCGGAGCGAGCTCTTCGGGGAGCAGCGAT
        730         740         750         760         770         780
GCGACCCTCCGGGACGGCCGGGGCAGCGCTCCTGGCGCTGCTGGCTGCGCTCTGCCCGGC
        790         800         810         820         830         840
GAGTCGGGCTCTGGAGGAAAAGAAAGTTTGCCAAGGCACGAGTAACAAGCTCACGCAGTT
        850         860         870         880         890         900
GGGCACTTTTGAAGATCATTTTCTCAGCCTCCAGAGGATGTTCAATAACTGTGAGGTGGT
        910         920         930         940         950         960
CCTTGGGAATTTGGAAATTACCTATGTGCAGAGGAATTATGATCTTTCCTTCTTAAAGAC
```

970 980 990 1000 1010 1020
CATCCAGGAGGTGGCTGGTTATGTCCTCATTGCCCTCAACACAGTGGAGCGAATTCCTTT
1030 1040 1050 1060 1070 1080
GGAAAACCTGCAGATCATCAGAGGAAATATGTACTACGAAAATTCCTATGCCTTAGCAGT
1090 1100 1110 1120 1130 1140
CTTATCTAACTATGATGCAAATAAAACCGGACTGAAGGAGCTGCCCATGAGAAATTTACA
1150 1160 1170 1180 1190 1200
GGAAATCCTGCATGGCGCCGTGCGGTTCAGCAACAACCCTGCCCTGTGCAACGTGGAGAG
1210 1220 1230 1240 1250 1260
CATCCAGTGGCGGGACATAGTCAGCAGTGACTTTCTCAGCAACATGTCGATGGACTTCCA
1270 1280 1290 1300 1310 1320
GAACCACCTGGGCAGCTGCCAAAAGTGTGATCCAAGCTGTCCCAATGGGAGCTGCTGGGG
1330 1340 1350 1360 1370 1380
TGCAGGAGAGGAGAACTGCCAGAAACTGACCAAAATCATCTGTGCCCAGCAGTGCTCCGG
1390 1400 1410 1420 1430 1440
GCGCTGCCGTGGCAAGTCCCCCAGTGACTGCTGCCACAACCAGTGTGCTGCAGGCTGCAC
1450 1460 1470 1480 1490 1500
AGGCCCCCGGGAGAGCGACTGCCTGGTCTGCCGCAAATTCCGAGACGAAGCCACGTGCAA
1510 1520 1530 1540 1550 1560
GGACACCTGCCCCCCACTCATGCTCTACAACCCCACCACGTACCAGATGGATGTGAACCC
1570 1580 1590 1600 1610 1620
CGAGGGCAAATACAGCTTTGGTGCCACCTGCGTGAAGAAGTGTCCCCGTAATTATGTGGT
1630 1640 1650 1660 1670 1680
GACAGATCACGGCTCGTGCGTCCGAGCCTGTGGGGCCGACAGCTATGAGATGGAGGAAGA
1690 1700 1710 1720 1730 1740
CGGCGTCCGCAAGTGTAAGAAGTGCGAAGGGCCTTGCCGCAAAGTGTGTAACGGAATAGG
1750 1760 1770 1780 1790 1800
TATTGGTGAATTTAAAGACTCACTCTCCATAAATGCTACGAATATTAAACACTTCAAAAA
1810 1820 1830 1840 1850 1860
CTGCACCTCCATCAGTGGCGATCTCCACATCCTGCCGGTGGCATTTAGGGGTGACTCCTT
1870 1880 1890 1900 1910 1920
CACACATACTCCTCCTCTGGATCCACAGGAACTGGATATTCTGAAAACCGTAAAGGAAAT
1930 1940 1950 1960 1970 1980
CACAGGGTTTTTGCTGATTCAGGCTTGGCCTGAAAACAGGACGGACCTCCATGCCTTTGA
1990 2000 2010 2020 2030 2040
GAACCTAGAAATCATACGCGGCAGGACCAAGCAACATGGTCAGTTTTCTCTTGCAGTCGT
2050 2060 2070 2080 2090 2100
CAGCCTGAACATAACATCCTTGGGATTACGCTCCCTCAAGGAGATAAGTGATGGAGATGT
2110 2120 2130 2140 2150 2160
GATAATTTCAGGAAACAAAAATTTGTGCTATGCAAATACAATAAACTGGAAAAAACTGTT
2170 2180 2190 2200 2210 2220
TGGGACCTCCGGTCAGAAAACCAAAATTATAAGCAACAGAGGTGAAAACAGCTGCAAGGC
2230 2240 2250 2260 2270 2280
CACAGGCCAGGTCTGCCATGCCTTGTGCTCCCCCGAGGGCTGCTGGGGCCCGGAGCCCAG

```
       2290        2300        2310        2320        2330        2340
GGACTGCGTCTCTTGCCGGAATGTCAGCCGAGGCAGGGAATGCGTGGACAAGTGCAACCT
       2350        2360        2370        2380        2390        2400
TCTGGAGGGTGAGCCAAGGGAGTTTGTGGAGAACTCTGAGTGCATACAGTGCCACCCAGA
       2410        2420        2430        2440        2450        2460
GTGCCTGCCTCAGGCCATGAACATCACCTGCACAGGACGGGGACCAGACAACTGTATCCA
       2470        2480        2490        2500        2510        2520
GTGTGCCCACTACATTGACGGCCCCCACTGCGTCAAGACCTGCCCGGCAGGAGTCATGGG
       2530        2540        2550        2560        2570        2580
AGAAAACAACACCCTGGTCTGGAAGTACGCAGACGCCGGCCATGTGTGCCACCTGTGCCA
       2590        2600        2610        2620        2630        2640
TCCAAACTGCACCTACGGATGCACTGGGCCAGGTCTTGAAGGCTGTCCAACGAATGGGCC
       2650        2660        2670        2680        2690        2700
TAAGATCCCGTCCATCGCCACTGGGATGGTGGGGGCCCTCCTCTTGCTGCTGGTGGTGGC
       2710        2720        2730        2740        2750        2760
CCTGGGGATCGGCCTCTTCATGCGAAGGCGCCACATCGTTCGGAAGCGCACGCTGCGGAG
       2770        2780        2790        2800        2810        2820
GCTGCTGCAGGAGAGGGAGCTTGTGGAGCCTCTTACACCCAGTGGAGAAGCTCCCAACCA
       2830        2840        2850        2860        2870        2880
AGCTCTCTTGAGGATCTTGAAGGAAACTGAATTCAAAAAGATCAAAGTGCTGGGCTCCGG
       2890        2900        2910        2920        2930        2940
TGCGTTCGGCACGGTGTATAAGGGACTCTGGATCCCAGAAGGTGAGAAAGTTAAAATTCC
       2950        2960        2970        2980        2990        3000
CGTCGCTATCAAGGAATTAAGAGAAGCAACATCTCCGAAAGCCAACAAGGAAATCCTCGA
       3010        3020        3030        3040        3050        3060
TGAAGCCTACGTGATGGCCAGCGTGGACAACCCCCACGTGTGCCGCCTGCTGGGCATCTG
       3070        3080        3090        3100        3110        3120
CCTCACCTCCACCGTGCAACTCATCACGCAGCTCATGCCCTTCGGCTGCCTCCTGGACTA
       3130        3140        3150        3160        3170        3180
TGTCCGGGAACACAAAGACAATATTGGCTCCCAGTACCTGCTCAACTGGTGTGTGCAGAT
       3190        3200        3210        3220        3230        3240
CGCAAAGGGCATGAACTACTTGGAGGACCGTCGCTTGGTGCACCGCGACCTGGCAGCCAG
       3250        3260        3270        3280        3290        3300
GAACGTACTGGTGAAAACACCGCAGCATGTCAAGATCACAGATTTTGGGCTGGCCAAACT
       3310        3320        3330        3340        3350        3360
GCTGGGTGCGGAAGAGAAAGAATACCATGCAGAAGGAGGCAAAGTGCCTATCAAGTGGAT
       3370        3380        3390        3400        3410        3420
GGCATTGGAATCAATTTTACACAGAATCTATACCCACCAGAGTGATGTCTGGAGCTACGG
       3430        3440        3450        3460        3470        3480
GGTGACCGTTTGGGAGTTGATGACCTTTGGATCCAAGCCATATGACGGAATCCCTGCCAG
       3490        3500        3510        3520        3530        3540
CGAGATCTCCTCCATCCTGGAGAAAGGAGAACGCCTCCCTCAGCCACCCATATGTACCAT
       3550        3560        3570        3580        3590        3600
CGATGTCTACATGATCATGGTCAAGTGCTGGATGATAGACGCAGATAGTCGCCCAAAGTT
```

3610 3620 3630 3640 3650 3660
CCGTGAGTTGATCATCGAATTCTCCAAAATGGCCCGAGACCCCCAGCGCTACCTTGTCAT
3670 3680 3690 3700 3710 3720
TCAGGGGGATGAAAGAATGCATTTGCCAAGTCCTACAGACTCCAACTTCTACCGTGCCCT
3730 3740 3750 3760 3770 3780
GATGGATGAAGAAGACATGGACGACGTGGTGGATGCCGACGAGTACCTCATCCCACAGCA
3790 3800 3810 3820 3830 3840
GGGCTTCTTCAGCAGCCCCTCCACGTCACGGACTCCCCTCCTGAGCTCTCTGAGTGCAAC
3850 3860 3870 3880 3890 3900
CAGCAACAATTCCACCGTGGCTTGCATTGATAGAAATGGGCTGCAAAGCTGTCCCATCAA
3910 3920 3930 3940 3950 3960
GGAAGACAGCTTCTTGCAGCGATACAGCTCAGACCCCACAGGCGCCTTGACTGAGGACAG
3970 3980 3990 4000 4010 4020
CATAGACGACACCTTCCTCCCAGTGCCTGAATACATAAACCAGTCCGTTCCCAAAAGGCC
4030 4040 4050 4060 4070 4080
CGCTGGCTCTGTGCAGAATCCTGTCTATCACAATCAGCCTCTGAACCCCGCGCCCAGCAG
4090 4100 4110 4120 4130 4140
AGACCCACACTACCAGGACCCCCACAGCACTGCAGTGGGCAACCCCGAGTATCTCAACAC
4150 4160 4170 4180 4190 4200
TGTCCAGCCCACCTGTGTCAACAGCACATTCGACAGCCCTGCCCACTGGGCCCAGAAAGG
4210 4220 4230 4240 4250 4260
CAGCCACCAAATTAGCCTGGACAACCCTGACTACCAGCAGGACTTCTTTCCCAAGGAAGC
4270 4280 4290 4300 4310 4320
CAAGCCAAATGGCATCTTTAAGGGCTCCACAGCTGAAAATGCAGAATACCTAAGGGTCGC
4330 4340 4350 4360 4370 4380
GCCACAAAGCAGTGAATTTATTGGAGCATGActtaagcttCGAATTCTGCAGTCGACGGT
4390 4400 4410 4420 4430 4440
ACCGCGGGCCCGGGATCCACCGGTCGCCACC**ATGGTGAGCAAGGGCGAGGAGCTGTTCA**
4450 4460 4470 4480 4490 4500
CGGGGTGGTGCCCATCCTGGTCGAGCTGGACGGCGACGTAAACGGCCACAAGTTCAGCGT
4510 4520 4530 4540 4550 4560
GTCCGGCGAGGGCGAGGGCGATGCCACCTACGGCAAGCTGACCCTGAAGTTCATCTGCAC
4570 4580 4590 4600 4610 4620
CACCGGCAAGCTGCCCGTGCCCTGGCCCACCCTCGTGACCACCCTGACCTACGGCGTGCA
4630 4640 4650 4660 4670 4680
GTGCTTCAGCCGCTACCCCGACCACATGAAGCAGCACGACTTCTTCAAGTCCGCCATGCC
4690 4700 4710 4720 4730 4740
CGAAGGCTACGTCCAGGAGCGCACCATCTTCTTCAAGGACGACGGCAACTACAAGACCCG
4750 4760 4770 4780 4790 4800
CGCCGAGGTGAAGTTCGAGGGCGACACCCTGGTGAACCGCATCGAGCTGAAGGGCATCGA
4810 4820 4830 4840 4850 4860
CTTCAAGGAGGACGGCAACATCCTGGGGCACAAGCTGGAGTACAACTACAACAGCCACAA
4870 4880 4890 4900 4910 4920
CGTCTATATCATGGCCGACAAGCAGAAGAACGGCATCAAGGTGAACTTCAAGATCCGCCA

4930 4940 4950 4960 4970 4980

CAACATCGAGGACGGCAGCGTGCAGCTCGCCGACCACTACCAGCAGAACACCCCCATCGG

4990 5000 5010 5020 5030 5040

CGACGGCCCCGTGCTGCTGCCCGACAACCACTACCTGAGCACCCAGTCCGCCCTGAGCAA

5050 5060 5070 5080 5090 5100

AGACCCCAACGAGAAGCGCGATCACATGGTCCTGCTGGAGTTCGTGACCGCCGCCGGGAT

5110 5120 5130 5140 5150 5160

CACTCTCGGCATGGACGAGCTGTACAAGTAAAGCGGCCGCGACTCTAGATCATAATCAGC

5170 5180 5190 5200 5210 5220

CATACCACATTTGTAGAGGTTTTACTTGCTTTAAAAAACCTCCCACACCTCCCCCTGAAC

5230 5240 5250 5260 5270 5280

CTGAAACATAAAATGAATGCAATTGTTGTTGTTAACTTGTTTATTGCAGCTTATAATGGT

5290 5300 5310 5320 5330 5340

TACAAATAAAGCAATAGCATCACAAATTTCACAAATAAAGCATTTTTTTCACTGCATTCT

5350 5360 5370 5380 5390 5400

AGTTGTGGTTTGTCCAAACTCATCAATGTATCTTAAGGCGTAAATTGTAAGCGTTAATAT

5410 5420 5430 5440 5450 5460

TTTGTTAAAATTCGCGTTAAATTTTTGTTAAATCAGCTCATTTTTTAACCAATAGGCCGA

5470 5480 5490 5500 5510 5520

AATCGGCAAAATCCCTTATAAATCAAAAGAATAGACCGAGATAGGGTTGAGTGTTGTTCC

5530 5540 5550 5560 5570 5580

AGTTTGGAACAAGAGTCCACTATTAAAGAACGTGGACTCCAACGTCAAAGGGCGAAAAAC

5590 5600 5610 5620 5630 5640

CGTCTATCAGGGCGATGGCCCACTACGTGAACCATCACCCTAATCAAGTTTTTTGGGGTC

5650 5660 5670 5680 5690 5700

GAGGTGCCGTAAAGCACTAAATCGGAACCCTAAAGGGAGCCCCCGATTTAGAGCTTGACG

5710 5720 5730 5740 5750 5760

GGGAAAGCCGGCGAACGTGGCGAGAAAGGAAGGGAAGAAAGCGAAAGGAGCGGGCGCTAG

5770 5780 5790 5800 5810 5820

GGCGCTGGCAAGTGTAGCGGTCACGCTGCGCGTAACCACCACACCCGCCGCGCTTAATGC

5830 5840 5850 5860 5870 5880

GCCGCTACAGGGCGCGTCAGGTGGCACTTTTCGGGGAAATGTGCGCGGAACCCCTATTTG

5890 5900 5910 5920 5930 5940

TTTATTTTTCTAAATACATTCAAATATGTATCCGCTCATGAGACAATAACCCTGATAAAT

5950 5960 5970 5980 5990 6000

GCTTCAATAATATTGAAAAAGGAAGAGTCCTGAGGCGGAAAGAACCAGCTGTGGAATGTG

6010 6020 6030 6040 6050 6060

TGTCAGTTAGGGTGTGGAAAGTCCCCAGGCTCCCCAGCAGGCAGAAGTATGCAAAGCATG

6070 6080 6090 6100 6110 6120

CATCTCAATTAGTCAGCAACCAGGTGTGGAAAGTCCCCAGGCTCCCCAGCAGGCAGAAGT

6130 6140 6150 6160 6170 6180

ATGCAAAGCATGCATCTCAATTAGTCAGCAACCATAGTCCCGCCCCTAACTCCGCCCATC

6190 6200 6210 6220 6230 6240

CCGCCCCTAACTCCGCCCAGTTCCGCCCATTCTCCGCCCCATGGCTGACTAATTTTTTTT

```
      6250        6260        6270        6280        6290        6300
ATTTATGCAGAGGCCGAGGCCGCCTCGGCCTCTGAGCTATTCCAGAAGTAGTGAGGAGGC
      6310        6320        6330        6340        6350        6360
TTTTTTGGAGGCCTAGGCTTTTGCAAAGATCGATCAAGAGACAGGATGAGGATCGTTTCG
      6370        6380        6390        6400        6410        6420
CATGATTGAACAAGATGGATTGCACGCAGGTTCTCCGGCCGCTTGGGTGGAGAGGCTATT
      6430        6440        6450        6460        6470        6480
CGGCTATGACTGGGCACAACAGACAATCGGCTGCTCTGATGCCGCCGTGTTCCGGCTGTC
      6490        6500        6510        6520        6530        6540
AGCGCAGGGGCGCCCGGTTCTTTTTGTCAAGACCGACCTGTCCGGTGCCCTGAATGAACT
      6550        6560        6570        6580        6590        6600
GCAAGACGAGGCAGCGCGGCTATCGTGGCTGGCCACGACGGGCGTTCCTTGCGCAGCTGT
      6610        6620        6630        6640        6650        6660
GCTCGACGTTGTCACTGAAGCGGGAAGGGACTGGCTGCTATTGGGCGAAGTGCCGGGGCA
      6670        6680        6690        6700        6710        6720
GGATCTCCTGTCATCTCACCTTGCTCCTGCCGAGAAAGTATCCATCATGGCTGATGCAAT
      6730        6740        6750        6760        6770        6780
GCGGCGGCTGCATACGCTTGATCCGGCTACCTGCCCATTCGACCACCAAGCGAAACATCG
      6790        6800        6810        6820        6830        6840
CATCGAGCGAGCACGTACTCGGATGGAAGCCGGTCTTGTCGATCAGGATGATCTGGACGA
      6850        6860        6870        6880        6890        6900
AGAGCATCAGGGGCTCGCGCCAGCCGAACTGTTCGCCAGGCTCAAGGCGAGCATGCCCGA
      6910        6920        6930        6940        6950        6960
CGGCGAGGATCTCGTCGTGACCCATGGCGATGCCTGCTTGCCGAATATCATGGTGGAAAA
      6970        6980        6990        7000        7010        7020
TGGCCGCTTTTCTGGATTCATCGACTGTGGCCGGCTGGGTGTGGCGGACCGCTATCAGGA
      7030        7040        7050        7060        7070        7080
CATAGCGTTGGCTACCCGTGATATTGCTGAAGAGCTTGGCGGCGAATGGGCTGACCGCTT
      7090        7100        7110        7120        7130        7140
CCTCGTGCTTTACGGTATCGCCGCTCCCGATTCGCAGCGCATCGCCTTCTATCGCCTTCT
      7150        7160        7170        7180        7190        7200
TGACGAGTTCTTCTGAGCGGGACTCTGGGGTTCGAAATGACCGACCAAGCGACGCCCAAC
      7210        7220        7230        7240        7250        7260
CTGCCATCACGAGATTTCGATTCCACCGCCGCCTTCTATGAAAGGTTGGGCTTCGGAATC
      7270        7280        7290        7300        7310        7320
GTTTTCCGGGACGCCGGCTGGATGATCCTCCAGCGCGGGGATCTCATGCTGGAGTTCTTC
      7330        7340        7350        7360        7370        7380
GCCCACCCTAGGGGGAGGCTAACTGAAACACGGAAGGAGACAATACCGGAAGGAACCCGC
      7390        7400        7410        7420        7430        7440
GCTATGACGGCAATAAAAAGACAGAATAAAACGCACGGTGTTGGGTCGTTTGTTCATAAA
      7450        7460        7470        7480        7490        7500
CGCGGGGTTCGGTCCCAGGGCTGGCACTCTGTCGATACCCCACCGAGACCCCATTGGGGC
      7510        7520        7530        7540        7550        7560
CAATACGCCCGCGTTTCTTCCTTTTCCCCACCCCACCCCCCAAGTTCGGGTGAAGGCCCA
```

```
        7570        7580        7590        7600        7610        7620
GGGCTCGCAGCCAACGTCGGGGCGGCAGGCCCTGCCATAGCCTCAGGTTACTCATATATA
        7630        7640        7650        7660        7670        7680
CTTTAGATTGATTTAAAACTTCATTTTTAATTTAAAAGGATCTAGGTGAAGATCCTTTTT
        7690        7700        7710        7720        7730        7740
GATAATCTCATGACCAAAATCCCTTAACGTGAGTTTTCGTTCCACTGAGCGTCAGACCCC
        7750        7760        7770        7780        7790        7800
GTAGAAAAGATCAAAGGATCTTCTTGAGATCCTTTTTTTCTGCGCGTAATCTGCTGCTTG
        7810        7820        7830        7840        7850        7860
CAAACAAAAAAACCACCGCTACCAGCGGTGGTTTGTTTGCCGGATCAAGAGCTACCAACT
        7870        7880        7890        7900        7910        7920
CTTTTTCCGAAGGTAACTGGCTTCAGCAGAGCGCAGATACCAAATACTGTCCTTCTAGTG
        7930        7940        7950        7960        7970        7980
TAGCCGTAGTTAGGCCACCACTTCAAGAACTCTGTAGCACCGCCTACATACCTCGCTCTG
        7990        8000        8010        8020        8030        8040
CTAATCCTGTTACCAGTGGCTGCTGCCAGTGGCGATAAGTCGTGTCTTACCGGGTTGGAC
        8050        8060        8070        8080        8090        8100
TCAAGACGATAGTTACCGGATAAGGCGCAGCGGTCGGGCTGAACGGGGGGTTCGTGCACA
        8110        8120        8130        8140        8150        8160
CAGCCCAGCTTGGAGCGAACGACCTACACCGAACTGAGATACCTACAGCGTGAGCTATGA
        8170        8180        8190        8200        8210        8220
GAAAGCGCCACGCTTCCCGAAGGGAGAAAGGCGGACAGGTATCCGGTAAGCGGCAGGGTC
        8230        8240        8250        8260        8270        8280
GGAACAGGAGAGCGCACGAGGGAGCTTCCAGGGGGAAACGCCTGGTATCTTTATAGTCCT
        8290        8300        8310        8320        8330        8340
GTCGGGTTTCGCCACCTCTGACTTGAGCGTCGATTTTTGTGATGCTCGTCAGGGGGGCGG
        8350        8360        8370        8380        8390        8400
AGCCTATGGAAAAACGCCAGCAACGCGGCCTTTTTACGGTTCCTGGCCTTTTGCTGGCCT
        8410        8420        8430        8440        8450        8460
TTTGCTCACATGTTCTTTCCTGCGTTATCCCCTGATTCTGTGGATAACCGTATTACCGCC
        8470
ATGCAT
```

pEGFP-N1 Vector Information PT3027-5

GenBank Accession #U55762 Catalog #6085-1

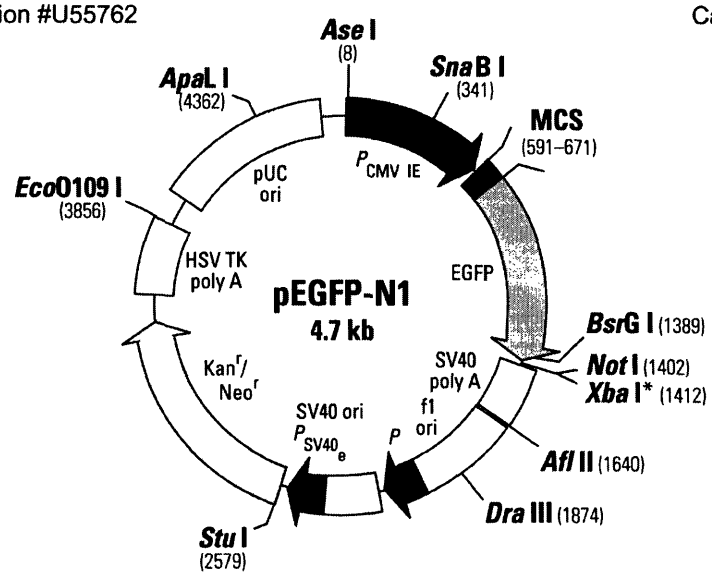

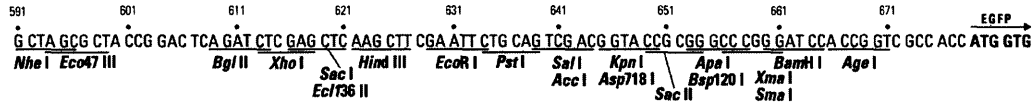

Restriction Map and Multiple Cloning Site (MCS) of pEGFP-N1 Vector. All restriction sites shown are unique. The *Not* I site follows the EGFP stop codon. The *Xba* I site (*) is methylated in the DNA provided by BD Biosciences Clontech. If you wish to digest the vector with this enzyme, you will need to transform the vector into a *dam*⁻ and make fresh DNA.

Description

pEGFP-N1 encodes a red-shifted variant of wild-type GFP (1–3) which has been optimized for brighter fluorescence and higher expression in mammalian cells. (Excitation maximum = 488 nm; emission maximum = 507 nm.) pEGFP-N1 encodes the GFPmut1 variant (4) which contains the double-amino-acid substitution of Phe-64 to Leu and Ser-65 to Thr. The coding sequence of the EGFP gene contains more than 190 silent base changes which correspond to human codon-usage preferences (5). Sequences flanking EGFP have been converted to a Kozak consensus translation initiation site (6) to further increase the translation efficiency in eukaryotic cells. The MCS in pEGFP-N1 is between the immediate early promoter of CMV ($P_{CMV\ IE}$) and the EGFP coding sequences. Genes cloned into the MCS will be expressed as fusions to the N-terminus of EGFP if they are in the same reading frame as EGFP and there are no intervening stop codons. SV40 polyadenylation signals downstream of the EGFP gene direct proper processing of the 3' end of the EGFP mRNA. The vector backbone also contains an SV40 origin for replication in mammalian cells expressing the SV40 T antigen. A neomycin-resistance cassette (Neo^r), consisting of the SV40 early promoter, the neomycin/kanamycin resistance gene of Tn5, and polyadenylation signals from the Herpes simplex virus thymidine kinase (HSV TK) gene, allows stably transfected eukaryotic cells to be selected using G418. A bacterial promoter upstream of this cassette expresses kanamycin resistance in *E. coli.* The pEGFP-N1 backbone also provides a pUC origin of replication for propagation in *E. coli* and an f1 origin for single-stranded DNA production.

pEGFP-N1 **Vector Information**

Use

Fusions to the N terminus of EGFP retain the fluorescent properties of the native protein allowing the localization of the fusion protein *in vivo*. The target gene should be cloned into pEGFP-N1 so that it is in frame with the EGFP coding sequences, with no intervening in-frame stop codons. The inserted gene should include the initiating ATG codon. The recombinant EGFP vector can be transfected into mammalian cells using any standard transfection method. If required, stable transformants can be selected using G418 (7). pEGFP-N1 can also be used simply to express EGFP in a cell line of interest (e.g., as a transfection marker).

Location of features

- Human cytomegalovirus (CMV) immediate early promoter: 1–589
  Enhancer region:59–465; TATA box: 554–560
  Transcription start point: 583
  C→G mutation to remove *Sac* I site: 569
- MCS: 591–671
- Enhanced green fluorescent protein (EGFP) gene
  Kozak consensus translation initiation site: 672–682
  Start codon (ATG): 679–681; Stop codon: 1396–1398
  Insertion of Val at position 2: 682–684
  GFPmut1 chromophore mutations (Phe-64 to Leu; Ser-65 to Thr): 871–876
  His-231 to Leu mutation (A→T): 1373
- SV40 early mRNA polyadenylation signal
  Polyadenylation signals: 1552–1557 & 1581–1586; mRNA 3' ends: 1590 & 1602
- f1 single-strand DNA origin: 1649–2104 (Packages the noncoding strand of EGFP.)
- Bacterial promoterfor expression of Kan^r gene:
  –35 region: 2166–2171; –10 region: 2189–2194
  Transcription start point: 2201
- SV40 origin of replication: 2445–2580
- SV40 early promoter
  Enhancer (72-bp tandem repeats): 2278–2349 & 2350–2421
  21-bp repeats: 2425–2445, 2446–2466 & 2468–2488
  Early promoter element: 2501–2507
  Major transcription start points: 2497, 2535, 2541 & 2546
- Kanamycin/neomycin resistance gene
  Neomycin phosphotransferase coding sequences: start codon (ATG): 2629–2631; stop codon: 3421–3423
  G→A mutation to remove *Pst* I site: 2811
  C→A (Arg to Ser) mutation to remove *Bss*H II site: 3157
- Herpes simplex virus (HSV) thymidine kinase (TK) polyadenylation signal
  Polyadenylation signals: 3659–3664 & 3672–3677
- pUC plasmid replication origin: 4008–4651

Primer Locations

- EGFP-N Sequencing Primer (#6479-1): 745–724
- EGFP-C Sequencing Primer (#6478-1): 1332–1353

Propagation in *E. coli*

- Suitable host strains: DH5a, HB101 and other general purpose strains. Single-stranded DNA production requires a host containing an F plasmid such as JM101 or XL1-Blue.
- Selectable marker: plasmid confers resistance to kanamycin (30 μg/ml) to *E. coli* hosts.
- *E. coli* replication origin: pUC
- Copy number: ≈500
- Plasmid incompatibility group: pMB1/ColE1

References:

1. Prasher, D. C., *et al.* (1992) *Gene* **111**:229–233.
2. Chalfie, M., *et al.* (1994) *Science* **263**:802–805.
3. Inouye, S. & Tsuji, F. I. (1994) *FEBS Letters* **341**:277–280.
4. Cormack, B., *et al.* (1996) *Gene* **173**:33–38.
5. Haas, J., *et al.* (1996) *Curr. Biol.* **6**:315–324.
6. Kozak, M. (1987) *Nucleic Acids Res.* **15**:8125–8148.
7. Gorman, C. (1985). In *DNA cloning: A practical approach, vol. II.* Ed. D.M. Glover. (IRL Press, Oxford, U.K.) pp. 143–190.